AD NUMBER
AD829121
LIMITATION CHANGES
TO: **Approved for public release; distribution is unlimited.**
FROM: **Distribution authorized to U.S. Gov't. agencies and their contractors; Critical Technology; 01 AUG 1967. Other requests shall be referred to Air Force Office of Scientific Research, Arlington, VA. This document contains export-controlled technical data.**
AUTHORITY
AFOSR ltr dtd 12 Nov 1971

University of Utah

Department of Chemical Engineering

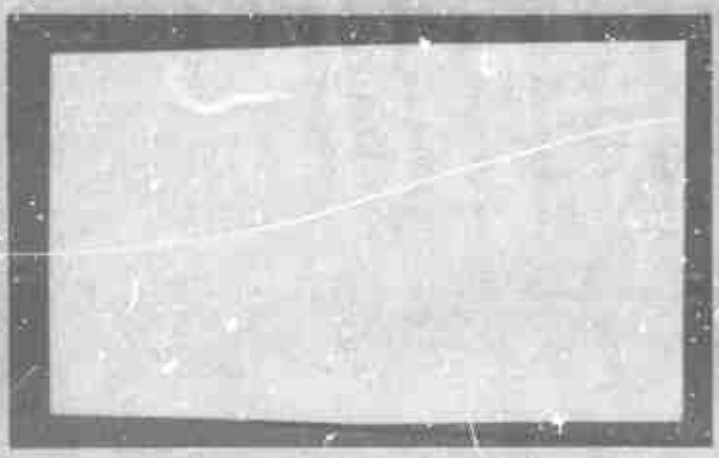

Salt Lake City, Utah

University of Utsh

Depsrtment of Chemical Engineering

Technical Report

on

SURFACE-TEMPERATURE MEASUREMENTS OF SOLID PROPELLANTS DURING IGNITION

Under Air Force Grants AFOSR 40-66 and 40-67

August 1, 1967

This resesrch under Grants AF AFOSR 40-66 and 40-67, Project Tssk No. 9711-01, for the period June, 1966, through July, 1967, was sponsored by the Air Force Office of Scientific Resesrch, Office of Aerospsce Research, United States Air Force.

The Technical Supervisor for this program is Dr. Bernard T. Wolfson, Project Scientist, Propulsion Division, Directorate of Engineering Sciences, Air Force Office of Scientific Research.

This report wss prepsred by John A. Keller, Alva D. Baer, snd Normsn W. Rysn.

Report approved by

Norman W. Ryan, Principal Investigator

TABLE OP CONTENTS

SUMMARY

An infrared detector, sensitive to radiation over the spectrum of one to ten microns, was used to measure surface temperature histories of solid propellant samples subjected to convective heat transfer in a shock-tube apparatus. In these experiments, the convective heat fluxes were in the range of 30 to 80 cal/(cm^2)(sec) and the heating gas velocity was about 100 m/(sec). This report describes the experimental procedure used and data obtained in tests on cast and pressed ammonium-perchlorate propellants.

The results of this study showed that surface temperature histories for samples having smooth surfaces, for the test conditions of this study, are in good agreement with those predicted by a thermal ignition model that considers the key ignition reaction to be localized at the propellant surface. For samples of propellant with rough surfaces, data obtained for only one test-gas velocity, about 100 m/(sec), indicate that the improved ignitibility for these samples is primarily the result of a higher heat-transfer rate to the roughened surface.

I. INTRODUCTION

This report describes the method used and data obtained in a study conducted for experimentally measuring surface temperatures on solid propellant samples during ignition. A fast-response infrared detector was used for monitoring radiation emitted by a propellant surface as the surface was exposed to transient convective heating in a shock tube.

Infrared detectors have not been extensively used in research on propellant ignition. Generally, photoelectric detectors, sensitive to radiation in the visible spectrum, have been used for monitoring the radiation from the propellant surface during ignition tests. Niesson and Bastress [1] report the use of an indium-arsenide infrared detector for observing ignition of propellant samples. In their study, the infrared detector was used primarily as a tool for measuring ignition time.

Powling and Smith [2, 3, 4] have successfully used infrared-detection methods for measuring temperatures at propellant surfaces during steady burning.

The experimental procedure used in the study reported here was to measure directly, as a function of time, the total radiation emitted by the propellant surface over the infrared spectrum of about one to ten microns. The Philco GPC-201A IR detector, a gold-doped germanium, photoconductive detector, and the detection system were calibrated dynamically for black-body radiation, using a blackened heat-flux gage as the source.

The following sections of this report describe the experimental apparatus and procedures, the calibration of the detection system, and the results of the propellant surface-temperature measurements.

II. EXPERIMENTAL APPARATUS

A. SHOCK TUBE

The shock tube used in this study was the one used previously for studies on propellant ignition by convective heating [5, 6, 7], and is described in considerable detail in Reference 6. Figure 1 shows a sketch of the driven end of the shock tube with the test section used in earlier studies. Heat transfer to the wall-mounted sample of propellant was controlled by initial shock-tube conditions and/or by the velocity of the heated gas through the test section. The test section and a propellant sample holder are shown in Figure 2.

For the work described in this report, the test section used in previous studies was modified, as shown in Figure 3, by the addition of a sharp-edged orifice upstream of the test position. This modification provided a means of increasing the rate of heat transfer to the test position without making other modifications to the apparatus. For temperature measurements with the IR detector, the quartz window used for monitoring ignition with the RCA 1P40 photodiode (Figure 2) was replaced with an infrared-transmitting window made of Kodak Irtran 2 (Figure 3).

The effective-test period in the shock-tube apparatus for a fixed total length is dependent on initial shock-tube conditions and the rate at which the shock-heated gases are exhausted through the test section. With a small flow-control orifice, the test period is approximately 35 and 20 milliseconds for incident shock Mach numbers of 2.0 and 3.5, respectively. Normally, even for small Mach numbers, the test period is terminated by mixing of driver gas with the shock-heated test gas before the reflected rarefaction wave arrives at the test section. When the mixed gases begin to flow through the test section, it is no longer possible to predict the heat-transfer rate to the test position.

With the modified test section shown in Figure 3, it was again necessary, as in earlier work [6] to measure experimentally heat transfer at the test position. The change in flow pattern produced by the addition of the sharp-edged orifice upstream of the test position precluded estimating

heat transfer with required precision from theoretical considerations alone. Heat tranafer was measured with heat-flux gages (thin-film resistance thermometers bonded to aubstratea of Pyrex 7740 or alumina) that were interchangesble with the propellant aample holder (aee Figure 2). The resulta from this study are discussed in Appendix A. It was found that the temperature-time data from heat-flux gages were well represented by the equation for transient heating of the surface of a semi-infinite solid from a high temperature gas, T_g, through a constant wall heat tranafer coefficient, h:

$$\frac{T_s - T_o}{T_g - T_o} = [1 - e^{N^2} (\text{erfc } N)] \qquad (1)$$

$$N = \frac{h(t)^{1/2}}{\Gamma}$$

The symbols used here are defined in the table of nomenclature, Appendix F.

The heat trsnsfer coefficients derived from experimental data were well represented as a function of mass flow rate, G, of the test gas through the test section and the temperature of the test gas, T_g. For high temperature air or nitrogen using flow-control orifice No. 3A, the heat transfer coefficient was defined by the following equation:

$$h = 2.784 \times 10^{-4} (T_g)^{0.3} (G)^{0.938}, \text{ cal/(cm}^2\text{)(sec)(°K)} \qquad (2)$$

B. INFRARED-RADIATION DETECTION SYSTEM

The infrared radiation detection system was designed to messure radiation emitted by the propellant surface over the IR spectrum of about one to ten microns. This is the region of most intense radiation for a gray or black body with temperatures of 30 to 600°C, the temperature range of interest for thia atudy. Figure 4 ahows the position of the IR detector and optical components in the apparatua.

1. Infrsred Detector

The IR detector used in this atudy was a Philco Model GPC-201A (a "P" type, gold-doped germanium) photoconductive detector with a cell

element 2-mm aquare and a detectivity, D*, of 2×10^9 cm/(watt). This detector has a time constant of about one microsecond and excellent detectivity over the wave-length spectrum from sbout one to ten microns when operated at liquid nitrogen temperature (77°K). The GPC-201A is linear in response to incident radiant flux in the range of 0.1 to 1000 microwstts/(cm^2). A sketch of the electrical circuit used with the detector is shown in Figure 5. Calibration data supplied by the Philco Corporation showed the best signal-to-noise ratio (425) for operstion at a bias current of 80 microamperes, and this wss the value for bias current used in this work. In our study, it was of advantage to ootain a direct-current reading of output from the IR detector; therefore, a second circuit was used to suppress the bsse voltage output for the detector (see Figure 5). It wse then possible to read output from the detector directly as a transient dc aignal on the CRT of a Tektronix, Model 502 oscilloscope.

2. Optics

A simple mirror system, shown in Figure 4, utilizing a 3-inch dismeter spherical mirror with a focal length of 12 inches was used for focusing the IR rsdiation from the source onto the detection cell of the GPC-201A detector.

An infrared window made of Kodsk Irtran 2 (polycrystalline zinc sulfide) was used in the test section in plsce of the quartz window used in earlier ignition studies. The window was one-hslf inch in diameter by one-eighth inch thick snd wss backed with a piece of Plexiglss machined to fit the port in the test section (see Figures 3 and 4). The Irtrsn 2 window mounted in this way withstood pressures of 350 psia and transient heating st heat fluxes of 100 cal/(cm^2)(sec) in the shock tube.

Irtrsn 2 gives excellent transmittsnce of infrared radiation over the spectrum of about one to ten microns. This is the same range of the spectrum over which the GPC-201A detector gives msximum detectivity.

At the start of the experimental progrsm, there was some concern sbout damaging the IR detector by excessive radiation from propellants

after ignition. The short wave-length cutoff at about one micron for Irtran 2 would be expected to provide some protection for the IR detector from intense radiation at shorter wave lengths after ignition. Overloading of the IR detector for short-time intervals, 100 to 200 milliseconds, did not damage it.

The optical system was assembled and then focused with visible radiation. A preliminary calibration of the entire optical system, detector in place, with a steady-state infrared source, indicated that focusing was not extremely critical; however, during all tests, the IR detector was held at the same position relative to the source (sample surface).

III. CALIBRATION OF INFRARED-RADIATION DETECTION SYSTEM

The infrared-radiation detection system was calibrated by measuring detector output for incident radiation received by the detector from a carbon-coated heat-flux gauge as the gage was subjected to transient, convective heating in the shock tube. The heat-flux gauge was directly interchangeable in the test section with the propellant sample holders used for ignition studies.

The shock-tube conditions for calibration of the IR detector were the same as those used later for measuring propellant surface temperatures. From this study, a relationship between IR-detector output for radiation from a black-body source (blackened heat-flux gauge) and temperature of the source (for transient heating) was obtained.

In theory, if sufficient information is known about the system optics and the detector, it is possible to calculate directly the relationship between detector output and the temperature of a black-body source (also for a gray body if the emissivity of the gray-body source is known). Investigators at the Avco-Everett Research Laboratory [8, 9] found good agreement between theory and experiment for a high-speed infrared bolometer which utilized an IR detector for sensing the temperature rise of a black-body source during transient heating.

In our work, unknown features about the IR detection system precluded a direct calculation of the relationship between detector output and source temperature. In the experimental apparatus, the source was on the opposite side of the flow channel from the optics (see Figure 4). One of the problems was that of determining the radiation from dust particles suspended in the hot test gas moving through the flow channel of the test section. A second problem was that of determining the radiation contribution of the Irtran 2 window, which was also undergoing transient heating.

The contribution of radiation from these sources was measured by using a highly-polished brass surface at the sample position in some of the shock-tube runs. The IR-detector output for runs with the brass surface represented what might be called "background radiation" (radiation from the IR window and dust particles in the convective gas), the contribution to the IR-detector output from the brass surface being negligible. The back-

ground radiation was found to be a function of time and Mach number of the incident shock wave for a given flow-control orifice at the downstream end of the test section. It is possible that background radiation would also be a weak function of pressure because of the dependence of mass flow rate on pressure, but all runs were made at approximately the same shock-tube pressure and no effect related to pressure was found.

A. DATA FOR BLACK-BODY SOURCE

A carbon-coated heat-flux gage was selected as a black-body source for calibrating the IR radiation detection system for the following reasons: (1) because of the problems already mentioned, a dynamic rather than a steady-state calibration procedure was required; (2) for dynamic calibration, a fast-response temperature sensing device was needed for recording the surface temperature of the black-body source; (3) in order to obtain a temperature rise of about 300°C for the source during tests, the thermal responsivity of the source had to be rather small (the thermal responsivity of Pyrex 7740 is less than two times as large as that for propellants); and (4) to obtain a temperature-time relationship which was similar to that for transient heating of propellant, a source with properties similar to those of a semi-infinite solid were desired.

The body for the heat-flux gage was constructed of Pyrex 7740 by methods described in Reference 6. The platinum-resistance, temperature-sensing element at the surface of the heat-flux gage was first coated with a thin layer of silicon monoxide (less than 0.1 micron thick) by a conventional vacuum deposition technique. Carbon was deposited over the SiO layer by thermally decomposing methyl iodide at the gage surface. The methods used for coating the heat-flux gage are described in more detail in Appendix B.

The emissivity of the carbon-coated heat-flux gage was not measured, and for the purposes of this study, it was assumed that the surface was a true black-body.

Figure 6 shows oscillographs for a shock-tube run with the blackened heat-flux gage as the source. The output from the IR detector is the gross output which includes the contribution from the source, dust particles in the convective gas, and the IR window. The temperature-time trace for the heat-flux gage (Figure 6a) is the temperature at the surface of the Pyrex which is overcoated with silicon monoxide and carbon. This temperature is smaller than the temperature seen by the detector by an amount equal to the temperature drop through the overcoating. The procedure used for calculating the temperature at the carbon surface from that measured at the Pyrex surface is described in Appendix C.

The oscillograph of Figure 6b shows a pressure-time trace measured with a Kistler, Model 601, pressure pickup. The pressure gage was mounted in the wall of the shock tube upstream of the test section (see Figure 1).

As mentioned earlier, mixing of driver gas with the shock-heated gas terminates the test before the reflected rarefaction wave arrives at the test section for some shock-tube runs. In Figure 6, both the IR detector and heat-flux gage output show a decrease in the rate of heat transfer about 10 milliseconds before the rarefaction wave reaches the test section. The useful test period for the data shown in Figure 6 is about 21 milliseconds.

From oscillographs of the kind shown in Figure 6, a relationship was obtained between the net infrared-detector output (IRDO) in millivolts and the surface temperature (ΔT_s) for the blackened heat-flux gage. Data showing this relationship are graphed in Figure 7. The data of Figure 7 represent ten different shock-tube tests in which the temperature of the shock-heated gas (nitrogen) was varied over the range of about 700 to 1500°K. The corresponding variation in mean heat flux to the blackened gage ranged from about 30 to 80 cal/(cm^2)(sec). All of the runs were made with the same flow-control orifice (No. 3A) downstream of the test position. Data used in the preparation of Figure 7 are given in Table 2C.

Based on the calibration data provided by the Philco Corporation for the GPC-201A detector, an output of 100 millivolts for a bias current of 80 microamperes represents about 1500 microwatts/(cm^2) of radiation incident on the cell. For the optics used in the detection system in this apparatus, an IRDO of 100 millivolts is equivalent to a black-body temperature of about 280°C (a ΔT_s of 250°C). Operation of the IR detector above the upper linear response limit of about 1000 microwatts/(cm^2) reported by Philco is not a problem if the detector is calibrated. Even though the response may not be linear for incident radiation above 1000 microwatts/(cm^2), the detector, based on our observations, could be used for measuring radiation of much higher intensity. It appears to be almost impossible to saturate the GPC-201A by massive overloading for short-time intervals. In some experiments on propellant ignition, IR detector outputs as large as 3 volts were observed during steady burning of blackened propellants. In the work described here, a screen was placed between the source and the IR detector to utilize better the linear response region for the detector. Some compromise was required in this respect because of the shock-sensitivity of the detector.

B. DATA ON BACKGROUND RADIATION

In this report, "background radiation" is the radiant flux incident on the IR detector cell that does not originate at the main IR source; in particular, radiation emitted by hot dust particles in the convective gas and radiation emitted from the infrared window in the wall of the test section. The surface of the IR window at the wall undergoes convective heating with the main source. As the thermal responsivity of the window is relatively large and the emissivity of the window material is small, the contribution from this source is small. Data on the magnitude of this background radiation were obtained by making tests with a polished brass plug as the source in place of the blackened heat flux gage. Data obtained from these tests were used for adjusting the gross IR-detector output for runs with the heat-flux gage and propellants. The oscillographs of

IR detector output shown in Figure 8 were obtained from runs with the brass plug as the main IR source. The cyclic fluctuations on the two traces represent the sensitivity of the IR detector to shock-tube vibrations. Since the magnitude of the fluctuations was approximately the same for all runs, the effect was only troublesome for measurements of radiant fluxes from low intensity sources.

The IR detector output for background radiation was found to be a function only of the Mach number of the incident shock wave and time measured from the passage of the incident shock through the test section. Data in the form of IRDO versus Mach number at the end of the driven section (M_E) for ten milliseconds after passage of the incident shock are graphed in Figure 9. Also, data on background radiation derived from runs with carbon-coated heat-flux gage are included in Figure 9. (The data obtained from runs with the brass plug were used for adjusting the gross IRDO obtained with the heat-flux gage as the source; in turn, the normalized curve of IRDO versus temperature for the heat-flux gage, Figure 7, was used to obtain additional data on background radiation.)

The scatter among the data given in Figure 9 appears to be related to variations in the concentration of dust in the test gas. Even though the shock tube was thoroughly cleaned and clean nitrogen was used for tests, it appears that some dust entered the shock tube each time it was opened for replacing diaphragms. Data obtained indicates that dust particles suspended in the test gas are the largest source of background radiation. Differences in background radiation for different runs, as shown in Figure 9, produced some scatter in IR-detector output data obtained from runs on propellants, particularly for the first few milliseconds of the heating period when surface temperatures were low.

IV. SURFACE-TEMPERATURE MEASUREMENTS ON PROPELLANTS

One of the problems that is encountered in the use of infrared detectors for surface temperature measurements ia that of determining the effective emissivity of the propellant surface. Ammonium perchlorate has a rather high transmissivity to radiation at some wave lengths in the infrared spectrum, and some radiation emitted by a heated sample of AP comes from below the aurface. For rapid transient heating of a propellant surface, some of the radiation received by the detector is emitted below the surface where the temperature is lower than that at the surface. For material with spectrally dependent emissivity, the effective emissivity for the material could be a function of the heating rate of the surface.

There are several ways to attack the problem. One approach is to measure radiation emitted by the propellant surface at selected wave lengths of high surface emissivity. This was the procedure employed by Powling and Smith [2, 3, 4] for measuring surface temperatures on burning solid propellanta. Another approach is to eliminate the problem, if possible, by blackening the propellant composition through the addition of carbon to the propellant or by coating the propellant surface with a thin layer of carbon or other suitable blackening material. For a propellant containing carbon and very fine ammonium perchlorate, e.g., one-micron AP particles, the surface properties of the propellant would be expected to reaemble cloaely those of a black-body surface.

For the study described in this report, total radiation emitted by the propellant surface during transient heating waa meaaured over the spectrum of about one to ten microns. Measurements were made on conventional propellants, blackened propellants, and propellant samples coated with carbon.

A. PROPELLANTS

Experimental data using the IR detector were obtained on several propellants and propellant ingredients as samples of these materials

were subjected to convective heating in the shock tube. Data on propellant compositions are given in Table 3 and the thermophysical properties of propellants and ingredients are listed in Table 4.

Samples of cast propellants were prepared by casting freshly mixed propellant into the cylindrical cup of the sample holder (see Figure 2). The cup was overfilled so that a fresh, smooth surface could be cut immediately before a test. A new single-edged razor blade was used for cutting away the excess propellant and for providing a smooth surface flush with the lip of the sample holder.

Samples of pressed propellants were prepared by bonding cylindrical pellets, with diameters slightly smaller than that of the cup, into the sample holder. Either an epoxy bonding agent or Fleck's (ceramic blend) inorganic cement were used for bonding pellets in the sample holder. For pellets of pressed propellant or pressed AP, that portion of the pellet and bonding material extending above the lip of the sample holder was removed by sanding with 600-A grit silicon carbide paper.

B. MEASUREMENTS ON CAST PROPELLANTS

1. Propellant UA

Oscillographs of infrared detector output as a function of time for cast propellant UA are shown in Figure 10. Propellant UA is a conventional cast propellant containing only PBAA binder, 15-micron AP, and copper-chromite catalyst (see Table 3A). For the oscillographs of Figure 10a, the oscilloscope sensitivity was increased to expand the first 16 milliseconds of the test that corresponds to heating of the propellant surface primarily by external heating by the hot, convective gas (nitrogen). Figure 10b shows data for the same run for a longer time interval and lower oscilloscope sensitivity.

For the trace shown in Figure 10a, the initial fast rise was produced by radiation from carbon particles in the test section. Carbon particles deposited on the walls of the flow-channel were loosened by the passage of the incident shock wave and were carried from the test section in the first one or two milliseconds of the test. Since it was not practical to clean

the test section after each run, some carbon remained on the flow-channel walls deposited as ignited propellant burned away.

In earlier work at this laboratory [5, 6, 7, 10], photocells sensitive to radiation at wave lengths close to the visible range of the spectrum were used for detecting propellant ignition. In these earlier studies, and also in this study, the experimental criterion for ignition was the same. Ignition time, t_i, is defined in our work as the time interval starting with the first application of external heat to the propellant and ending with the appearance of a flame at the propellant surface. Experimentally, ignition time is determined from a recording of the output signal from a radiation detector monitoring the propellant surface. The experimental criterion for ignition is the time from the start of heating at which the signal from the detector rises very rapidly with time. For the detector output versus time trace shown in Figure 10a, this criterion for ignition is indicated by the arrow. For this particular test, the ignition time was about 15.5 milliseconds.

As would be expected, the surface emisaivity of conventional composite propellants containing AP, such as Propellant UA, is not as large as that for a black surface, and, furthermore, the emissivity is spectrally dependent. Consequently, temperature histories for samples of Propellant UA could not be derived directly from data for the blackened heat-flux gage used for calibrating the IR-radiation detection system. For Propellant UA, IR-detector output data were compared directly with calculated temperature-time data for linear heating of the propellant samples for surface temperatures (ΔT_s) up to about 400°C, and the IRDO data were then extrapolated to higher temperatures. (We use the term "linear heating" to describe the process in which the temperature rise at the propellant, assumed to be inert for this calculation, is produced by externally applied heat flux only.) Net IR-detector output versus calculated surface temperature (ΔT_s) for four tests on Propellant UA with nitrogen as the test gas, are graphed in Figure 11. Each data point represents a specific time in the total test period.

Temperature-time data for linear heating were calculated with Equation (1), using experimental heat-transfer data. An experimental study (see Appendix A) of heat transfer in the shock-tube test section showed that the temperature rise at the wall could be represented with good precision by Equation (1). Equation (1) defines the surface temperature of a semi-

infinite solid subjected to transient heating from a high temperature gas (T_g) through a constant wall heat transfer coefficient. In making this calculation for each run, it was assumed: (1) that the temperature was uniform over the propellant surface and that the thermal responsivity of the bulk propellant represented the properties of the surface; (2) that the thermal responsivity of the propellant was not temperature dependent and values determined experimentally or estimated for a temperature of 60°C were used, (3) the latent heat for the crystalline phase transition of AP could be neglected in surface temperature calculations; and (4) that during the greater part of the heating period, until the temperature of the surface had reached about 400°C above room temperature, the temperature rise at the surface was produced only by externally applied heat flux. A discussion of these assumptions follows.

The first assumption about a uniform temperature distribution over the propellant surface is a reasonable one. Propellant UA was prepared with AP having a weight-average particle size of 15 microns (many of the AP particles had diameters of less than one micron). Bouck [11] has numerically solved the heat conduction equation for heating of a heterogeneous propellant composed of alternate slabs of AP and PBAA binder. The results of that study for a propellant composed of slabs of AP, 45 microns wide, alternated with slabs of PBAA binder, 5 microns wide, for an applied heat flux to the surface of 60 cal/(cm^2)(sec), showed a maximum temperature difference of about 35°C between the center of a slab of AP and a slab of PBAA binder. The results of Bouck's study also indicate that the interface temperature between the binder and AP, perhaps the most meaningful temperature with respect to ignition, is a good approximation to the surface temperature calculated using bulk thermophysical properties. Experimentally, in this work, the infrared detector cell receives radiation from area of about 4 square millimeters on the propellant surface, and thus, effectively measures a mean surface temperature over this area.

The second assumption about temperature independent thermophysical properties for the propellant is less tenable. We do not have sufficient information on propellant thermophysical properties to include their temperature dependence in surface-temperature calculations. The most complete

set of data on thermal diffusivity of propellant ingredients is that for pure AP determined experimentally by Rosser, Inami and Wise [12] over the temperature range of 50 to 240°C. The results of the study by Rosser *et al.*, are given in Table 4. These data, when anaylzed with respect to temperature dependence of thermal responsivity, $\Gamma(T)$, show that Γ varies less than 3 percent, relative to data at 50°C, over the range of 50 to 240°C. Our experience indicates that a variation of 3 percent will give essentially the same variation in calculated surface temperatures.

With regard to the latent heat of phase change for AP, the effect is small. We do not have information on the kinetics of this phase transition, but one might expect that the transition is sufficiently slow so that the endothermic process occurs over a rather wide temperature range for rapid heating of the propellant surface.

On the last assumption used, we have found in our experimental work on propellant samples with smooth surfaces that the surface temperature rise up to about 400°C is of the form that would be expected for linear heating. For different test conditions the results could be different. The test conditions used in this work were convective heating of propellant samples with air or nitrogen at externally applied heat fluxes of about 30 to 80 cal/(cm^2 (sec). For samples with rough surfaces, the results are different and this assumption is not valid.

As already mentioned, data for samples of Propellant UA with smooth surfaces are plotted in the form of net IRDO (mv) versus ΔT_s(°C) in Figure 11, and are compared with the data obtained with the carbon-coated heat-flux gage. Heat tranafer data used for calculating temperature-time data for these runs are given in Table 5A. Also, listed in Table 5A is an approximate mean heat flux for each run. Values of ΔT_s^L (calculated for linear heating) and net IR detector output are tabulated as a function of time for each run in Table 6A. The data graphed in Figure 11 are for values of ΔT_s^L up to about 400°C, the temperature range over which propellant reactions do not appear to contribute energy for heating the surface.

Ignition occurred during Run Nos. 611-6-21 and -22 which were tests conducted at higher heat fluxes. (Oscillographs for Run No. 611-6-21 are shown in Figure 10.) The same sample with a smooth, cut surface was used

for Run Nos. 611-6-20 and -21. The sample used in Run 611-6-22 had a polymer-rich surface of the kind that forms on an exposed surface of propellant during the curing process.

The good correlation of data in the form net IRDO versus ΔT_s for Propellant UA in Figure 11 indicates that the method used for calculating surface temperatures is consistent and that the experimental heat transfer data represent rather well the heat transfer process in the test section. This good agreement also suggests that the sample surfaces were uniform and each sample had nearly the same surface emissivity. Scatter among data points is more apparent at lower temperatures (lower values of IRDO) which correspond to the initial part of the heating process for each run. These are conditions for which variations in background radiation (primarily radiation from dust particles in the test gas) are a larger fraction of the total IR-detector output.

The displacement of the data for propellant UA above the data for the carbon-coated heat-flux gage is a measure of the difference in emissivity for the two surfaces. These data indicate the apparent emissivity of the propellant surface is about 35 percent of that for the heat-flux gage, which is assumed to be an opaque, black surface. Other factors that could affect the displacement of the two sets of data are: (1) differences between the actual and calculated temperature histories for the propellant surface (for calculations, it was assumed that the thermophysical properties of the propellant were not temperature dependent), and (2) non-linear response of the IR detector to incident radiant flux (this particular property of the detector was not evaluated and the information would not be useful unless the spectral emissivity of the propellant surface were known).

The different slope for the set of data on Propellant UA relative to that observed for the heat-flux gage could be caused by the following factors: (1) variation of propellant thermophysical properties with temperature, (2) changes in the spectral emissivity and total emissivity of the propellant surface with temperature and heating rate (the heating rate is slightly lower at higher surface temperatures); and (3) exothermic reactions

at the propellant surface at the higher temperatures resulting in a faster temperature rise than that predicted for linear heating.

The data graphed in Figure 11 were extrapolated above 400°C and the result was used for estimating surface temperature from IR-detector output in the higher temperature region. Surface temperature data derived in this way for samples that ignited are listed with calculated temperatures and IR-detector data in Table 6. The surface temperature history, for Run No. 611-6-21, a sample that ignited (oscillographs for this run are shown in Figure 10), is shown in Figure 12. The ignition time, t_i, for this run waa about 15.5 milliseconds. The measured surface temperature departs from the linear heating curve about 11 milliseconds after heating started (at a ΔT_s of about 385°C). The actual ignition temperature (the portion of the curve where temperature begins to change rspidly with time) is about 460°C (730°K). This corresponds to an ignition temperature for linear heating, T_{si}^{L}, of about 430°C. After the sharp break in the curve of figure 12, the IR detector output may no longer represent the true temperature of the surfsce, for as soon as exothermic gaa-phase reactions become important, some radiation incident on the detector is emitted by hot combustion products.

2. Blackened Propellants

Propellanta AR snd AQ blackened by the addition of fine-particle carbon (Philblack E) were used in part of this study. Like Propellant UA, the blackened propellants were made with 15-micron AP to facilitate the preparation of smooth surfaces on samples. Propellant AR and AQ contained 70 and 65 percent of 15-micron AP, respectively, and 3 percent of Philblack E. The powdered ingredients used in the two propellants (see Table 3) were thoroughly blended by passing them through a 270-mesh screen three times. This procedure was used in attempt to coat the individual AP particles with carbon.

Propellant AR

Samplea with Smooth Surfaces: Data for samples of Propellant AR with smooth surfacea in the form of IR-detector output versus calculated surface temperature for linear heating (the same analysis procedure used for Propellant UA) are graphed in Figure 13. These data are grouped closer to the data for the blackened heat-flux gage than were the data for Propellant UA (Figure 11). The apparent mean surface emisaivity for Propellant AR, compared with that for the heat-flux gage, is about 0.6.

The data for individual tests on Propellant AR show about the same amount of scatter as that for Propellant UA; however, the data for all tests fall in a wider band. Differences between individual tests are probably produced by two main factors: (1) heterogeneities at the surface that alter the emissivity, and (2) variations in the predicted heat transfer. In general, auccesaive testa on the same sample, tests at heat fluxes too low to produce ignition, were reasonably consistent.

Samples with Blackened Surfaces: As a means of increasing the surface emissivity of Propellant AR, a few samples with smooth aurfaces were coated with a thin layer of Thilblack E. The thickness of the carbon layer waa not meaaured, but it was estimated to be of the order of two to five microns thick. The carbon layer would affect the heating of the sample in that there would be a temperature drop of 5 to 15°C through the carbon layer. The heating process is still closely approximated by equations that describe the heating of a aemi-infinite solid with the properties of the propellant.

Dats for the carbon-coated samples are graphed in Figure 14. These data are grouped near the curve that represents the data for the carbon-coated heat-flux gage. The maximum deviation of data for samples of Propellant AR from the curve for the heat-flux gage is about 25°C. The results of this study on samples with artificially blackened surfaces indicate that surface-temperature histories calculated sssuming linear heating and constant thermophysical properties for the propellant (temperature independent) closely approximate the actual heating procesa, as long as ignition temperstures are not too closely approached.

Samples with Rough Surfaces: Surfaces on samples of Propellant AR were roughened by sanding a small area near the center of a smooth, cut surface with 320 grit-size paper. Since the sanding process changes the surface features of the sample, particularly with respect to blackness, carbon was dusted on the sanded area and the excess along with loose particles of propellant was brushed off. For this part of the study, it was assumed that the emissivity of the rough surface prepared in this way was about the same as that for a smooth, uncoated surface. This approximation could introduce errors as large as 30°C in the derived temperature-time data for an individual test. The mean surface roughness on samples prepared in this way is estimated to be about 20 microns.

Figures 15 and 16 are oscillographs of IR-detector output as a function of time for runs on samples of Propellant AR with smooth and rough surfaces, respectively. The oscilloscope trace for the sample with the rough surfaces, Figure 16, shows several small fluctuations in the detector output, features that are not present on the trace for the smooth aample. Both of the samples ignited during the tests. The post-ignition rise of IR-detector output for the smooth-surfaced sample (Figure 15b) was more rapid than that for the rough-surfaced sample (Figure 16b). This result indicates that the sample with the rough surface ignited locally only over the roughened area, while the entire surface of the amooth sample ignited almost instantaneously. High-speed motion pictures of ignition for samples with rough and smooth surfaces have generally confirmed this observation. Since radiation from hot combustion products produced upstream of the detector field of view contribute to the total flux incident on the detector, the output is greater if the entire surface ignites.

Data for the IR detector output obtained from the oscillographs of Figure 16 were converted to temperature-time data using the IRDO-ΔT_s curve for Propellant AR in Figure 13. Data for Run No. 611-6-25 are given in Table 6b. These data are graphed in Figure 17 along with the predicted temperature-time data calculated for linear heating using experimental heat transfer data. Figure 17 shows that the surface temperature of the rough-surfaced sample prior to ignition increased considerably faster than that predicted for linear heating of a smooth-surfaced sample, and ignition occurred in a shorter time than that expected for a sample with a smooth

surface. It is interesting to note that the measured surface temperature at the time ignition occurred is about the same as that for smooth-surfaced samples for an equivalent externally applied heat flux. For smooth-surfaced samples, the measured ignition temperatures, ΔT_{si}, were between 450 and 520°C. The data for Run No. 611-6-25 are in reasonable agreement with data on other samples with rough surfaces. For example, see data for Run Nos. 611-7-7, 611-7-9, and 611-8-1 tabulated in Table 6b.

The data for the sample with the rough surface, shown in Figure 17, indicates that the faster temperature rise observed for this sample is primarily the result of increased heat transfer to the propellant surface. The temperature history for the sample with the rough surface (Figure 17) is somewhat different than that for convective heating of a semi-infinite solid through a constant heat-transfer coefficient. It is to be expected that the form of the measured temperature-time relationship for heating of a rough-surfaced sample of propellant will be different for different samples and will be dependent on the magnitude of the surface roughness for a given set of test conditions.

We know from earlier studies on ignition by convective heating (6, 7) that factors other than heat transfer are important in the ignition of samples with rough surfaces. We found in earlier work that as the gas velocity across the sample was increased, for a given externally applied heat flux based on measurements for a smooth surface, that ignition times also increased. This result suggested that the ignition process for propellants with rough surfaces, particularly the rate of temperature rise at the surface, was affected by a combination of processes, a higher heat transfer rate and secondary ignition reactions at the surface.

In the work described in this report, surface temperatures were measured at one test-gas velocity, about 100 m/(sec). Data are needed over a wider range of gas velocities for comparison with our earlier results.

One can only speculate about the small fluctuations observed on IR-detector traces for the rough-surfaced sample (Figure 16). For the test section used in this study, the test position is very near the leading edge for boundary layer development. Since the flow in the channel is turbulent, the viscous sublayer at the test position is very thin. It is possible that the small fluctuations observed on the IR-detector output trace represent

radiation from protrusions at the roughened surface that extend into the turbulent zone. On the other hand, these fluctuations could indicate initiation and quenching of localized reactions at the propellant surface, particularly near hot spots on the surface produced by two-dimensional heating of protrusions and sharp corners on AP crystals. The IR detector as used in this work cannot distinguish between the two processes and some form of high-speed IR spectroscopy would be required to probe for the presence of chemical reactions.

Propellant AQ

Propellant AQ was prepared with the same ingredients as Propellant AR, but had a lower concentration of AP (65 percent of 15-micron AP versus 70 percent for Propellant AR).

In general, IR-detector data for runs with Propellant AQ were the same as those observed on Propellant AR. Data in the form of net IRDO versus ΔT_s for smooth-surfaced samples are graphed in Figure 18. This set of data is reasonably consistent, but the data are oriented differently relative to the data for the blackened heat-flux gage than those for Propellant AR. The lower slope for Propellant AQ could indicate a higher temperature dependence for thermal properties for this propellant or a different surface emissivity than that for Propellant AR.

C. MEASUREMENTS ON PRESSED PROPELLANTS

Pressed propellants are of interest for ignition studies in that they can be made from a variety of solid materials with a wide range of fuel-to-oxidizer ratios. Furthermore, it is not too difficult to incorporate a rather large concentration of carbon in pressed propellants. Data on propellant compositions and thermophysical properties are given in Tables 3 and 4, respectively. Heat transfer data are given in Table 5 and experimental data on surface-temperature measurements are tabulated in Table 6.

1. Pressed Propellant PP-CBM

Pressed Propellant PP-CBM contained 16 percent Philblack E, 2 percent copper chromite, and 80 percent, 15 micron, AP. Two kinds of samples were

used for surface temperature measurements, regular samples with smooth surfaces and samples coated with a thin layer of Philblack E.

Oscillographs of IR detector output versus time had about the same form as those for cast propellants. Data for regular samples of Propellant PP-CBM are plotted in the form of net IRDO versus calculated surface temperature, ΔT_s, in Figure 19. The data for Propellant PP-CBM lie above the curve for the carbon-coated heat-flux gage with about the same displacement as that for samples of cast Propellant AR with smooth surfaces.

Data for two runs on samples coated with Philblack E are shown in Figure 20. This was the first set of data on propellant that was found to lie below the line that describes the data for the carbon-coated gage. The curve representing these data has about the same slope as that for the regular samples, and for lower temperatures, is steeper than that for the blackened gage.

There may be more than one reason for the data points on coated samples of Propellant PP-CBM to lie below the curve for the blackened heat-flux gage. It appears, however, that the larger values of IR-detector output for lower surface temperatures are produced by loose particles of carbon on the surface. The start of heating in the shock tube begins when the incident shock wave reaches the end of the tube. It is suspected that carbon particles at the surface of the pellet are loosened by the shock wave and are then swept from the surface by the convective gas. A small concentration of carbon particles in the hot test gas would be sufficient to provide the additional radiant flux that was observed. (Pressed propellants with smaller concentration of carbon did not show this type of behavior.) At higher temperatures, near the end of the test period, the data for the carbon-coated samples of Pressed Propellant PP-CBM are in excellent agreement with the data for the blackened heat-flux gage. The fact that reasonable agreement is found between coated samples of Propellant PP-CBM and the blackened heat-flux gage again indicates that the assumption of constant properties used for calculating surface temperatures is a reasonable assumption.

2. Other Pressed Propellants and Pressed Ammonium Perchlorate

IR-detector measurements were made on two other pressed propellants containing the following ingredients: Propellant PP-E with 4.5 percent Sterling VR carbon, 2.5 percent copper chromite, and 93.0 percent AP; and Propellant PP-F with 5.0 percent copper chromite and 95.0 percent AP. Since the concentration of ingredients other than AP was small, the thermal properties of these propellants would almost be identical and the properties would be similar to those for pressed ammonium perchlorate. Data on these samples should give an excellent approximation of the effect of added carbon on surface emissivity.

Data for Propellants PP-E and PP-F in the form of net IRDO versus calculated surface temperatures, ΔT_s, are graphed in Figure 21. Both sets of data lie above that for the carbon-coated heat-flux gage, and the curves through the two sets of data are almost parallel with the curve for the carbon-coated gage.

Oscillographs of IR-detector output for the two runs, one for Propellant PP-E and one for Propellant PP-F, in which ignition occurred, are shown in Figure 22a and 22b, respectively. The oscillograph traces are very similar to those observed on cast propellants shown in Figures 10, 15 and 16. The rate of change of detector output with time is smaller for these propellants but this would be expected since the fuel level is much lower in the pressed propellants. As the oscillographs show, both samples were extinguished before burn-out.

In tests on samples of pressed AP, no indication of ignition was observed even at higher heat fluxes, at conditions which were sufficiently severe to ignite all other propellants tested.

The data for three runs on pressed AP are graphed in Figure 23. It is interesting to note that the net IRDO versus ΔT_s graph for pressed AP is almost identical to that for Pressed Propellant PP-F containing 5 percent copper chromite. This result shows that copper chromite does not appreciably improve the surface emissivity of propellants. The data for pressed AP are also very similar to those for cast Propellant UA (compare Figures 11 and 23). Apparently, the emissivity of conventional propellants is approximately that for pure AP.

D. MEASUREMENTS ON DOUBLE-BASE PROPELLANT JPN

It had been observed from some earlier studies on the ignition of JPN propellant that under some test conditions JPN propellant exhibited rather unusual ignition characteristics. The output from a photocell sensitive to radiation of about 0.8 microns showed that samples of JPN ignited and extinguished several times during ignition tests by convective heating. The oscillograph of Figure 24 (Run No. 69-21-12) is the IR-detector output for a test on JPN propellant that exhibited this behavior.

Net IRDO versus ΔT_s data for Propellant JPN are plotted in Figure 25. Surface temperature data on JPN propellant show that this propellant ignites when the surface temperature reachea a value of about 330°C, in contrast to 450 to 520°C for AP composite propellants at similar test conditions.

E. MEASUREMENTS ON PROPELLANT BINDERS

Samples of polyurethane and polybutadiene-acrylic acid copolymer (PBAA) binders containing Philblack E were made for surface-temperature measurements during convective heating in the shock tube. The reason for conducting these experiments was to determine if the oxygen in air reacts with the polymer surface at temperatures encountered during ignition. In most of the tests, the final surface temperatures for the binder samples were much higher than ignition temperatures of composite AP propellants.

Data on net IR-detector output versus calculated surface temperature (ΔT_s) for samples of PBAA and polyurethane binder for tests conducted in air and nitrogen are graphed in Figures 26 and 27, respectively. For both kinds of binder, oscillographs of IR-detector output versus time for tests in air and nitrogen are very nearly the same. This suggests that for the conditions of the experiment there were no significant reactions between air and the binder samples. The blackened PBAA binder based on these data appears to have a much lower surface emissivity than the blackened polyurethane binder. The same thermophysical properties were assumed for both kinds of binder and were based on values obtained experimentally for PBAA binder at 60°C. If the properties of the two binders were significantly different, and have a different temperature dependence, the calculated temperatures could be wrong. It appears, based on microscopic examination

of the two binders, that the carbon was dispersed more uniformly in the polyurethane binder. In the PBAA binder, even though the same processing procedures were used, the carbon particles were agglomerated to some extent, indicating that the PBAA polymer does not wet the carbon particles as well as the polyurethane polymer. It is possible that this observed difference in the two systems could make a significant difference in surface emissivity.

The fact that data for the carbon-coated sample of PBAA binder (Figure 26) is also displaced above the data for the carbon-coated heat flux gage probably means that the sample surface was not uniformly coated.

Even though calculated surface temperatures for samples of binder showed temperatures at the surface as high as 600°C for some tests, the IR-detector data were of the form expected for linear heating of the sample. There were no sharp discontinuities or other trends that would indicate the polymer was decomposing or vaporizing. It was observed, however, for some tests with the polyurethane binder for high temperature runs that some polymer flowed over the edge of the sample holder indicating a decrease in viscosity of the polymer at higher temperatures. This could also mean that some depolymerization of the polyurethane polymer occurred during heating.

V. PROPELLANT IGNITION

A. IGNITION THEORY

In earlier studies [6, 7] on ignition of composite AP propellants by convective heating, we have shown that experimental ignition data are in good agreement with that predicted by thermal ignition theory. The thermal theory of propellant ignition predicts that experimental data plotted in the form of heat flux at the propellant surface during the ignition test versus the square root of ignition time should be represented by a straight line on logarithmic-coordinate paper. Furthermore, theory predicts that the slope of the line that represents the data plotted in this form is related to the activation energy of the key ignition reaction.

The thermal theory of ignition suggested by Baer [10] which assumes that the key ignition reaction is a surface reaction was found to give the best agreement between theory and experiment. The partial differential equation which describes the ignition process is:

$$\rho c \frac{\partial T}{\partial t} = k \frac{\partial^2 T}{\partial x^2} \tag{3}$$

at $x = 0$,

$$F_T = -k(\partial T/\partial x) = F_s + be^{-E_a/RT}$$

at $x = +\infty$,

$$T(t) = T_o, \text{ all } t$$

at $t = 0$

$$T(x) = T_o, \text{ all } x$$

From numerical solutions to Equation (3) for various related parameters characteristic of propellants, it was shown that ignition times for propellants that ignite thermally can be expressed with a good approximation by:

$$(t_i)^{1/2} = \frac{\Gamma_p (\pi)^{1/2}}{2F_s} \left[\frac{E_a/R}{1 - 1.04 \ln (F_s/b)} - T_o \right] \qquad (4)$$

Where E_a is the activation energy for the key ignition reaction and is related to the slope of the line that represents ignition data plotted in the form of $\ln(F_s)$ versus $\ln(t_i)^{1/2}$ by the following equation:

$$S = 4.2 \frac{RT_0}{E_a} - 1 \qquad (5)$$

In an earlier study [6, 7] on ignition by convective heating and in this work, it was found that ignition times for propellants with smooth surfaces are not appreciably affected by environmental factors, such as oxygen in the test gas, gas temperature, and gas velocity, and data are well represented by Equation (4). From the earlier studies, it was found that a line with a slope of -0.92 represents the data for composite AP propellants. This value for the slope used in conjunction with a T_o of about 300°K gives an activation energy, E_a/R, of about 15,500°K.

B. EXPERIMENTAL DATA

Data for propellant samples that ignited during tests in this study were evaluated to give a set of data in the form of $\ln(\overline{F}_s)$ versus $\ln(t_i)^{1/2}$. Shock-tube, heat-transfer, and ignition data for propellants are given in Table 7. Most of the data were obtained from tests in which the propellant surface-temperature history was also measured. Included with these data are some ignition results on Propellant UA obtained with an RCA 1P40 gas photodiode having maximum sensitivity to radiation at a wave length of about 0.8 microns. In all experiments, as already indicated, ignition time was the time in heating process that the output signal from the detector monitoring the propellant surface began to increase rapidly with time.

A special circuit for differentiating the output signal was used with the RCA 1P40 photocell to increase measurement precision.

Data for Propellant UA from this study and from an earlier one are plotted in the form of $\ln(\overline{F}_s)$ versus $\ln(t_i)^{1/2}$ in Figure 28. The three data points for ignition as observed with the GPC-201A IR detector are in good agreement with results obtained with the RCA 1P40 photocell. The data of Figure 28 are for three different flow-control orifices and thus, represent tests at different gas velocities across the propellant surface. The range of velocities is from about 50 to 110 m/(sec). Since the surfaces on these samples were smooth, there is no observable effect of gas velocity on ignition time. These data represent what we have called "simple thermal ignition" of Propellant UA and the ignition time to a very good approximation is defined by Equation (4).

The line through the data has a slope of -0.92 and corresponds to an activation energy, E_a/R, of about 15,500°K. Using this value for the activation energy, the pre-exponential factor, b, which appears in Equations (3) and (4) has a value of approximately 2.35×10^{10} cal/(cm^2)(sec) for Propellant UA. Ignition time for Propellant UA can also be represented by the equation for the straight line that defines the data. In this form, the ignition time for Propellant UA as a function of externally applied heat flux is

$$t_i(\text{sec}) = 28.9/(\overline{F}_s)^{1.84} \qquad (6)$$

where $\overline{F}_s$ has the units of cal/(cm^2)(sec).

Ignition data for cast Propellants AR and AQ, obtained with GPC-201A IR detector, are plotted in Figure 29. The straight line on this graph is the one for Propellant UA shown in Figure 28.

The results on the three cast propellants are in good agreement with those obtained on smooth-surfaced propellants in earlier work [6, 7].

Data on ignition of pressed propellants are also given in Table 7. Ignition data for Propellant PP-CBM, the one with 16 percent carbon, show considerable scatter and were not graphed. Ignition data were obtained in only one test on each of the Pressed Propellants PP-E and PP-F. We have

found that ignition data on pressed propellants are usually more scattered than data for smooth-surfaced, cast propellants. Even though samples are carefully prepared, ignition, as observed by high-speed photography, is quite frequently initiated at the interface between the bonding agent and the pellet. Also, we have observed on some samples, recovered from tests in which ignition had not occurred, that small surface cracks had developed. If the small cracks formed during heating rather than cooling, they could significantly alter the ignition characterstics of ths sample.

C. IGNITION THEORY AND SURFACE-TEMPERATURE MEASUREMENTS

For the purpose of comparing measured surface-temperature histories with those predicted by thermal ignition theory, temperature-time data were calculated for a few runs on cast Propellants AR and UA, using the equations that describe thermal ignition with the key ignition reaction localized at the propellant surface. For heating of a semi-infinite slab of homogeneous propellant convectively from a high-temperature gas, T_g, through a constant, surface hest-transfer coefficient, h, the following equation applies:

$$\rho c \frac{\partial T}{\partial t} = k \frac{\partial^2 T}{\partial x^2} \tag{7}$$

at $x = 0$, $F_T = -k \left(\frac{\partial T}{\partial x}\right) = h(T_g - T_o) + be^{-E_a/RT}$

at $x = +\infty$, $T(t) = T_o$, all t

at $t = 0$, $T(x) = T_o$, all x

Based on our experience with ignition of propellants in the shock tube, one would not expect complete agreement between calculated and experimental results. One reason is that it is not possible to predict precisely the heat transfer to a propellant sample. It is estimated that heat transfer to the surface, based on experimental measurements, can be predicted with an average deviation of about 5 percent. For some individual tests, the predicted heat transfer could be in error by 10 percent. All calculated temperature-time data are based on experimental heat transfer data obtained in a separate study (see Appendix A). (Heat transfer to

some of the propellant samples could be slightly higher than expected, since sample surfaces are a little rougher than the surfaces on heat flux gagea used for measuring heat transfer.) Another reason for expecting differences between experimental and calculated results is that the entire propellant surface does not always ignite simultaneously. High-speed photography of ignition runs has shown that, depending on surface characteristics of the sample and teat conditions, ignition is initiated either upstream or downstream of the detector field of view. At very high heat fluxes, ssy 60 to 100 cal/(cm^2)(sec), the entire surface ignites almost simultaneously; at lower heat fluxes, when ignition occurs near the end of the test period, ignition is sometimes initiated downstream of the detector field of view and then propagates slowly upstream at sbout the time that cold gases begin to flow through the test-section flow channel. Under these conditions, it could take as long as 20 milliseconds for the flame to spread over the entire surface. Some of these features of the ignition process are visible on oscillographs of IR-detector output.

Temperature-time data were calculated for Run No. 611-6-21 on Propeliant UA, and for Run Nos. 611-6-11, -13, and -14 on Propellant AR. The calculated temperature-time data are tabulated in Table 8A. The various parameters used in the numerical solution of Equation (7) for these runs are given in Table 8B. The value for activation energy, E_a, and the pre-exponential factor, b, were those evaluated from experimental ignition data on Propellant UA. The other parameters were evaluated from initial shock-tube conditions and the experimental dsta on heat transfer.

The temperature-time data for ignition of Propellsnt UA calculated with Equation (7) is graphed with the experimental data in Figure 30 for Run No. 611-6-21. The curve for linear heating of the sample calculated with Equstion (1) for the same test conditions is also included. The observed ignition time for this run was about 15.5 milliseconds and that predicted by theory was about 14.0 milliseconds. The graph of net IRDO versus ΔT_s for Propellant UA in Figure 11 was used to convert measured IR-detector output versus time data to temperature-time data of the kind shown in Figure 30.

Measured and calculated surface-temperature histories for thres runs on samples of Propellant AR in which ignition occurred, Run Nos. 611-6-11, -13 and -14 are graphed in Figures 31, 32 and 33, respectively. The measured data in Figure 31 are in reasonable agreement with the temperature-time data calculated using Equation (7). The experimental data graphed in Figures 32 and 33, although showing the same general form as the calculated data, have different ignition times than those predicted by Equation (7). The experimental temperature-time data for Propellant AR shown in these figures were derived from oscillographs of IR-detector output versus time with aid of Figure 13.

The curves representing the experimental data which are graphed in Figures 30, 31, 32 and 33 have about the same form as those calculated with Equation (7). The form of the curves representing the experimental data, as ignition temperature is approached, would be expected to be somewhat different than that predicted by Equation (7). For calculations made with Equation (7) it is assumed that the entire surface is heated uniformly and that the entire surface is ignited at the same time. Experimentally, we know from viewing high-speed motion pictures of ignition that the entire surface does not always ignite simultaneously. Quite frequently, ignition, the appearance of a flame, is initiated at one or more locations on the surface. Local ignition is followed by a rapid spreading of the flame across the entire surface. The form of the experimentally measured temperature-time curve is thus somewhat dependent on the following physical features of the ignition process: (a) simultaneous ignition over the entire surface, (b) localized ignition upstream of the detector field of view followed by flame spread, and (c) localized ignition downstream of the detector field of view followed by flame spread upstream into the field of view of the detector.

VI. CONCLUSIONS

The results of this study show that the thermal ignition model proposed by Beer and Ryan [10] with the key ignition reaction considered to be localized at the propellant surface closely represents the kind of surface-temperature histories observed experimentally. Data obtained from this study do not provide any new information about the chemistry of the key ignition reaction.

Some of the more specific conclusions arrived at from this work are:

1. Infrared detectors, used as total radiation sensors, can be used for making transient, surface-temperature measurements on solid propellants during ignition tests. After ignition is initiated at the sample surface, the detector no longer gives a reliable reading of the surface temperature because radiation from gas-phase processes and hot combustion products is then the major source of radiant flux.

2. Data on smooth-surfaced samples of AP propellants show, as expected, that the surface of the propellant behaves as a passive solid for the greater portion of the heating process. Only after the temperature of the surface, for propellants used in this study, rises to about 400°C, relative to room temperature, for test conditions employed in this study do reactions involving propellant ingredients become important. Oscillographs of infrared detector output versus time do not reveal an effect of strong endothermic processes at the propellant surface.

3. Data on samples with roughened surfaces indicate that these samples ignite at about the same surface temperature as samples with smooth surfaces for the test conditions of this study. However, the surface temperature rises at a faster rate than that predicted for heating of samples with smooth surfaces. It appears that the faster temperature rise is the result of a higher rate of heat transfer to the surface than that measured at the test position

with a smooth-surfaced heat-flux gage. More data on rough-surfaced samples at different test-gas velocities are needed to substantiate fully this observation. It appeared, based on earlier ignition studies [6, 7], that a combination of factors, higher heat tranafer rates and exothermic aecondary ignition reactions, affected the ignition process for samples with rough surfaces.

4. A comparison of measured and calculated surface-temperatura histories, particularly for samples blackened with carbon, shows that the thermal responsivity, Γ_p, of AP propellants is not a strong function of temperature; and temperature-time data calculated assuming constant properties closely approximates the actual heating proceaa until the sample surface reaches a temperature, ΔT_s, of about 400°C.

APPENDIX A

CONVECTIVE HEAT TRANSFER TO WALL OF TEST-SECTION FLOW CHANNEL

Heat transfer to the wall of the modified test section (see Figure 3) was measured with heat-flux gages. The manufacture and calibration of heat-flux gagea for measuring heat transfer are described in Appendix H of Reference 6. The methods used for analyzing experimental temperature-time data from heat-flux gage measurements are described in Appendix I of Reference 6.

The temperature-time data obtained from heat-flux gages mounted with their faces flush with the flow-channel wall were, as was found in earlier studies [6, 7], well represented by the equation for transient convective heating of a semi-infinite solid through a constant wall heat-transfer coefficient (see page 72 of Reference 13):

$$\frac{T_s - T_o}{T_g - T_o} = [1 - e^{N^2} (\text{erfc } N)] \qquad (A - 1)$$

$$= \frac{h(t)^{1/2}}{\Gamma}$$

Where T_o, T_s and T_g are the initial heat-flux gage temperatures, time-dependent surface temperature, and gas temperature respectively; and Γ is the thermal responsivity for the heat-flux gage (square root of the product of thermal conductivity, density and heat capacity). In this work, T_g is the temperature of the test gas behind the reflected shock wave which has been sdjusted for isentropic compression as the preasure in the driven end of the shock tube increases with time after the passage of the shock wave.

Heat transfer coefficients were obtained from temperature-time data, after adjustments were made for temperature dependent gage properties, by comparing experimental data with Equation (A-1). Most of the data were obtained with heat-flux gages made with substrates of Pyrex 7740, but some data were obtained with gages made with substrates of alumina (Alsimag 614). For the heat transfer study, three different flow-control

orifices, No. 3A, 4A, and 5A, having flow areas of 0.0284, 0.01865 and 0.01441 square inches, respectively, were used for controlling gas flow through the test section. When measuring surface temperatures, only the 3A orifice was used, which provides a mean gas velocity of about 100 m/sec or a flow Mach No. 0.13 in the flow channel. The flow channel has a cross section 0.50 inches wide by 0.25 inches high. The rectangular, sharp-edged orifice at the entrance to the flow channel has a minimum opening of 0.48 inches by 0.10 inches.

Data obtained from this study are tabulated in Table 1, and data for flow-control orifices No. 3A, 4A, and 5A are graphed in the form $\ell n(G)$ versus $\ell n[h/(T_g)^{0.3}]$ in Figures 34, 35, and 36, respectively. This is one of the conventional ways of correlating heat-transfer coefficients for convective, turbulent heat transfer (see Appendix C of Reference 6). The data for the modified test section and different flow-control orifices, as expected, could not be correlated by a single equation. With the sharp-edged orifice upstream, the point of reattachment for separated flow would be at a different location for different flow-control orifices downstream. Wall heat-transfer coefficients for the smaller orifices, No. 5A and No. 4A, were found to be dependent on $(G)^{0.8}$, a value expected for turbulent-flow heat transfer. For the larger orifice, the dependence of h on G was slightly higher. Wall heat-transfer coefficients (with dimensions of cal/[sec][cm^2][°K]) for the three flow-control orifices for heat transfer from high-temperature nitrogen are well represented by the following equations:

Flow-control Orifice No. 3A:

$$h = 2.784 \times 10^{-4}(T_g)^{0.3}(G)^{0.938} \qquad \text{(A-2)}$$

Flow-control Orifice No. 4A:

$$h = 5.30 \times 10^{-4}(T_g)^{0.3}(G)^{0.8} \qquad \text{(A-3)}$$

Flow-control Orifice No. 5A:

$$h = 5.11 \times 10^{-4}(T_g)^{0.3}(G)^{0.8} \qquad \text{(A-4)}$$

Here the mean gas mass velocity, G, has dimensions of g/(sec)(cm^2) and the gas temperature, T_g, is in °K.

Wall heat-transfer coefficients for all flow-control orifices for the regular test section, with the bell-mouthed entrance, were measured in a previous study [6] and were found to be represented by the following equation for heat transfer from high-temperature air or nitrogen:

$$h = 1.435 \times 10^{-4}(T_g)^{0.3}(G)^{0.905} \qquad \text{(A-5)}$$

The mass flow rate, G, used as a correlating parameter for all heat-transfer coefficients is calculated assuming choked flow at the throat of flow-control orifice.

APPENDIX B

PROCEDURE FOR COATING HEAT-FLUX GAGE WITH CARBON

A variation of the procedure deacribed by Camac and Feinberg [8, 9], the thermal decomposition of methyl iodide at a hot surface, waa uaed for depoaiting a thin layer of carbon over the face of a heat-flux gage. The heat-flux gage waa firat coated with a thin layer of ailicon monoxide (leaa than about 0.1 micron thick) to provide electrical inaulation for the platinum resiatance thermometer. The SiO layer waa then overcoated with a layer of carbon about 5 microna thick.

The SiO layer waa applied to the face of the gage uaing a vacuum depoaition method. Here the term "face" refers to the flat end face of a small, solid cylinder of Pyrex 7740 on which the platinum resiatance thermometer had been painted and fired. The Pyrex cylindera (gage elementa) were about 0.40 inchea in diameter, and about one inch in length. For coating, the gage elementa were auapended by wires with their facea about two inchea above a molybdenum boat containing a 50/50 mixture of powdered ailicon metal and silicon dioxide (Cab-O-Sil). To reduce heat loaaea from the ayatem, the molybdenum boat (3 inchea long by 3/4 inch deep by 3/4 inch wide) waa partially embedded in a fire brick, and the entire ayatem waa covered with aluminum foil. A coil made of 25-mil molybdenum wire waa used aa the heating element. The ailicon-ailica mixture waa placed in the molybdenum boat to a level that just covered the entire heating element, about one to two millimetera above the heating coil. The entire proceaa was carried out in a vacuum bell at a presaure of leaa than 10^{-4} torr. An excellent coat of SiO depoaited on the gage face in 30 minutea when the bed temperature waa held at about 1500°C. The gages were wrapped with heavy aluminum foil to prevent deposition of SiO on the walla of the Pyrex cylindera.

For overcoating the SiO layer with carbon, the method deacribed by Camac and Feinberg [8, 9] waa uaed, but waa modified for coating the more maaaive heat-flux gagea. Thia method takea advantage of the apecial propertiea of methyl iodide in that it decompoaea at a hot aurface leaving

a deposit of dense carbon. This method gives excellent deposits on thin discs or sheets of Pyrex or ceramic material, sufficiently thin so that they can be heated uniformly by a platinum foil heating element.

For coating heat-flux gages, the platinum foil heating element (1/2 inch wide by 0.001 inch thick) was suspended above the face of the gage with a gap of about two millimeters between the gege face and the foil when the temperature of the foil was at steady-state conditions. The coating process was conducted in an argon atmosphere at a pressure of 5 to 10 inches of Hg abaolute. After the system was closed and argon admitted, the temperature of the platinum foil was increased until it glowed with a dull red color, a temperature in the range of 800 to 900°C. After about 10 minutes, time for the gage surface to heat up, methyl iodide was slowly bled into the system through a copper tube. The end of the copper tube was placed so that the methyl iodide entering the system was directed at the face of the heat-flux gage. In this way, about two milliliters of liquid methyl iodide were added to the aystem in 10 minutes.

Although good carbon deposits were obtained using this general procedure, no standard operating procedure was found that would always give good deposits. Normally, this procedure was repeated two or three times with variations in platinum foil temperature and/or feed rate of methyl iodide before good deposita were obtained.

APPENDIX C

ANALYSIS OF DATA FOR CARBON-COATED HEAT-FLUX GAGE

Data obtained with carbon-coated heat-flux gage (HFG-23), uaed for calibrating the infrared detector, required careful analysis to ensure that data for the IR detector would be meaningful. This required that the temperature at the surface of the heat-flux gage as a function of time be known quite accurately. Furthermore, it was necessary to know the temperature drop through the carbon layer at the surface so that adjustments could be made for the temperature measured at the Pyrex surface.

The temperature coefficient of resistivity of the thin-film platinum resistsnce thermometer waa carefully measured over the range of 0 to 200°C. The data obtained over this range were extrapolated to 300°C so that experimental temperature-time data, measured at the Pyrex surface, could be adjuated for variations in temperature coefficient of resistivity of platinum film with temperature.

For estimating the effective thermal barrier at the heat-flux gage surface provided by the carbon layer, two different experimental methods were uaed for estimating the properties of the carbon layer. It is well known that the thermal conductivity and density of carbon are atrongly dependent on the deposition proceas used, and, ccnsequently, it is not possible to estimate the properties of a carbon deposit from theoretical considerations alone. The problem was further complicated because the only carbon sample available was that on the gage surface.

It was found, as expected, that temperature data obtained for ahock-tube runs with the blackened heat-flux gage were lower than thoae obtained with an uncoated gage for the same test conditions. By comparing data obtained witn different heat-flux gages, it was possible to ahow that the layer of carbon on the surface of the heat-flux gage was equivalent to a layer of Pyrex about 5 microna thick. In other words, during the transient heating process in the ahock tube, the temperature-time data for the carbon-coated heat-flux gage, measured at the Pyrex surface, were lower than the temperature at the surface of the carbon layer by an amount equivalent to the temperature drop through a 5-micron thick layer of Pyrex.

Approximately the same result was obtained from a different experimental method. One of the simplest ways of messuring the thermal responsivity of heat-flux gsges st room temperature is to messure the gage surface temperature by conventional heat-flux gage thermometry, as the gsge at room temperature is ropidly immersed in a bath of csrbon tetrschloride held at 0°C. This process simulates the bringing together of two semi-infinite solids of different temperatures with zero contsct resistance at their interface. As the gsge contacts the liquid, there is a shsrp discontinuity in the gage surface temperature as the temperature drops to a new value that is dependent on the initial temperatures of the two bodies and their thermal properties. The relationship between temperatures and thermal properties for the two bodies is expressed by the following equation:

$$\frac{T_{ga} - T_i}{T_i - T_\ell} = \frac{\Gamma_\ell}{\Gamma_{ga}} \qquad \text{(C-1)}$$

Where: T_{gs}, T_ℓ, and T_i are the initial uniform gage temperature, initial uniform liquid temperature, snd the temperature at the interface between the gage and the liquid at the instant of contact, respectively.

Figure 37a is sn oscillograph of temperature versus time for an uncoated gage rspidly immersed in csrbon tetrachloride. Note the sharp discontinuities in the temperature-time trsce. For the costed heat-flux gsge, Figure 37b, the measured temperature adjusts more slowly to the sudden tempersture chsnge. By carefully measuring the temperature-time dsta on oscillographs of the kind shown in Figure 37 with an optical comparator snd then compsring the experimentslly determined profile st Pyrex surface (under the layer of csrbon) with profiles calculsted for various distsnces below the surfsce for this special cooling process, the results agsin showed that the carbon layer was spproximately equivslent to a 5-micron thick layer of Pyrex.

With this information sbout the carbon layer, it was now possible to cslculate the temperature at the carbon surface as a function of time from the experimental temperature-time dsta st the Pyrex surfsce. We knew from preliminary studies thst temperature-time data from shock-tube runs are well represented by equations for heating of a semi-infinite solid through a constant wsll heat-trsnsfer coefficient. The experimentsl data for s position

5 microns below the surface were well represented by the following equation (see page 72 of Reference 13):

$$\frac{T - T_o}{T_g - T_o} = \text{erfc}\ \frac{x}{2(\alpha t)^{1/2}} - \left[e^{hx/k + N^2}\right]\left[\text{erfc}\left(\frac{x}{2(\alpha t)^{1/2}} + N\right)\right] \qquad \text{(C-2)}$$

$$N = \frac{h(t)^{1/2}}{\Gamma}$$

Heat-transfer coefficients obtained by comparing experimental data to Equation (C-2) were then used to calculate temperature-time data at the surface of the carbon layer. In performing these calculations, it was necessary to take into consideration temperature-dependent thermophysical properties of the Pyrex substrate. The method used in this work is described in Appendix I of Reference 6.

Temperature-time data for the carbon-coated heat-flux gage are tabulated in Table 2C. Two sets of temperature-time data are given. ΔT_{sp} is the experimental temperature measured at the Pyrex surface, and ΔT_s is that calculated for the carbon surface. The temperature drop through the carbon layer, as these data show, is of the order of 5 to 15°C. Consequently, a rather large error, say 20 percent, in the experimentally determined properties of the carbon layer would not greatly affect the observed results.

APPENDIX D

TABLES OF DATA

TABLE I

SUMMARY OF HEAT TRANSFER DATA FOR MODIFIED TEST SECTION

(Heat Transfer from High-temperature Nitrogen)

A. SHOCK-TUBE DATA

Run No.	Orifice	M_E	T_0 (°K)	T_4 (°K)	T_4' (°K)	P_4 (atm)	P_4' (atm)
		Heat-Flux Gage No. 5 (Pyrex 7740)					
62-1-2	3A	2.21	294	835	881	17.5	21.5
62-1-3	3A	2.57	294	1050	1138	14.2	19.7
62-1-4	3A	2.75	294	1154	1251	13.4	18.7
62-1-5	3A	3.05	295	1329	1427	14.4	19.5
62-1-6	3A	3.24	295	1463	1592	13.1	18.9
62-1-7	3A	3.45	295	1609	1757	13.0	19.1
62-1-8	3A	3.16	295	1414	1531	12.9	18.2
62-1-9	3A	2.50	295	1010	1088	10.3	13.8
62-1-10	3A	2.13	296	798	867	10.8	14.9
62-1-11	4A	2.16	296	813	853	17.1	20.3
62-1-12	4A	2.53	296	1029	1105	14.2	18.9
62-1-13	4A	3.03	296	1331	1451	13.8	19.9
62-1-14	4A	3.13	296	1396	1509	13.3	18.5
62-1-15	4A	3.48	296	1633	1779	12.9	19.7
62-2-1	5A	2.13	295	798	839	17.9	21.6
62-2-2	5A	2.57	295	1046	1131	15.0	20.5
62-2-3	5A	2.58	295	1052	1136	15.3	20.8
62-2-4	5A	2.83	295	1200	1280	15.4	20.0
62-2-5	5A	2.77	295	1285	1380	14.1	19.0
62-2-6	5A	3.12	295	1383	1486	14.7	20.0
62-2-7	5A	3.45	295	1609	1771	13.3	20.6
62-2-8	5A	2.97	295	1285	1377	10.3	13.8
610-15-9	3A	2.13	295	793	840	15.4	19.3
610-15-10	3A	2.53	295	1022	1106	13.3	18.3
610-15-11	3A	3.04	294	1324	1449	12.5	18.3

TABLE I (continued)

A. SHOCK-TUBE DATA

Run No.	Orifice	M_E	T_0 (°K)	T_4 (°K)	T_4' (°K)	P_4 (atm)	P_4' (atm)
		Heat-Flux Gage No. 11 (Pyrex 7740)					
610-15-1	3A	2.04	296	752	796	15.7	19.5
610-15-2	3A	2.15	296	812	860	15.9	19.9
610-15-3	3A	2.52	296	1022	1110	13.3	18.6
610-15-4	3A	2.73	296	1146	1237	13.2	18.0
610-15-5	3A	3.04	296	1331	1443	13.1	18.5
610-15-6	3A	3.03	296	1327	1445	12.7	18.2
610-15-7	3A	3.20	295	1438	1562	13.0	18.6
		Heat-Flux Gage No. 1 (Alumina)					
63-15-1	3A	3.44	297	1603	1787	12.5	20.0
63-15-2	3A	3.47	297	1627	1800	12.4	19.3
63-15-3	3A	3.28	297	1501	1614	14.1	19.4
63-15-4	3A	3.18	297	1438	1566	13.9	20.0
63-15-5	3A	2.76	297	1171	1255	14.7	19.5
		Heat-Flux Gage No. 9 (Alumina)					
610-15-12	3A	2.12	294	785	831	15.2	18.8
610-15-13	3A	3.01	294	1307	1433	12.5	18.4

B. HEAT TRANSFER DATA

Run No.	$(T_4')^{0.3}$ $(°K)^{0.3}$	h $\frac{cal}{(cm^2)(sec)(°K)}$	$h/(T_4')^{0.3}$ $\frac{cal}{(cm^2)(sec)(°K)^{1.3}}$	G $\frac{g}{(cm^2)(sec)}$	Time Interval[1] (msec)
		Heat-Flux Gage No. 5 (Pyrex 7740)			
62-1-2	7.65	10.98×10^{-2}	14.35×10^{-3}	65.7	4-30
62-1-3	8.26	8.93	10.81	52.6	5-30
62-1-4	8.48	8.65	10.19	47.4	2-25
62-1-5	8.84	8.80	9.95	46.2	3-20
62-1-6	9.13	8.28	9.07	42.4	3-18
62-1-7	9.41	8.30	8.82	40.7	2-12
62-1-8	9.03	8.22	9.10	41.7	2-20
62-1-9	8.15	6.97	3.55	37.8	5-30
62-1-10	7.61	7.75	10.18	45.9	2-40
62-1-11	7.57	8.88	11.73	41.9	5-40
62-1-12	8.18	7.07	8.64	33.6	5-35
62-1-13	8.88	6.93	7.80	30.7	2-25
62-1-14	8.99	6.90	7.67	28.0	2-17
62-1-15	9.47	7.41	7.83	27.3	1-20
62-2-1	7.53	7.34	9.75	34.4	5-40
62-2-2	8.24	5.96	7.23	27.9	2-35
62-2-3	8.25	6.00	7.28	28.2	5-35
62-2-4	8.55	6.16	7.21	25.6	2-25
62-2-5	8.75	5.42	6.19	23.3	5-25
62-2-6	8.96	5.64	6.29	23.5	5-25
62-2-7	9.44	5.82	6.16	22.1	5-20
62-2-8	8.74	4.76	5.45	16.9	5-25
610-15-9	7.53	9.58	12.73	60.3	5-35
610-15-10	8.20	8.51	10.38	49.7	1-25
610-15-11	8.88	7.73	8.70	43.1	1-20

[1]This is the interval for which the time-temperature data could be represented to within ±5 percent by Eq. (A-1).

TABLE I (continued)

B. HEAT TRANSFER DATA (continued)

Run No.	$(T_4')^{0.3}$ $(°K)^{0.3}$	h $\frac{cal}{(cm^2)(sec)(°K)}$	$h/(T_4')^{0.3}$ $\frac{cal}{(cm^2)(sec)(°K)^{1.3}}$	G $\frac{g}{(cm^2)(sec)}$	Time Interval[1] (msec)
		Heat-Flux Gage No. 11 (Pyrex 7740)			
610-15-1	7.41	11.56×10^{-2}	15.50×10^{-3}	62.7	5-40
610-15-2	7.60	10.07	13.24	61.7	5-35
610-15-3	8.23	8.58	10.43	50.3	3-30
610-15-4	8.45	9.24	10.93	46.1	1-22
610-15-5	8.87	8.56	9.64	43.7	1-20
610-15-6	8.88	8.34	9.39	42.9	1-21
610-15-7	9.08	8.52	9.38	42.1	1-20
		Heat-Flux Gage No. 1 (Alumina)			
63-15-1	9.44	8.67	9.19	42.1	2-13
63-15-2	9.47	8.47	8.99	40.6	1-15
63-15-3	9.19	9.08	9.08	43.2	2-20
63-15-4	9.11	8.53	9.36	45.3	1-25
63-15-5	8.51	8.99	10.56	49.6	1.30
		Heat-Flux Gage No. 9 (Alumina)			
610-15-12	7.52	10.59	14.08	59.4	1-40
610-15-13	8.84	8.55	9.67	43.7	1-30

[1]Time interval over which the temperature-time data could be represented within 5 percent by equation for transient heating of a semi-infinite solid through a constant heat transfer coefficient.

TABLE II

DATA FOR SHOCK-TUBE RUNS WITH
CARBON-COATED HEAT-FLUX GAGE

A. SHOCK-TUBE DATA

Run No.	M_E	T_o (°K)	T_4 (°K)	T_4' (°K)	P_4 (atm)	P_4' (atm)
66-10-8-12	2.13	301.4	814	858	16.1	19.7
66-10-8-13	2.18	301.6	842	881	17.2	20.5
66-10-8-14	2.52	301.7	1041	1138	12.9	18.4
66-10-8-15	2.77	301.7	1192	1285	14.1	19.3
66-10-8-16	3.04	302.1	1363	1476	13.9	19.5
66-10-8-17	2.95	302.1	1305	1408	13.7	18.9
66-11-6-1	1.95	297.0	698	754	6.9	9.2
66-11-6-2	2.34	297.3	922	995	11.4	15.4
66-11-6-3	2.44	297.7	982	1059	12.7	17.1
66-11-7-3	3.00	297.4	1315	1393	13.3	16.9

B. HEAT-TRANSFER DATA

Run No.	$(T_4')^{0.3}$ $(°K)^{0.3}$	h $\frac{cal}{(cm^2)(sec)(°K)}$	$h/(T_4')^{0.3}$ $\frac{cal}{(cm^2)(sec)(°K)^{1.3}}$	G $\frac{g}{(cm^2)(sec)}$
66-10-8-12	7.56	0.1012	13.39×10^{-3}	60.9
66-10-8-13	7.64	0.1054	14.80×10^{-3}	62.8
66-10-8-14	8.24	0.0888	10.78×10^{-3}	49.3
66-10-8-15	8.56	0.0934	10.91×10^{-3}	48.3
66-10-8-16	8.92	0.0874	9.80×10^{-3}	45.4
66-10-8-17	8.80	0.0890	10.11×10^{-3}	45.2
66-11-6-1	7.30	0.06079	8.33×10^{-3}	-
66-11-6-2	7.93	0.07697	9.71×10^{-3}	44.1
66-11-6-3	8.08	0.08449	10.46×10^{-3}	47.6
66-11-7-3	8.76	0.08345	9.53×10^{-3}	40.7

TABLE II (continued)

C. SURFACE TEMPERATURE AND IR-DETECTOR OUTPUT DATA FOR SHOCK-TUBE RUNS WITH CARBON-COATED HEAT-FLUX GAGE.

Time (msec)	ΔT_{ps}, Measured Temperature at Pryex Surface (°C)	ΔT_{s}, Temperature Calculated for Carbon Surface (°C)	Net IRDO (mv)
Run No. 66-10-8-12			
0	0	0	0
1	52.5	62.3	3.5
2	70.0	77.6	5.8
3	81.0	88.5	7.0
5	97.8	104.9	11.1
10	130.8	137.4	22.6
15	147.5	153.7	28.5
20	157.3	164.1	33.4
25	171.2	176.7	40.2
30	180.4	185.8	45.8
35	188.5	193.7	51.1
Run No. 66-10-8-13			
0	0	0	0
1	55.5	63.4	3.7
2	74.5	82.7	6.2
3	80.5	88.5	8.0
5	101.9	109.5	11.9
10	135.9	143.0	24.0
15	159.0	165.6	32.9
20	171.2	177.4	40.7
25	183.3	187.2	47.2
30	193.1	198.8	52.1
35	199.5	205.0	56.6
Run No. 66-10-8-14			
[illegible]	0	0	0
1	64.0	74.4	5.3
2	85.0	95.2	9.5
3	97.1	107.1	12.4
5	125.0	134.7	21.2
10	164.1	173.0	37.8
15	194.9	203.3	57.3
20	217.0	225.1	72.6
25	234.7	242.4	86.8
Run No. 66-10-8-15			
0	0	0	0
1	80.5	93.4	6.0
2	101.3	113.8	13.1
3	116.9	129.2	17.0
5	153.8	165.6	31.2
10	200.1	211.0	61.8
15	234.6	244.9	86.7
20	260.0	269.9	108.8

TABLE II (continued)

C. SURFACE TEMPERATURE AND IR-DETECTOR OUTPUT DATA FOR SHOCK-TUBE RUNS WITH CARBON-COATED HEAT-FLUX GAGE (continued).

Time (msec)	ΔT_{pa}, Meaaured Temperature at Fyrex Surface (°C)	ΔT_{a}, Temperature Calculated for Carbon Surface (°C)	Net IRDO (mv)
Run No. 66-10-8-16			
0	0	0	0
1	92.0	106.4	8.5
2	114.0	128.1	18.9
3	136.6	150.5	26.5
5	171.2	184.6	44.1
10	225.0	237.9	82.6
15	262.6	274.3	122.5
20	291.4	302.7	153.0
Run No. 66-10-8-17			
0	0	0	0
1	80.5	93.2	9.2
2	112.3	124.7	17.4
3	125.0	137.2	22.3
5	155.0	166.8	35.2
10	197.8	208.9	64.0
15	235.6	246.1	95.9
20	262.1	272.1	122.9
Run No. 66-11-6-1			
0	0	0	0
1	27.0	31.0	0.9
2	33.0	37.0	1.0
3	41.0	44.9	2.1
5	51.0	54.9	3.3
10	70.0	73.7	7.5
15	84.0	87.5	10.3
20	93.2	96.6	10.7
25	101.8	105.1	14.3
30	109.4	112.6	15.2
35	112.9	116.1	17.1
Run No. 66-11-6-2			
0	0	0	0
1	48.0	55.6	3.5
2	65.0	72.5	6.2
3	72.0	79.4	6.9
5	91.0	98.2	11.8
10	122.1	128.8	22.4
15	147.6	154.1	32.9
20	164.8	171.0	42.0
25	179.9	185.9	51.6
30	192.8	198.6	59.3

TABLE II (continued)

C. SURFACE TEMPERATURE AND IR-DETECTOR OUTPUT DATA FOR SHOCK-TUBE RUNS WITH CARBON-COATED HEAT-FLUX GAGE (continued).

Time (msec)	ΔT_{ps}, Measured Temperature at Pyrex Surface (°C)	ΔT_{s}, Temperature Calculated for Carbon Surface (°C)	Net IRDO (mv)
Run No. 66-11-6-3			
0	0	0	0
1	58.0	67.0	4.2
2	78.0	86.9	7.6
3	87.0	95.7	9.6
5	109.4	117.9	16.0
10	146.4	154.3	32.9
15	169.5	177.0	46.9
20	189.2	196.3	61.4
25	205.6	212.5	76.8
30	215.8	222.4	85.0
Run No. 66-11-7-3			
0	0	0	0
1	87.0	99.7	10.3
2	103.6	116.3	14.4
3	120.9	133.3	19.5
5	153.3	165.4	33.7
10	205.4	216.7	65.2
15	229.6	250.8	92.5
20	248.2	275.8	117.0

TABLE III

PROPELLANT COMPOSITIONS

Ingradienta (Weight Percent)

Propellant Code	Fuel	Catalyst	Ammonium Perchlorate	Ammonium Perchlorate Particle Size (a)
		A: CAST PROPELLANTS		
AR	25.0 PBAA (b) 3.0 Philblack E (c)	2.0 Copper Chromite (d)	70.0	15 Micron
AQ	30.35 PBAA, 2.79 Philblack E	1.86 Copper Chromite	65.0	15 Micron
FM	18.0 PBAA	2.0 Copper Chromite	40.0 40.0	15 Micron 200 Micron
UA	25.0 PBAA	2.0 Copper Chromite	73.0	15 Micron
		B: PRESSED PROPELLANTS (e)		
PP-CBM (f)	16.0 Philblack E	2.0 Copper Chromite	82.0	15 Micron
PP-E (g)	4.5 Sterling VR Carbon Black (h)	2.5 Copper Chromite	46.5 46.5	15 Micron 45 Micron
PP-F (f)	-	5.0 Copper Chromite	95.0	15 Micron

(a) Ammonium perchlorate of the designated particle size means that the 50 weight percent of the particles have diameters less than the value indicated. For particle sizes greater than 35 microns, a screen analysis was used to determine particle diameters. For particles less than 15 microns in diameter, particle sizes were determined microscopically by first dispersing ammonium perchlorate in dry carbon tetrachloride with the aid of a wetting agent and then measuring diameters of 200 to 300 particles. All ammonium perchlorate was obtained from the American Potash and Chemical Corporation.

(b) The PBAA binder-fuel for these propellants was composed of 85.0 percent of a liquid polybutadiene-acrylic acid copolymer cured 15.0 percent Epon 828 (manufactured by Shell Chemical Company).

(c) A rubber-reinforcing carbon black obtained from Phillips Petroleum Company.

TABLE III (continued)

(d) Copper Chromite Catalyst Cu0202 P from Harshaw Chemical Company contains approximately 82 percent CuO and 17 percent Cr_2O_3.

(e) The ingredients for pressed propellants were prepared by blending all fine-particle size ingredients and then passing the dry blend of ingredients through a 270-mesh screen several times.

(f) Dry-blended material, slightly moistened, was pressed into pallets under a pressure of 100,000 psig. Pellets formed at 100,000 psig were powdered and repressed at 200,000 psig.

(g) Dry-blended material, slightly moistened, was pressed into pellets under a pressure of 100,000 psig.

(h) Sterling VR carbon black was obtained from the Cabot Corporation.

TABLE IV

THERMOPHYSICAL PROPERTIES OF PROPELLANT AND PROPELLANT INGREDIENTS

Propellant or Ingredients	Test Temp. (°C)	Heat Capacity, c cal/(g)(°K)	Denaity ρ g/(cm)^3	Thermal Oiffusivity, & $(cm^2)/(sec)$	Thermal Conductivity, k cal/(cm)(sec)(°K)	Thermal Responsivity, Γ $(kpc)^{1/2}$ $cal/(cm^2)(eec)^{1/2}$ (°K)
			A. INGREDIENTS			
Ammonium Perchlorate (a)	50	0.271	1.952	2.27×105^3	1.20×10^{-3}	2.520×10^{-2}
	100	0.291	1.952	2.04×10^{-3}	1.16×10^{-3}	2.567×10^{-2}
	150	0.312	I.952	1.81×10^{-3}	1.10×10^{-3}	2.588×10^{-2}
	200	0.333	1.952	1.58×10^{-3}	1.03×10^{-3}	2.588×10^{-2}
	240	0.349	1.952	1.41×10^{-3}	0.96×10^{-3}	2.557×10^{-2}
	60	0.275	1.92	2.182×10^{-3}	1.152×10^{-3}	2.45×10^{-2}
Copper Chromite Catalyst Cu0202 (b)	60	0.147	6.15	-	-	-
Philblack E (c)	60	0.195	2.0	-	2.10×10^{-3}	-
PBAA Binder with 5% Philblack E (e)	60	0.452	1.004	-	0.46×10^{-3}	1.44×10^{-2}
Polyurethane Binder with 5% Philblack E (e)	60	-	-	-	-	1.44×10^{-2}
			8: CAST PROPELLANTS			
AR (f)	60	0.313	1.53	-	0.855×10^{-3}	2.02×10^{-2}
AQ (f)	60	0.316	1.50	-	0.819×10^{-3}	1.97×10^{-2}
FM (g)	60	0.316	1.63	1.70×10^{-3}	0.876×10^{-3}	2.12×10^{-2}
UA (f)	60	0.322	1.56	1.63×10^{-3}	0.819×10^{-3}	2.03×10^{-2}
JPN (Double-Base)(h)	-	-	-	-	-	1.77×10^{-2}
			C: PRESSED PROPELLANTS			
PP-CBM (k)	60	0.260	1.91	-	1.245×10^{-3}	2.48×10^{-2}
PP-E (ℓ)	60	-	1.92	-	-	2.44×10^{-2}
PP-F (ℓ)	60	-	I.92	-	-	2.44×10^{-2}

TABLE IV (continued)

(a) Data for pressed ammonium perchlorate powder. Thermal diffusivity and thermal conductivity are based on work of Rosser, Inami, and Wise [12].

(b) Data for copper chromite were estimated from data on CuO and Cr_2O_3 given by *Lange's Handbook of Chemistry*, Sixth Edition.

(c) Thermal conductivity data for Philblack E was estimated from measured thermal diffusivity on pressed propellants made from Philblack E and ammonium perchlorate.

(d) PBAA Binder composed of 5 percent Philblack E and 95 percent PBAA polymer. The polymer consisted of 85 percent liquid polybutadiene-acrylic copolymer and 15 percent Epon 828 curing agent. The tbermophysical properties for the binder were estimated from data on Philblack E and measured vslues on cured, unloaded polymer.

(e) The polyurethane binder consisted of the following ingredients by weight percent: estane, 96.6; trimethylol propane (TMP), 2.3; 1, 4 butanedial (1,4BD), 0.7; and triethanolamine (TEA), 0.4. No thermophysical properties were available. Data for PBAA binder with Philblack E were used in calculations.

(f) Thermophysical properties for this propellant were not measured directly, but were estimated from dsta on similar propellants.

(g) Thermophysical properties were measured by the methods described in Ref. 5.

(h) Thermal responsivity of JPN(Double-Base) propellant calculated from data on double-base propellant given in Ref. 14.

(i) Thermophysical properties were based on measurements on pellets of PP-CBM of lower density and sdjustments were made for poroaity.

(j) Thermal responsivity assumed to be the same as that for pressed AP of equivalent density.

TABLE V

HEAT-TRANSFER DATA FOR SHOCK-TUBE RUNS FOR MEASUREMENT OF SURFACE TEMPERATURES ON PROPELLANTS AND PROPELLANT INGREDIENTS

Run No.	M_E	T_o °K	T_8 °K	P_4' (atm)	G $\frac{g}{(cm^2)(sec)}$	h $\frac{cal}{(cm^2)(sec)(°K)}$	$\overline{F}_s$ (a) $\frac{cal}{(cm^2)(sec)}$
				A. PROPELLANT UA			
611-6-20	2.46	300	1079	17.8	49.0	0.0871	43.2
611-6-21	2.99	300	1421	17.4	41.5	0.0809	59.2
611-6-22	2.89	300	1337	16.8	41.3	0.0791	54.1
611-6-23	2.66	300	1208	17.6	45.5	0.0840	49.2
				B. PROPELLANT AR			
69-21-14	2.10	301	835	18.8	59.2	0.0963	31.3
69-21-15	2.55	301	1134	19.4	52.1	0.0936	48.1
69-21-16	2.56	301	1146	19.4	51.6	0.0931	48.6
69-22-5	2.52	301	1118	18.2	49.2	0.0883	45.4
69-22-6	2.74	301	1258	19.0	48.2	0.0897	53.8
69-22-7	2.66	301	1220	17.3	44.5	0.0826	49.1
69-22-8	2.74	301	1253	18.6	48.0	0.0893	53.4
611-6-11	3.01	300	1426	17.1	40.6	0.0793	58.7
611-6-12	2.99	300	1424	17.3	41.1	0.0802	59.0
611-6-13	3.09	300	1493	17.8	41.2	0.0816	63.3
611-6-14	2.58	300	1168	17.4	45.9	0.0839	46.9
611-6-19	2.97	300	1416	17.8	42.5	0.0827	59.7
611-6-25	2.69	300	1231	17.5	44.9	0.0834	50.1
611-7-6	2.45	298	1065	18.3	50.6	0.0895	43.1
611-7-7	2.42	298	1042	17.3	48.4	0.0851	40.5
611-7-8	1.98	298	748	17.1	57.0	0.0900	25.4
611-7-9	1.94	298	740	17.7	59.2	0.0928	25.4
611-8-1	2.10	294	804	18.2	59.2	0.0952	29.7
611-8-3	2.47	294	1061	19.3	53.4	0.0939	44.4

TABLE V (continued)

Run No.	M_E	T_o °K	T_g °K	P_4' (stm)	$\frac{G}{g}$ $\frac{}{(cm^2)(sec)}$	h_{cal} $\frac{}{(cm^2)(sec)(°K)}$	$\overline{F}_{s_{cal}}$ (s) $\frac{}{(cm^2)(sec)}$
				C. PROPELLANT AQ			
611-6-4	2.02	299	783	17.8	57.9	0.0925	27.5
611-6-5	2.52	299	1109	18.6	50.3	0.0900	45.2
611-6-6	2.70	299	1217	18.1	46.7	0.0863	50.0
611-6-7	3.04	299	1465	18.8	44.2	0.0866	63.6
611-6-8	2.66	300	1186	17.2	45.0	0.0828	47.0
611-6-9	3.01	300	1427	17.8	42.3	0.0826	59.7
611-6-10	2.67	300	1208	18.8	48.8	0.0898	50.6
				D. PRESSED PROPELLANT PP-CEM			
610-25-13	2.56	303	1149	20.0	53.2	0.0956	53.6
610-25-14	2.74	303	1246	19.6	50.0	0.0926	58.4
610-25-15	2.55	303	1137	19.5	52.2	0.0939	52.2
610-25-16	2.73	302	1261	18.1	45.9	0.0857	56.4
610-25-17	3.03	302	1469	18.2	42.5	0.0836	67.5
611-6-17	2.05	300	807	18.4	58.7	0.0946	31.9
611-6-18	2.66	300	1203	17.3	45.0	0.0831	52.1
				E. PRESSED PROPELLANT PP-E			
610-25-5	2.66	301	1208	17.3	44.9	0.0831	52.0
610-25-6	2.58	301	1162	19.3	50.9	0.0923	52.9
610-25-7	2.98	302	1414	18.2	43.4	0.0842	64.3
				F. PRESSED PROPELLANT PP-F			
611-7-4	2.73	298	1254	18.2	46.3	0.0864	56.3
611-7-5	3.01	298	1444	18.6	44.0	0.0859	67.2
				G. PRESSED AMMONIUM PERCHLORATE			
610-25-2	2.70	300	1236	19.5	49.8	0.0921	57.4
610-25-3	2.97	301	1427	17.7	42.0	0.0820	64.0
610-25-4	3.20	301	1566	17.6	39.9	0.0802	70.8
				H. DOUBLE-BASE PROPELLANT JPN			
69-21-11	1.97	301	768	19.4	63.6	0.1005	26.5
69-21-12	2.75	302	1266	19.1	48.3	0.0902	51.6

TABLE V (continued)

Run No.	M_E	T_o °K	T_g °K	P_4' (atm)	G $\frac{g}{(cm^2)(sec)}$	h $\frac{cal}{(cm^2)(sec)(°K)}$	$\overline{F}_s$ (a) $\frac{cal}{(cm^2)(sec)}$
				I. PBAA BINDER			
610-25-8	2.74	302	1245	18.9	48.3	0.0896	45.7
610-25-9	2.70	302	1227	18.1	47.3	0.0875	44.3
610-25-10	2.68	302	1222	18.2	46.8	0.0866	43.8
610-25-11	3.15	302	1549	18.5	42.8	0.0855	59.0
610-25-12	3.21	303	1607	18.5	41.3	0.0836	61.0
				J. POLYURETHANE BINDER			
69-22-1	2.71	298	1228	19.1	49.1	0.0907	45.4
69-22-2	2.75	298	1254	19.1	49.4	0.0918	46.9

(a) $\overline{F}_s$ is the mean externally applied heat flux. This value is based on the mean heating rate for first 20 milliseconds of test:

$$\overline{F}_s = \frac{\Gamma_p}{2}\left(\frac{\pi}{t}\right)^{1/2}\left(T_{20}{}^{L} - T_o\right)$$

Where: $T_{20}{}^{L}$ is the temperature at the surface of the sample 20 milliseconds after start of linear heating through a constant heat transfer coefficient.

TABLE VI

DATA FROM SURFACE-TEMPERATURE MEASUREMENTS ON PROPELLANTS

A. DATA FOR PROPELLANT UA

Time (msec)	Net IRDO (a) (mv)	ΔT_s^L (b) (calc.) (°C)	ΔT_s (c) (Exp.) (°C)
Run No. 611-6-20 (Smooth Surface)			
0	0	0	-
2	6.1	144	-
3	9.5	170	-
5	19.4	209	-
10	41.2	270	-
15	62.8	310	-
20	84.2	339	-
25	100.0	363	-
30	109.8	382	-
Run No. 611-6-21 (Same Sample used in 611-6-20, Ignited)			
0	0	0	0
1	7.9	143	160
2	14.4	194	199
3	22.5	230	231
4	30.5	259	260
5	41.6	283	289
6	49.1	304	305
7	57.6	323	321
8	67.1	339	340
9	73.6	354	350
10	83.4	368	369
11	92.8	381	380
12	105.2	393	399
13	118.6	404	411
14	129.0	414	428
14.5	136.7	-	436
15	153.4	424	451
15.5	159.	-	460
16	345	433	598
17	555	442	740

Time (msec)	Net IRDO (a) (mv)	ΔT_s^L (b) (calc.) (°C)	ΔT_s (c) (Exp.) (°C)
Run No. 611-6-22 (Polymer-Rich Surface, Ignited)			
0	0	0	0
1	5.8	130	142
2	10.4	176	178
3	14.0	209	196
5	30.0	258	258
10	62.8	335	332
12	81.0	358	361
13	83.6	368	368
14	86.3	377	371
15	97.0	386	386
16	101.9	395	397
17	119.8	403	416
18	205	411	500
20	408	425	615
Run No. 611-6-23 (Smooth Surface)			
0	0	0	-
1	3.4	120	-
2	7.7	162	-
3	10.0	193	-
5	21.8	236	-
10	49.4	306	-
15	74.7	352	-
20	98.2	387	-
25	117.4	414	-
30	134.6	437	-

TABLE VI (continued)

B. DATA FOR PROPELLANT AR

Time (msec)	Net IRDO (a) (mv)	ΔT_a^L (b) (calc.) (°C)	ΔT_s (c) (exp.) (°C)
Run No. 69-21-14 (Smooth Surface, Coated with Thin Film of Philblack E)			
0	0	0	-
2	13.8	108	-
3	18.2	127	-
5	24.1	155	-
10	42.9	199	-
15	59.5	227	-
20	73.0	248	-
25	81.1	264	-
30	98.2	278	-
35	111.7	289	-
Run No. 69-21-15 (Same Sample Uaed in 69-21-14)			
0	0	0	-
2	30.1	164	-
3	38.1	194	-
5	65.9	237	-
10	133.5	304	-
15	188.	348	-
20	254	380	-
25	272	406	-
Run No. 69-21-16 (Same Sample uaed in 69-21-15, Ignited)			
0	0	0	0
2	33.0	166	173
3	41.5	196	192
5	71.8	239	240
10	139	307	310
15	183	352	346
17	208	366	360
20	255	384	390
22	265	395	396
25	273	410	400
26	288	415	408
27	319	-	424
28	350	-	439
29	490	-	495
30	600	-	530

Time (msec)	Net IRDO (a) (mv)	ΔT_s^L (b) (calc.) (°C)	ΔT_s (c) (exp.) (°C)
Run No. 69-22-5 (Smooth Surface)			
0	0	0	-
1	9.5	113	-
2	15.8	153	-
3	20.3	181	-
5	36.0	222	-
10	70.7	287	-
15	101.6	329	-
20	130.7	360	-
25	151	384	-
30	187	405	-
Run No. 69-22-6 (Same Sample Used in 69-22-5, Ignited)			
0	0	0	0
1	15.1	135	142
2	25.1	182	179
3	32.9	215	200
5	50.9	263	240
10	112.7	339	325
15	149.7	389	362
20	189	425	395
21	196	432	400
22	202	438	403
23	203	443	403
24	230	449	425
25	266	454	446
26	290	-	460
27	490	-	555
Run No. 69-22-7 (Smooth Surface)			
0	0	0	-
1	14.6	120	-
2	22.7	163	-
3	28.4	193	-
5	45.2	234	-
10	82.4	307	-
15	111.4	353	-
20	150	388	-
25	183	416	-

TABLE VI (continued)

B. DATA FOR PROPELLANT AR (continued)

Time (msec)	Net IRDO (c) (mv)	ΔT_s^L (b) (calc.) (°C)	ΔT_s (c) (exp.) (°C)
Run No. 69-22-8 (Same Sample Used in 69-22-7, Ignited) (Teat Gas: Air)			
0	0	0	0
1	23.1	133	171
2	32.0	180	198
3	39.8	213	216
5	60.8	261	256
10	106.6	336	319
15	164.6	386	375
20	230	422	425
25	264	451	448
28	294	-	462
29	290	-	461
30	288	-	460
31	293	-	462
32	294	-	462
33	340	-	488
34	580	-	590
Run No. 611-6-11 (Smooth Surface, Ignited)			
0	0	0	0
1	19.6	142	160
2	33.2	193	200
3	51.6	229	240
4	69.7	257	270
5	90.8	281	300
6	108	302	320
7	124	321	338
8	152	337	364
9	172	352	380
10	203	366	405
11	218	379	417
12	232	391	428
12.5	245	-	433
13	267	402	448
13.5	311	-	473
14	381	412	510
14.5	525	-	570

Time (msec)	Net IRDO (a) (mv)	ΔT_s^L (b) (calc.) (°C)	ΔT_s (c) (exp.) (°C)
Run No. 611-6-12 (Smooth Surface, Ignited)			
0	0	0	0
1	17.8	143	153
2	33.4	194	200
3	50.5	231	240
4	70.1	259	270
5	91.7	284	300
6	109	304	321
7	127	323	340
8	152	340	365
9	175	355	383
10	203	368	405
11	218	381	415
12	242	393	432
13	262	404	445
14	281	415	458
14.5	291	-	461
15.0	351	425	495
15.5	510	-	560
16.0	660	-	620
17.0	825	-	860
18.0	1180	-	750
Run No. 611-6-13 (Smooth Surface, Ignited)			
0	0	0	0
2	40.3	209	217
3	59.0	248	252
4	71.3	279	271
5	86.7	305	295
6	104.8	327	319
7	123	347	339
8	138	365	350
9	154	381	367
10	185	396	390
11	204	409	405
12	220	222	419
13	247	434	433
14	272	445	450
14.5	301	-	470
15	563	455	582
16	1180	-	755

TABLE VI (continued)

B. DATA FOR PROPELLANT AR (continued)

Time (msec)	Net IRDO (a) (mv)	T_s^L (b) (calc.) (°C)	T_s (c) (exp.) (°C)
Run No. 611-6-14 (Smooth Surface, Ignited)			
0	0	0	0
2	20.8	156	164
3	30.8	185	193
5	55.0	227	246
10	105	294	319
15	157	338	370
18	193	358	398
19	214	365	412
20	218	370	416
21	232	376	429
22	251	382	440
22.5	270	-	450
23	426	387	530
24	640	392	610
Run No. 611-6- 19 (Smooth Surface, Ignited)			
0	0	0	0
2	25.4	198	180
3	42.4	235	211
4	62.4	264	260
5	90.4	288	300
6	106.5	309	319
7	118.5	328	331
8	133	345	346
9	149	360	361
10	175	374	375
11	207	386	410
12	306	398	470
13	417	409	525
14	1135	420	740

Time (msec)	Net IRDO (a) (mv)	T_s^L (b) (calc.) (°C)	T_s (c) (exp.) (°C)
Run No. 611-6-25 (Surface Roughened and Coated with Philblack E, Ignited)(d)			
0	0	0	0
1	46.1	123	230
2	63.6	166	260
3	80.0	197	284
4	95.8	222	305
5	104	242	317
6	133	260	345
7	134	275	346
8	144	289	357
9	165	302	375
10	155	314	368
11	165	324	375
12	179	334	388
13	191	344	397
14	202	352	403
15	202	361	403
16	218	368	417
17	250	376	437
18	262	383	444
19	301	389	469
20	411	396	521
21	590	402	590
Run No. 611-7-6 (Smooth Surface)			
0	0	0	-
1	8.7	108	-
2	15.1	145	-
3	20.6	172	-
5	35.4	211	-
10	75.4	272	-
15	108	311	-
20	135	341	-
25	166	364	-
30	191	383	-

TABLE VI (continued)

B. DATA FOR PROPELLANT AR (continued)

Time (msec)	Net IRDO (a) (mv)	ΔT_s^L (b) (calc.) (°C)	ΔT_s (c) (exp.) (°C)
Run No. 611-7-7 (Surface Roughened and Coated with Philblack E, Ignited (d)			
0	0	0	0
1	39.9	100	216
2	60.2	135	255
3	62.7	160	260
4	77.6	180	281
5	94.6	196	303
6	105.4	211	318
7	115.2	223	329
8	127	235	340
9	138	245	350
10	157	254	369
11	182	263	390
12	232	271	425
13	324	278	480
Run No. 611-7-8 (Smooth Surface Coated with Thin Film of Philblack E)			
0	0	0	0
1	5.8	64	-
2	7.8	86	-
3	11.7	101	-
5	14.5	124	-
10	31.7	170	-
15	42.3	183	-
20	51.2	200	-
25	62.2	214	-
30	69.4	225	-
35	73.1	235	-
40	80	243	-
Run No. 611-8-3 (Smooth Surface)			
0	0	0	-
1	9.9	112	-
2	13.4	151	-
3	22.8	179	-
5	34.9	218	-
10	61.5	281	-
15	88.4	321	-
20	119.8	350	-
25	142.7	374	-

Time (msec)	Net IRDO (a) (mv)	ΔT_s^L (b) (calc.) (°C)	ΔT_s (c) (exp.) (°C)
Run No. 611-7-9 (Same Sample Used in Run 611-7-8, Surface Roughened and Coated with Philblack E)			
0	0	0	0
1	16.8	64	150
2	22.0	86	169
3	27.0	102	182
5	32.5	125	199
10	55.4	160	248
15	64.5	184	262
20	70.9	201	271
25	83.9	214	290
30	96.8	225	308
35	100.9	235	311
Run No. 611-8-1 (Same Sample Used in Run 611-7-9, Test Gas: Air)			
0	0	0	0
1	17.1	76	151
2	22.3	102	170
3	37.1	120	210
5	42.1	147	220
8	64.6	174	262
10	71.1	188	271
14	74.2	210	277
15	84.0	215	290
20	99.1	235	310
23	91.6	244	300
25	99.6	250	311
30	108.4	263	320
35	113.2	274	325

TABLE VI (continued)

C. DATA FOR PROPELLANT AQ

Time (msec)	Net IRDO (a) (mv)	ΔT_a^L (b) (calc.) (°C)	ΔT_a (c) (exp.) (°C)
Run No. 611-6-4 (Smooth Surface)			
0	0	0	-
1	3.7	72	-
2	8.1	96	-
3	12.6	114	-
5	19.4	140	-
10	37.6	178	-
15	57.0	204	-
20	67.0	223	-
25	80.1	238	-
30	87.1	250	-
35	92.8	260	-
40	99.7	269	-
Run No. 611-6-5 (Same Sample Used in 611-6-4)			
0	0	0	-
5	43.2	228	-
10	98.8	293	-
15	153.3	335	-
20	208	366	-
25	251	391	-
Run No. 611-6-6 (Same Sample Used in 611-6-5)			
0	0	0	-
1	7.0	128	-
2	19.1	172	-
3	31.0	204	-
5	65.7	250	-
10	141	322	-
15	210	370	-
20	263	405	-

Time (msec)	Net IRDO (a) (mv)	ΔT_a^L (b) (calc.) (°C)	ΔT_a (c) (exp.) (°C)
Run No. 611-6-7 (Same Sample Used in 611-6-6, Ignited)			
0	0	0	0
1	10.5	162	141
2	39.4	219	225
3	54.8	260	250
4	83.9	291	289
5	119	318	321
6	144	341	341
7	175	361	370
8	203	379	384
9	231	395	399
10	271	410	420
11	310	425	440
12	405	437	475
13	675	449	555
Run No. 611-6-8 (Smooth Surface)			
0	0	0	-
1	14.3	119	-
2	17.7	161	-
3	24.0	190	-
5	41.8	234	-
10	98.4	302	-
15	167	347	-
20	217	381	-
25	254	408	-

TABLE VI (continued)

C. DATA FOR PROPELLANT AQ (continued)

Time (msec)	Net 1RDO (a) (mv)	ΔT_s^L (b) (calc.) (°C)	ΔT_s (c) (exp.) (°C)
Run No. 611-6-9 (Same Sample Used in 611-6-8, Ignited)			
0	0	0	0
1	13.7	151	154
2	31.4	204	208
3	37.6	242	220
5	85.7	296	290
8	146	354	345
10	195	384	375
11	200	397	380
12	232	409	400
13	262	420	412
14	283	431	425
15	375	441	462
16	615	-	540
17	845	-	600
Run No. 611-6-10 (Smooth Surface; surface temperature started to rise near end of test.)			
0	0	0	0
1	11.3	131	145
2	17.7	176	170
3	30.0	208	205
5	53.8	255	250
10	112.4	328	318
15	197	375	380
20	256	410	410
25	296	438	430
30	313	-	440
32	331	-	447
35	401	-	472
37	450	-	490
38	455	-	492
40	425	-	482
45	413	-	479

TABLE VI (continued)

D. DATA FOR PRESSED PROPELLANT PP-CBM

Time (msec)	Net IRDO (a) (mv)	ΔT_s^L (b) (calc.) (°C)	ΔT_s (c) (exp.) (°C)
Run No. 610-25-13 (Smooth Surface)			
0	0	0	-
1	8.0	105	-
2	16.9	143	-
3	24.2	170	-
5	40.0	209	-
10	79.4	272	-
15	113.8	314	-
20	145.3	345	-
25	152.8	370	-
Run No. 610-25-14 (Same Sample Used in 610-25-13, Ignited)			
0	0	0	0
1	11.	114	111
2	24.6	154	161
3	34.0	184	188
5	57.7	226	240
10	107.6	295	318
12	128.4	316	340
13	139.2	325	351
14	148	333	362
15	172	341	389
16	231	349	440
17	276	356	471
18	471	363	585
Run No. 610-25-15 (Smooth Surface)			
0	0	0	-
1	11.1	102	-
2	16.9	138	-
3	24.2	164	-
5	38.1	203	-
10	74	264	-
15	96	305	-
20	120	336	-
25	140	360	-
30	151	381	-
Run No. 610-25-16 (Same Sample Used in 610-25-15)			
0	0	0	-
1	12.7	108	-
2	22.6	147	-
3	28.0	175	-
5	52.7	216	-
10	81.6	283	-
15	111.8	329	-
20	140.3	363	-
25	160.3	390	-
Run No. 610-25-17 (Same Sample Used in 610-25-16, Ignited)			
0	0	0	0
1	17.6	128	138
2	36.4	175	194
3	49.7	208	223
5	76.0	258	271
7	90.0	295	291
10	128	339	340
12	156	362	361
13	168	373	381
14	176	383	391
15	189	393	400
16	198	402	410
17	215	411	426
18	245	419	450
19	295	427	487
20	566	434	630

TABLE VI (continued)

D. DATA FOR PRESSED PROPELLANT PP-CBM (continued)

Time (msec)	Net IRDO (a) (mv)	ΔT_s^L (b) (calc.) (°C)	ΔT_s (c) (exp.) (°C)
Run No. 611-6-17 (Smooth Surface, Coated with Thin Layer of Philblack E)			
0	0	0	-
1	7.2	62	-
2	12.0	85	-
3	15.4	101	-
5	21.3	124	-
10	33.9	162	-
15	52.8	186	-
20	61.9	205	-
25	68.9	220	-
30	76.8	233	-
35	84.5	243	-
Run No. 611-6-18 (Same Sample Used in 611-6-17)			
0	0	0	-
1	17.3	99	-
2	27.7	135	-
3	36.0	161	-
5	61.8	199	-
10	109.4	261	-
15	144.6	303	-
20	183	335	-
21	192	341	-
22	205	346	-
23	219	351	-
24	236	356	-
25	239	361	-
26	253	365	-

TABLE VI (continued)

E. DATA OF PRESSED PROPELLANT PP-E

Time (msec)	Net IRDO (a) (mv)	ΔT_s^* (b) (calc.) (°C)	ΔT_s (c) (exp.) (°C)
Run No. 610-25-5			
0	0	0	-
1	5.9	101	-
2	9.7	137	-
3	15.5	163	-
5	28.8	202	-
10	59.9	265	-
15	90.8	308	-
20	114.2	340	-
25	133.4	366	-
30	148.6	388	-
Run No. 610-25-6			
0	0	0	-
1	7.8	105	-
2	12.9	143	-
3	19.0	169	-
5	34.0	209	-
10	64.1	272	-
15	95.6	314	-
20	125.0	346	-
25	153.4	371	-
30	169.4	393	-
Run No. 610-25-7 (Same Sample Used in 610-25-6 Ignited)			
0	0	0	0
1	13.0	125	139
2	24.4	170	180
3	34.4	202	208
5	60.4	250	261
10	111.6	328	335
11	120.2	340	342
12	136.8	351	361
13	150.4	362	373
14	167.9	371	390
15	191.2	381	412
16	235	389	449
17	319	398	500

TABLE VI (continued)

F. DATA FOR PRESSED PROPELLANT PP-P

Time (msec)	Net IRDO (a) (mv)	ΔT_s^L (b) (calc.) (°C)	ΔT_s (c) (exp.) (°C)
Run No. 611-7-4			
0	0	0	-
1	3.8	110	-
2	8.6	150	-
3	11.0	178	-
5	21.7	220	-
10	41.6	288	-
15	63.8	333	-
20	98.2	368	-
25	115.2	396	-
Run No. 611-7-5 (Same Sample Used in 611-7-4, Ignited)			
0	0	0	0
1	3.7	131	118
2	10.4	178	175
3	15.6	212	203
5	28.8	262	255
10	52.2	344	319
15	100.2	398	400
20	162.8	439	475
21	215	-	515
22	265	-	560
23	310	-	595

TABLE VI (continued)

G. DATA FOR PRESSED AMMONIUM PERCHLORATE

Time (msec)	Net IRDO (a) (mv)	T_s^L (b) (calc.) (°C)
Run No. 610-25-2		
0	0	0
2	7.7	155
3	10.0	184
5	19.7	227
10	39.0	295
15	56.2	341
20	77.7	376
25	94.8	403
Run No. 610-25-3 (Same Sample Uaed in 610-25-2)		
0	0	0
1	5.5	123
2	9.9	168
3	15.9	200
5	27.9	248
10	43.8	326
15	75.4	378
20	97.0	418
Run No. 610-25-4 (Same Sample Used in 610-25-3)		
0	0	0
1	4.1	136
2	13.3	185
3	21.4	221
5	37	274
10	56	361
15	96	419
20	136	463

TABLE VI (continued)

H. DATA FOR DOUBLE-BASE PROPELLANT JPN			
Time (msec)	Net IRDO (a) (mv)	ΔT_g^L (b) (calc.) (°C)	ΔT_g (c) (exp.) (°C)
Run No. 69-21-11			
0	0	0	-
2	4.6	109	-
3	6.9	127	-
5	9.7	154	-
7	12.9	173	-
10	19.0	195	-
15	25.7	220	-
20	31.0	239	-
25	37.7	253	-
30	41.8	265	-
35	45.8	275	-
40	49.8	283	-
Run No. 69-21-12 (Same Sample Used in 69-21-11, Ignited)			
0	0	0	0
2	24.0	205	220
3	31.8	242	241
4	39.9	271	261
5	49.0	294	283
6	95.9	-	359
6.5	88.9	-	348
7	106.3	-	370
8	72.8	-	325
8.5	58.2	-	300
9	59.7	-	302
10	149.6	-	412
10.5	182.8	-	440
11.5	68.6	-	320

TABLE VI (continued)

I. DATA FOR PBAA BINDER:

Time (msec)	Net IRDO (s) (mv)	ΔT_s^L (b) (calc.) (°C)
Run No. 610-25-8		
0	0	0
1	2.8	178
2	6.1	236
3	10.0	276
5	19.7	332
10	42.6	416
15	62.6	469
20	84.2	506
25	99.2	535
30	116.5	558
Run No. 610-25-9 (Same Sample Used in 610-25-8, Tested in Air)		
0	0	0
2	6.6	227
3	12.5	266
5	24.7	321
10	51.0	403
15	78.2	454
20	99.7	491
25	112	520
30	125	543
Run No. 610-25-10 (Sample Costed with Philblack E)		
0	0	0
1	14.2	168
2	25.7	224
3	37.0	262
5	59.8	316
10	113.2	398
15	159.5	449
20	194	486
24	220	509
Run No. 610-25-11 (Tested in Air)		
0	0	0
2	13.7	301
3	19.4	352
5	37.0	425
10	75.5	536
15	109.4	604
20	139	654
Run No. 610-25-12 (Same Sample Used in 610-25-11)		
0	0	0
1	6.0	232
2	16.2	309
3	28.6	362
5	56.0	438
10	105.6	552
15	152	624

TABLE VI (continued)

J. DATA FOR POLYURETHANE BINDER		
Time (msec)	Net IRDO (a) (mv)	ΔT_s^L (b) (calc.) (°C)
Run No. 69-22-1		
0	0	0
2	26.3	235
3	35.0	275
5	68.0	331
10	138	414
15	184	466
20	233	503
Run No. 69-22-2 (Teated in Air)		
0	0	0
1	17.0	184
2	26.0	244
3	40.8	285
5	76.8	342
10	177	429
15	239	482
20	291	520
25	315	549

(a) Net IRDO is the total IR detector output after adjustment for background effects.

(b) The term ΔT_s^L is the temperature at the propellant's surface relative to room temperature that is calculated assuming the propellant is a semi-infinite body undergoing transient heating through a constant heat transfer coefficient from a hot gas of temperature, T_g. It is further assumed that the temperature rise is produced only by external heating with no contributions from reactions at the surface of the propellant (linear heating).

(c) The term ΔT_s is the propellant surface temperature relative to room temperature determined experimentally by comparing the Net IRDO with the generalized graph of Net IRDO versus ΔT_a^L, extrapolated for temperatures above about 400°C.

(d) Surface was roughened over a small area near the center of the sample by sanding with silicon carbide paper (320-A grit size). Loose material on the surface was brushed off.

TABLE VII

IGNITION DATA ON PROPELLANTS

A. IGNITION TIME AND HEAT FLUX

Run No.	ΔT_{si}^{L} (°K)	T_{si}^{L} (°K)	t_i (msec)	$(t_i)^{1/2}$ $(msec)^{1/2}$	$\overline{F}_s$ (a) cal/(cm^2)(sec)	Sample Surface
		1. Dsts Obtained with RCA 1P40 Photocell				
		Propellant UA-14, Flow-Control Orifice: No. 5A(b)				
61-11-4	403	698	12.5	3.54	64.8	Smooth
62-2-10	407	703	25.3	5.04	46.0	Smooth
62-2-11	394	690	15.5	3.94	56.8	Smooth
62-2-12	382	678	11.7	3.42	63.5	Smooth
62-2-13	402	699	24.1	4.91	46.6	Smooth
		Propellsnt UA-14, Flow-Control Orifice: No. 4A(c)				
62-3-11	414	710	9.3	3.05	77.0	Smooth
62-4-1	408	700	19.5	4.41	52.6	Smooth
62-4-2	396	688	12.7	3.56	63.2	Smooth
62-4-3	399	692	8.6	2.93	77.3	Smooth
62-4-5	394	688	13.2	3.64	61.8	Smooth
		Propellant UA-14, Flow-Control Orifice: No. 3A(d)				
61-11-5	432	728	6.3	2.51	97.9	Smooth
62-3-6	457	752	5.9	2.43	106.9	Smooth
62-3-7	439	734	7.9	2.81	88.7	Smooth
62-3-8	453	749	14.6	3.82	67.4	Smooth
62-3-9	411	707	12.0	3.46	67.5	Smooth
62-3-10	433	729	24.0	4.90	50.2	Smooth
		2. Data Obtained with Philco GPC-201A IR Detector (d)				
		Propellant UA-18				
69-3-4	459	752	10.1	3.18	82.1	Smooth
611-6-21	428	728	15.5	3.94	61.9	Smooth
611-6-22	407	706	17.5	4.19	55.3	Polymer-Rich
611-6-24	203	503	3.6	1.90	49.1	Rough

A. IGNITION TIME AND HEAT FLUX (continued)

Run No.	ΔT_{ai}^{L} (°K)	T_{ai}^{L} (°K)	t_i (msec)	$(t_i)^{1/2}$ $(maec)^{1/2}$	$\overline{F}_s$ (a) cal/(cm^2)(sec)	Sample Surface
			Propellant AR-1			
69-21-16	427	729	29.0	5.39	44.9	Smooth
69-22-6	459	760	25.9	5.09	51.0	Smooth
69-22-8	465	767	28.8	5.36	49.1 (Test Gas: Air)	Smooth
611-6-11	412	711	14.0	3.72	62.3	Smooth
611-6-12	426	726	15.2	3.90	61.9	Smooth
611-6-13	455	754	14.8	3.84	70.0	Smooth
611-6-14	386	685	22.8	4.78	45.7	Smooth
611-6-19	409	709	13.0	3.60	64.3	Smooth
611-6-25	392	692	19.5	4.41	50.3	Rough
611-7-7	275	573	12.6	3.55	43.9	Rough
611-8-2	309	604	14.2	3.77	46.4	Rough
			Propellant AQ-1			
611-6-7	437	736	12.0	3.46	69.6	Smooth
611-6-9	449	749	15.9	3.99	62.2	Smooth
			Propellant FM-86			
69-3-2	360	652	20.9	4.57	46.7	Rough
69-3-5	329	622	11.2	3.34	58.3	Rough
			Double-Base Propellant JPN			
69-21-9	289	590	9.1	3.02	47.5	Smooth
69-21-10	338	640	13.6	3.68	45.5	Smooth
69-21-12	317	618	6.1	2.47	63.7	Smooth
			Preased Propellant PP-CBM-1			
68-15-3	377	682	35.2	5.94	44.1	Smooth
68-18-9	386	689	18.2	4.26	62.9	Smooth
68-18-10	376	679	16.5	4.06	64.3	Smooth
69-2-13	320	615	15.8	3.98	56.0	Smooth
69-2-14	361	655	22.7	4.76	52.6	Smooth
69-3-1	425	718	29.2	5.40	54.7	Smooth
610-25-14	360	663	17.6	4.20	59.7	Smooth
610-25-17	427	730	19.1	4.37	67.9	Smooth
			Preaaed Propellant PP-E-1			
610-25-7	360	663	16.1	4.01	66.5	Smooth
			Preaaed Propellant PP-F-1			
611-7-5	450	748	21.5	4.64	66.3	Smooth

TABLE VII (continued)

B. SHOCK-TUBE AND HEAT-TRANSFER DATA

Run No.	M_E	T_0 (°K)	T_g (°K)	P_4' (atm)	$\frac{G}{g}$ $\frac{}{(cm^2)(aec)}$	$\frac{h}{cal}$ $\frac{}{(cm^2)(aec)(°K)}$
			Propellant UA			
61-11-4	3.43	295	1751	20.6	22.3	0.0567
62-2-10	3.04	296	1428	20.1	24.2	0.0579
62-2-11	3.26	297	1593	20.6	23.5	0.0584
62-2-12	3.41	297	1729	20.1	21.9	0.0566
62-2-13	3.04	297	1434	20.2	24.3	0.0580
62-3-11	3.42	296	1735	19.5	27.4	0.0702
62-4-1	2.99	291	1388	18.6	29.4	0.0694
62-4-2	3.20	292	1513	19.3	29.1	0.0707
62-4-3	3.42	293	1698	19.9	28.4	0.0717
62-4-5	3.06	294	1443	20.6	32.0	0.0751
61-11-5	3.45	296	1764	19.9	42.2	0.0878
62-3-6	3.49	296	1813	21.4	44.8	0.0935
62-3-7	3.23	296	1594	21.1	47.3	0.0947
62-3-8	3.03	296	1427	19.4	46.0	0.0893
62-3-9	2.84	296	1318	21.4	52.9	0.0993
62-3-10	2.60	296	1072	21.2	56.4	0.1015
69-3-4	3.41	293	1698	17.8	38.7	0.0799
611-6-21	2.99	300	1421	17.4	41.5	0.0809
611-6-22	2.89	300	1337	16.8	41.3	0.0791
611-6-24	2.66	300	1215	16.9	43.8	0.0812
			Propellant AR			
69-21-16	2.56	301	1146	19.4	51.6	0.0931
69-22-6	2.74	301	1258	19.0	48.2	0.0897
69-22-8	2.74	301	1253	18.6	47.2	0.0880
611-6-11	3.01	300	1426	17.1	40.6	0.0793
611-6-12	2.99	300	1424	17.3	41.1	0.0802
611-6-13	3.09	300	1498	17.8	41.1	0.0815
611-6-14	2.58	300	1168	17.4	45.9	0.0839
611-6-19	2.97	300	1416	17.8	42.5	0.0827
611-6-25	2.69	300	1231	17.5	44.9	0.0834
611-7-7	2.42	298	1042	17.3	48.4	0.0851
611-8-2	2.48	295	1076	18.2	50.0	0.0887
			Propellant AQ			
611-6-7	3.04	299	1465	18.8	44.2	0.0866
611-6-9	3.01	300	1427	17.8	42.3	0.0826
			Propellant FM			
69-3-2	2.52	293	1101	19.0	51.8	0.0923
69-3-5	2.74	293	1232	18.4	47.1	0.0873

TABLE VII (continued)

B. SHOCK-TUBE AND HEAT-TRANSFER DATA (continued)

Run No.	M_E	T_0 (°K)	T_g (°K)	P_4' (atm)	$\frac{G}{g}$ $\frac{}{(cm^2)(aec)}$	$\frac{h_{cal}}{(cm^2)(sec)(°K)}$
			Pressed Propellant PP-CBM			
68-15-3	2.48	305	1091	19.5	53.2	0.0943
68-18-9	2.77	303	1292	20.1	50.2	0.0940
68-18-10	2.70	303	1273	20.9	52.7	0.0979
69-2-13	2.69	294	1197	18.4	47.8	0.0878
69-2-14	2.68	295	1185	18.6	48.8	0.0892
69-3-1	2.77	293	1248	19.3	49.2	0.0913
610-25-14	2.74	303	1246	19.6	50.0	0.0926
610-25-17	3.03	302	1469	18.2	42.5	0.0836
			Pressed Propellant PP-E			
610-25-7	2.98	302	1414	18.2	43.4	0.0842
			Pressed Propellant PP-P			
611-7-5	3.01	298	1444	18.6	44.0	0.0859
			Double-Base Propellant JPN			
69-21-9	2.45	301	1059	18.8	52.1	0.0918
69-21-10	2.50	301	1103	18.0	49.0	0.0876
69-21-12	2.75	302	1266	19.1	48.3	0.0902

Notes:

(a) $\overline{F}_s$ is the mean externally applied surface heat flux. This is the value of constant heat flux required to bring the propellant surface to the temperature ΔT_{si}^{L} in the observed ignition time.

$$\overline{F}_s = \frac{\Gamma_p}{2} \left(\frac{\pi}{t_i}\right) \left(\Delta T_{si}^{L}\right)$$

(b) Flow-control orifice No. 5A gave an area ratio (A_{or}/A_{ts}) relative to the test-section area of 0.115, and a Mach number (M_{ts}) of 0.07 for gas flowing through the test section.

(c) Flow-control orifice No. 4A gave an area ratio of 0.149 and a M_{ts} of 0.09.

(d) Flow-control orifice No. 3A was used for all runs with the IR detector. This orifice gave an area ratio of 0.227 and a M_{ts} of 0.13.

TABLE VIII

CALCULATED TEMPERATURE HISTORIES FOR THERMAL IGNITION

A. TEMPERATURE-TIME DATA

Run No. 611-6-11
(Propellant AR)

Time (msec)	ΔT_s (°K)	T_s (°K)
0	0	299.5
0.20	67.9	367.4
0.79	128.4	427.9
1.99	191.8	491.3
3.97	260.0	555.5
5.96	300.7	600.2
7.94	336.2	635.7
9.93	367.2	666.7
11.92	397.9	697.4
12.71	411.9	711.4
13.11	419.9	719.4
13.51	429.0	728.5
13.90	440.5	740.0
14.10	447.8	747.4
14.30	457.5	757.0
14.50	472.1	771.6
14.70	511.1	810.6
14.74	544.9	844.4

Run No. 611-6-13
(Propellant AR)

0	0	299.5
0.14	61.4	360.9
0.82	140.8	440.3
1.84	201.2	500.7
5.25	309.9	609.4
6.96	346.2	645.7
8.67	378.9	678.4
10.37	413.5	713.0
10.88	426.5	726.0
11.23	437.2	736.7
11.57	451.5	751.0
11.74	461.7	761.2
11.91	477.9	777.4
12.05	509.3	808.8
12.08	533.7	833.3

Run No. 66-11-6-14
(Propellant AR)

Time (msec)	ΔT_s (°K)	T_s (°K)
0	0	299.5
0.30	67.3	366.8
1.49	137.4	436.9
2.98	184.2	483.7
5.97	242.3	541.8
8.95	281.7	581.2
11.94	312.2	611.7
14.92	337.6	637.1
17.91	360.1	659.6
20.89	382.1	681.6
22.38	393.6	693.1
23.88	406.5	706.0
24.47	412.5	712.0
25.07	419.3	718.8
25.67	427.2	726.7
26.56	444.1	743.6
26.86	453.1	752.6
27.15	467.5	767.0
27.45	515.7	815.2
27.52	623.3	922.8

Run No. 66-11-6-21
(Propellant UA)

0	0	299.7
0.20	68.2	367.9
0.98	143.0	442.7
1.97	193.7	493.4
3.93	258.5	558.2
5.90	303.6	603.3
7.87	339.4	639.1
9.83	370.8	670.5
10.82	386.2	685.9
11.80	402.6	702.3
12.59	417.7	717.4
12.98	426.7	726.4
13.37	437.7	737.4
13.77	453.1	752.8
13.96	465.1	764.8
14.16	488.0	787.7
14.24	511.4	811.1
14.28	546.4	846.1

TABLE VIII (continued)

B. DATA USED FOR CALCULATIONS

Run No. Propellant Code	611-6-11 AR	611-6-13 AR	611-6-14 AR	611-6-21 UA
Γ_p, cal/(cm^2)(sec)$^{1/2}$(°K)	0.0203	0.0203	0.0203	0.0203
T_g, °K	1426	1493	1168	1421
T_o, °K	299.5	299.5	299.5	299.7
E_a/R, °K	15,500	15,500	15,500	15,500
B, cal/(cm^2)(sec)	2.35×10^{10}	2.35×10^{10}	2.35×10^{10}	2.35×10^{10}
h, cal/(cm^2)(sec)(°K)	0.0793	0.0816	0.0839	0.0809

APPENDIX E. FIGURES

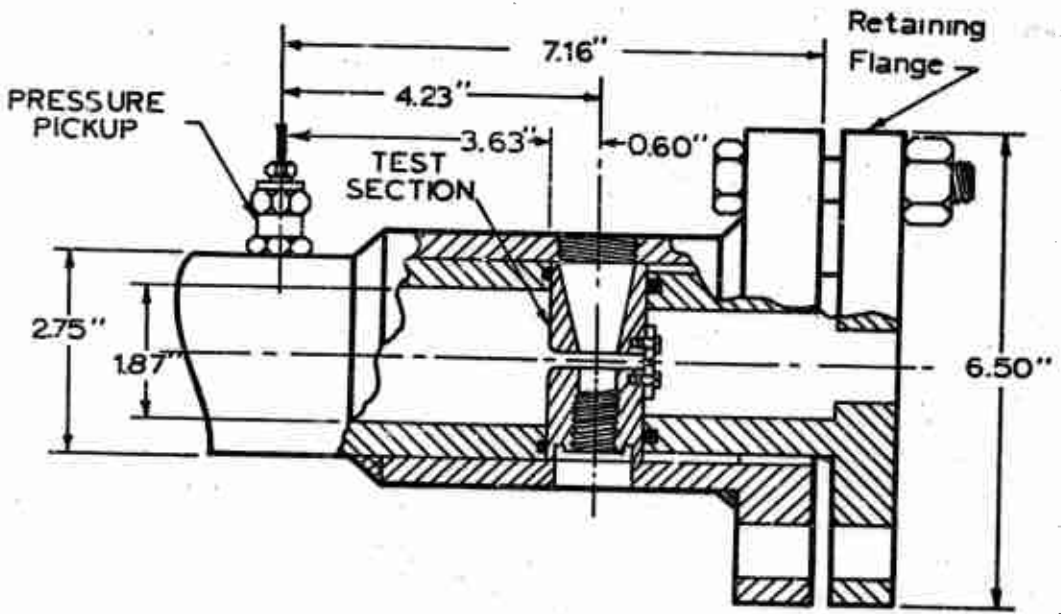

Figure 1. Sketch of Driven End of Shock Tube, Showing Position of the Test Section.

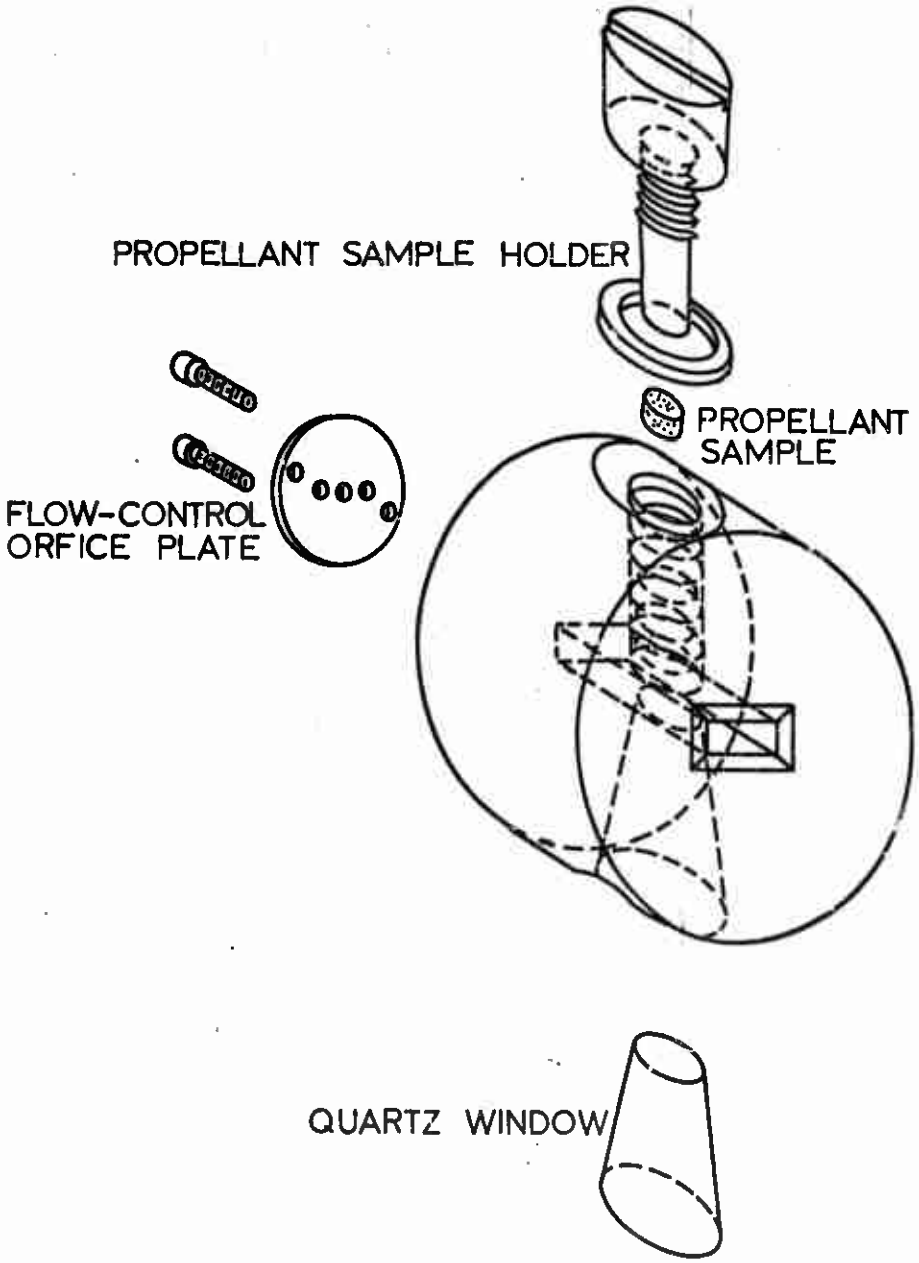

FIGURE 2. Sketch of Test Section.

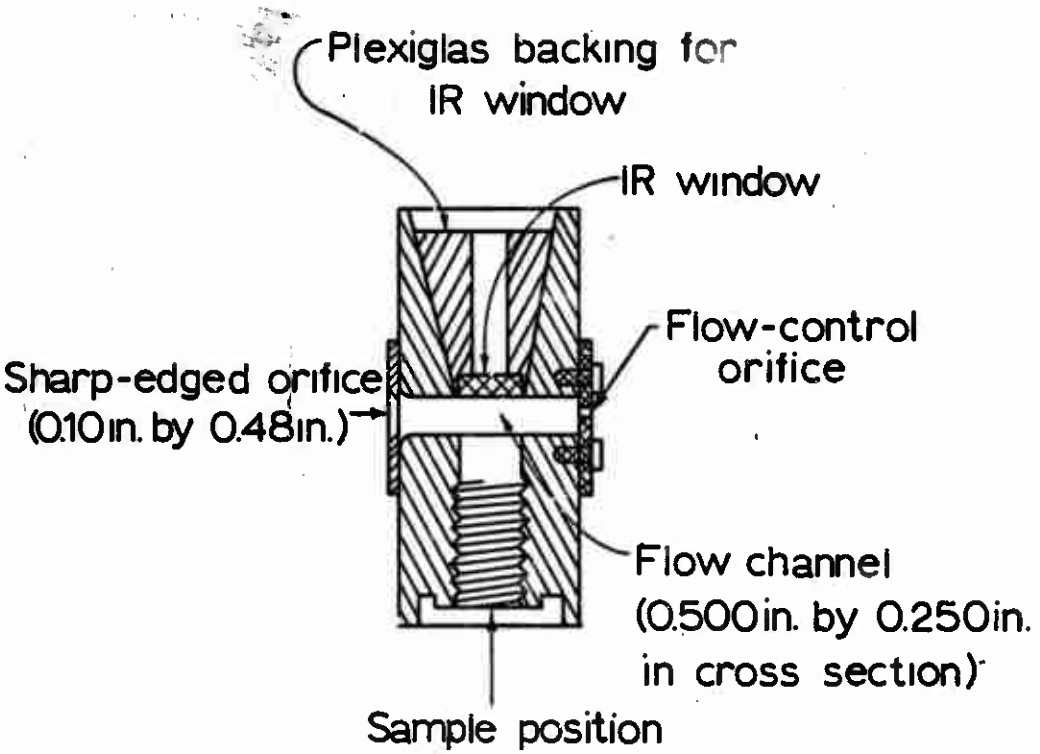

FIGURE 3. Shock-tube Test Section as Modified for Measuring Surface Temperatures on Propellants During Ignition.

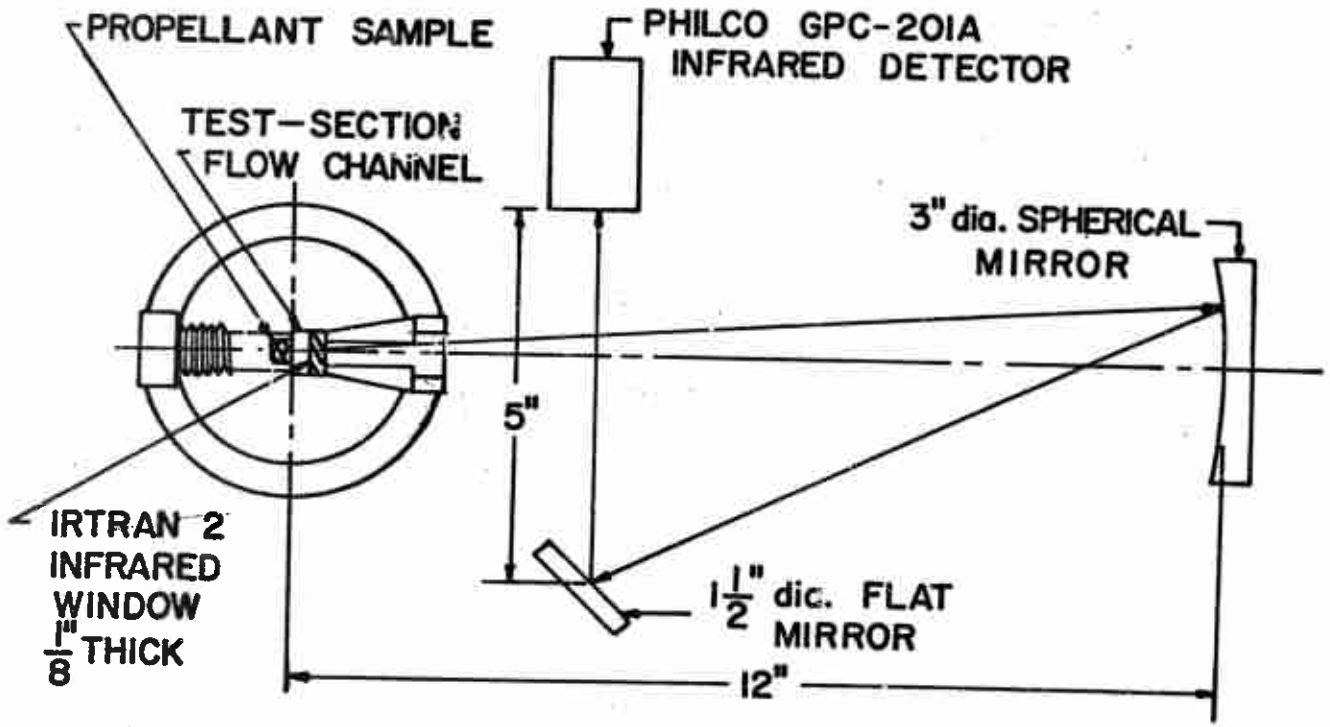

FIGURE 4. Radiation Detection System for Temperature Measurements.

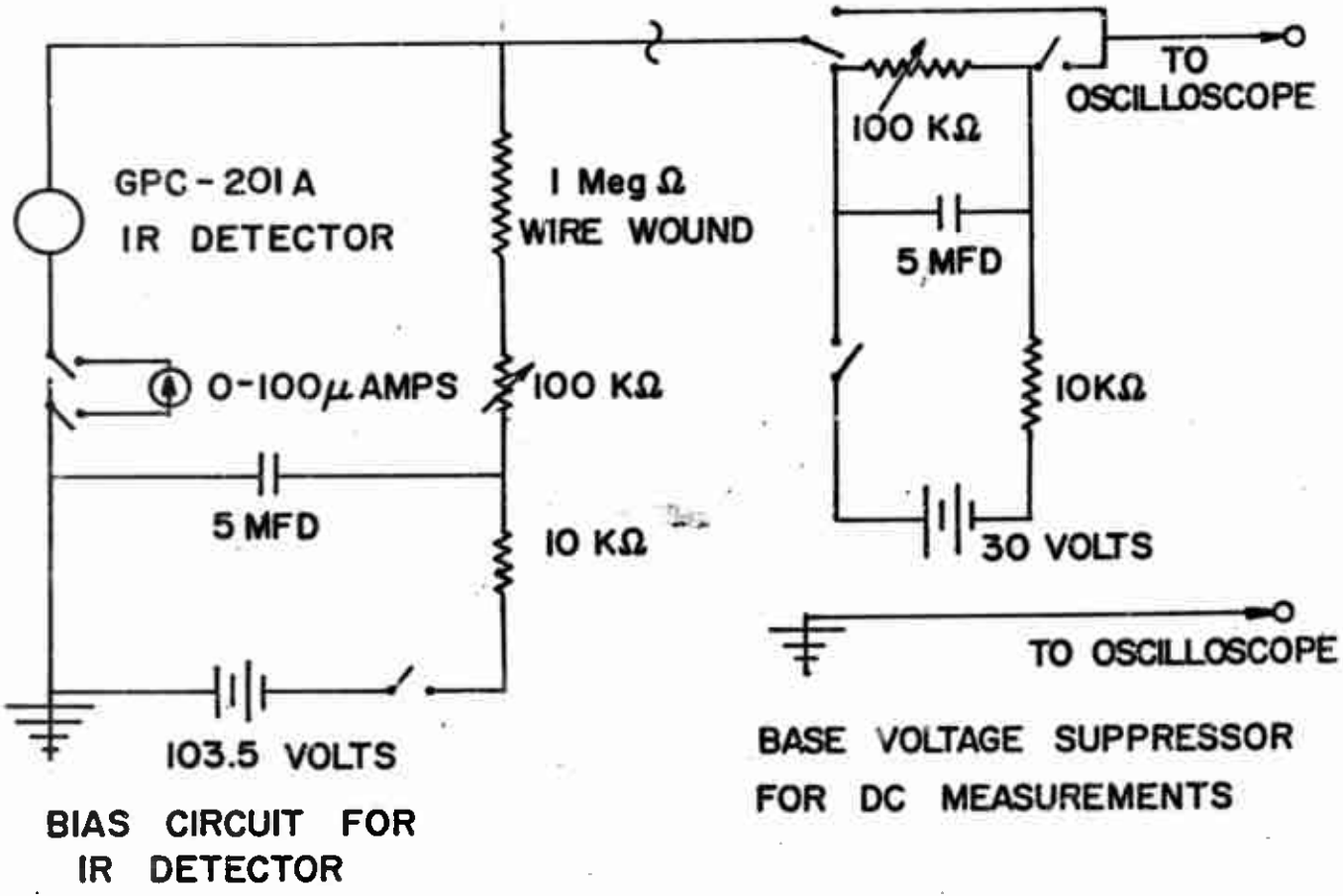

FIGURE 5. Electrical Circuit for Infrared Detector.

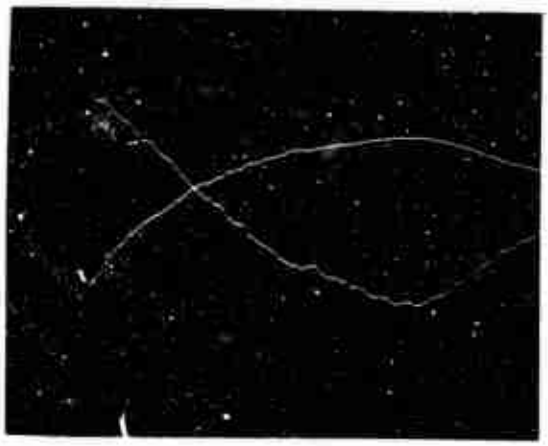

a. Invarted Trace: IR Detector Output, 40 mv/(div.). Normal Trace: Heat-flux Gage Temperature, 50°C/(div.). Sweep Rate: 5 maec/(div.) (Left to Right).

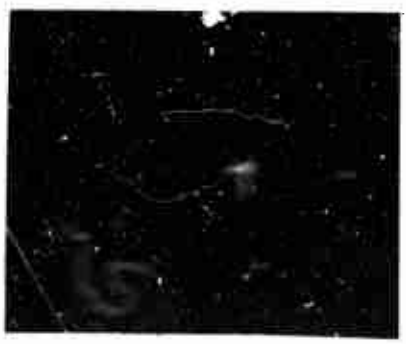

b. Inverted Trace: IR Detector Output: 40 mv/(div.). Normal Trace: Pressure in Shock-tube Driven Section, 50 paig/(div.) Sweep Rate: 5 maec/(div.) (Right to Left).

FIGURE 6. Oscillographa of Shock-tube Runa for Calibration of IR Detector with Carbon-coated Heat-flux Gage aa the Infrared Source. Run No. 66-10-8-1/. Shock Mach No.: 2.95. Convective Gas Temperature: 1410°K.

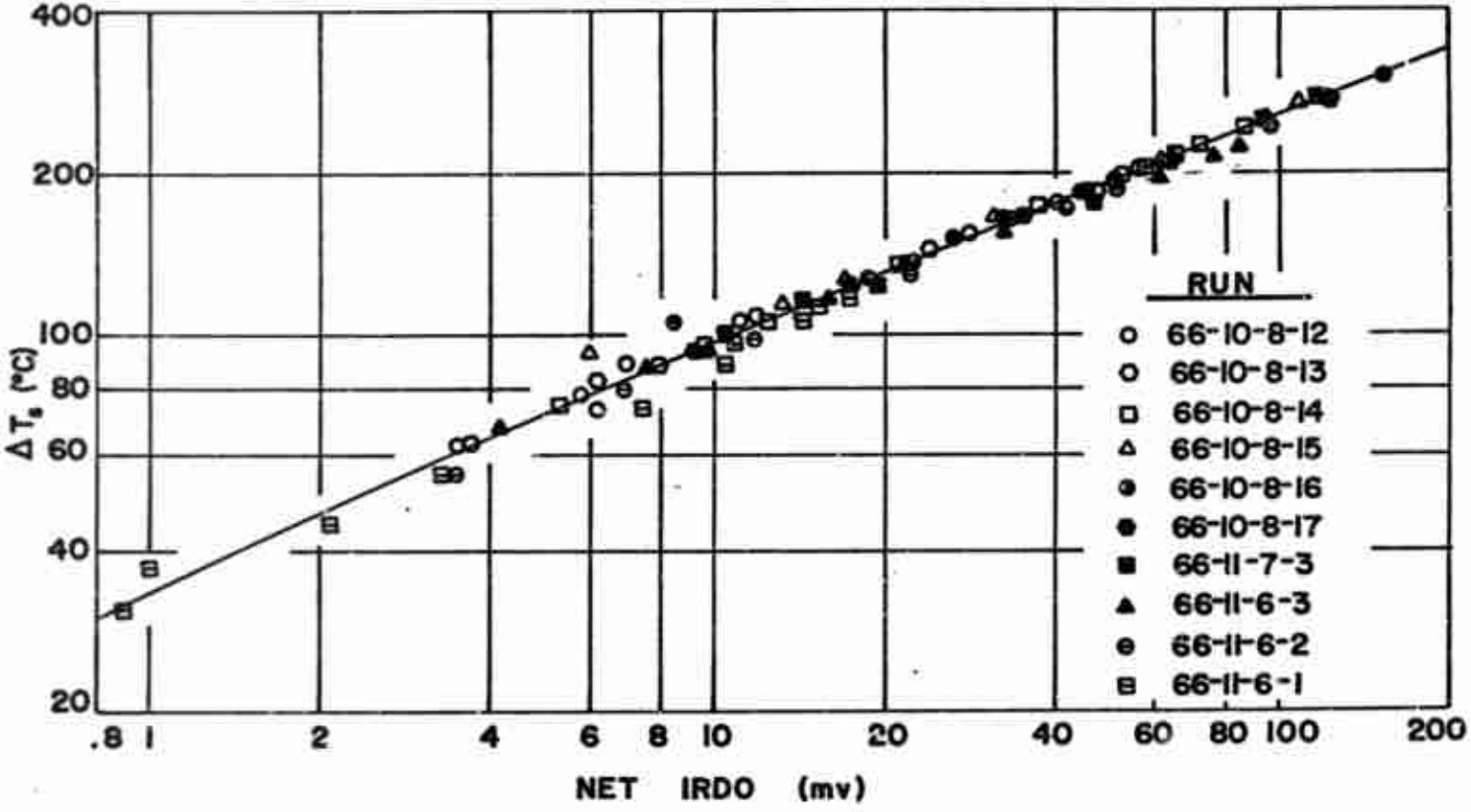

FIGURE 7. Surface Temperature for Blackened Heat-flux Gage Veraua Net Infrared-detector Output. (Temperature Measured at Platinum Film was Adjusted for Carbon Layer on the Surface.)

a. Run No. 610-8-5. Shock Mach No.: 2.52, Gas Temperature: 1115°K.

b. Run No. 610-8-8, Shock Mach No.: 3.09, Gas Temperature: 1345°K.

FIGURE 8. Oscillographs of Shock-tube Runs for Measurement of Background Radiation (IR Source: Polished Brass Surface). Inverted Trace: IR Detector Output 5 mv/(vert. div.). Normal Trace: Pressure in Driven Section, 50 psig/(vert. div.). Sweep Rate: (Right to Left), 5 msec/(div.)

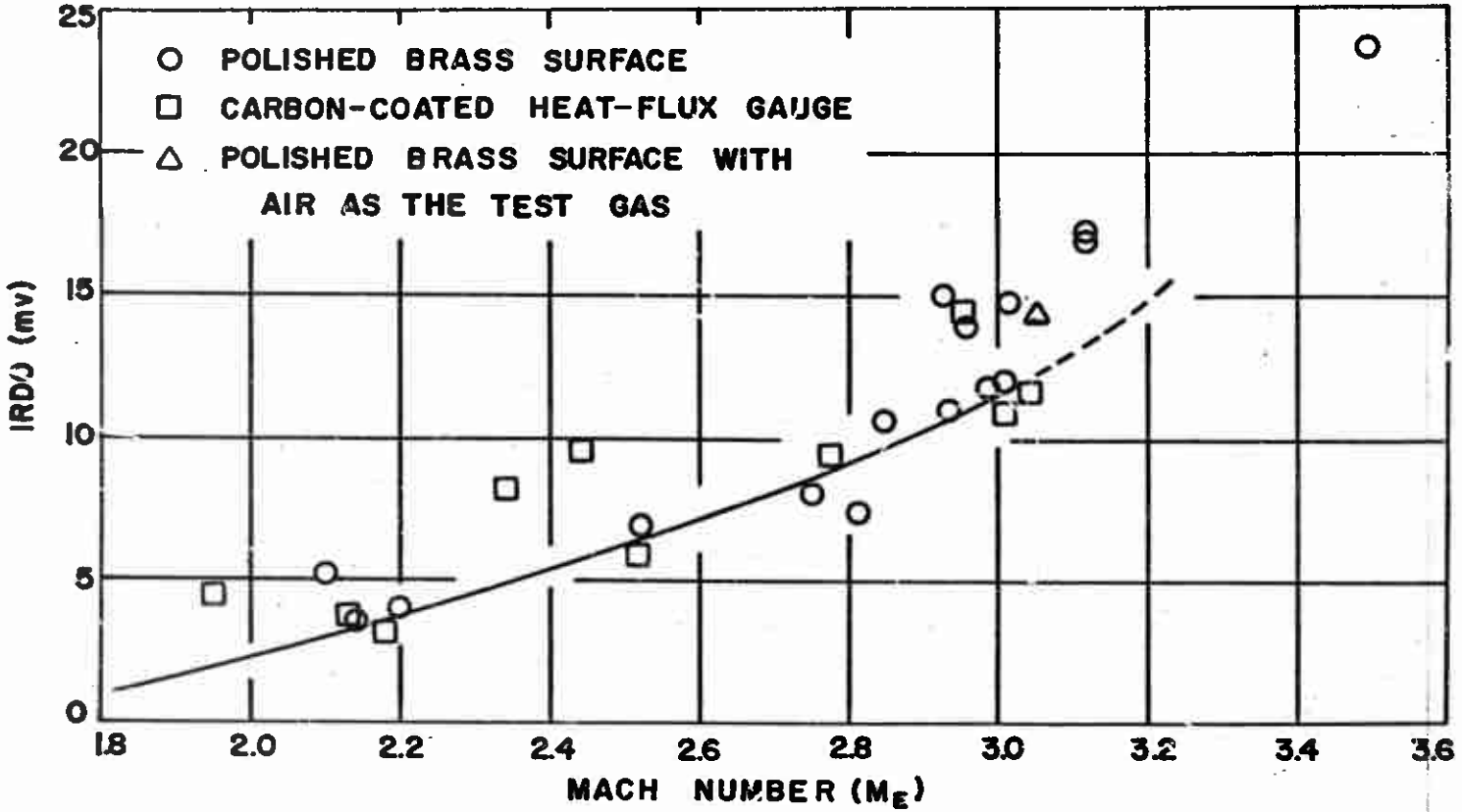

FIGURE 9. Background Radiation Data for Infrared Detection System (10 Milliseconds of Test)(Test Gas: Nitrogen).

a. IR Detector Output, 40 mv/(div.). Sweep Rate (Right to Left), 2 msec/(div.).

b. Inverted Trace: IR Detector Output, 200 mv/(div.). Normal Trace: Pressure in Shock Tube, 50 psig/(div.). Sweep Rate (Right to Left) 5 msec/(div.).

FIGURE 10. Oscillographs for Surfsce Temperature Messurements on Propellant UA with IR Detector. Run No. 611-6-21. Shock Mach Number: 3.0. Convective Gas Temperature: 1420°K.

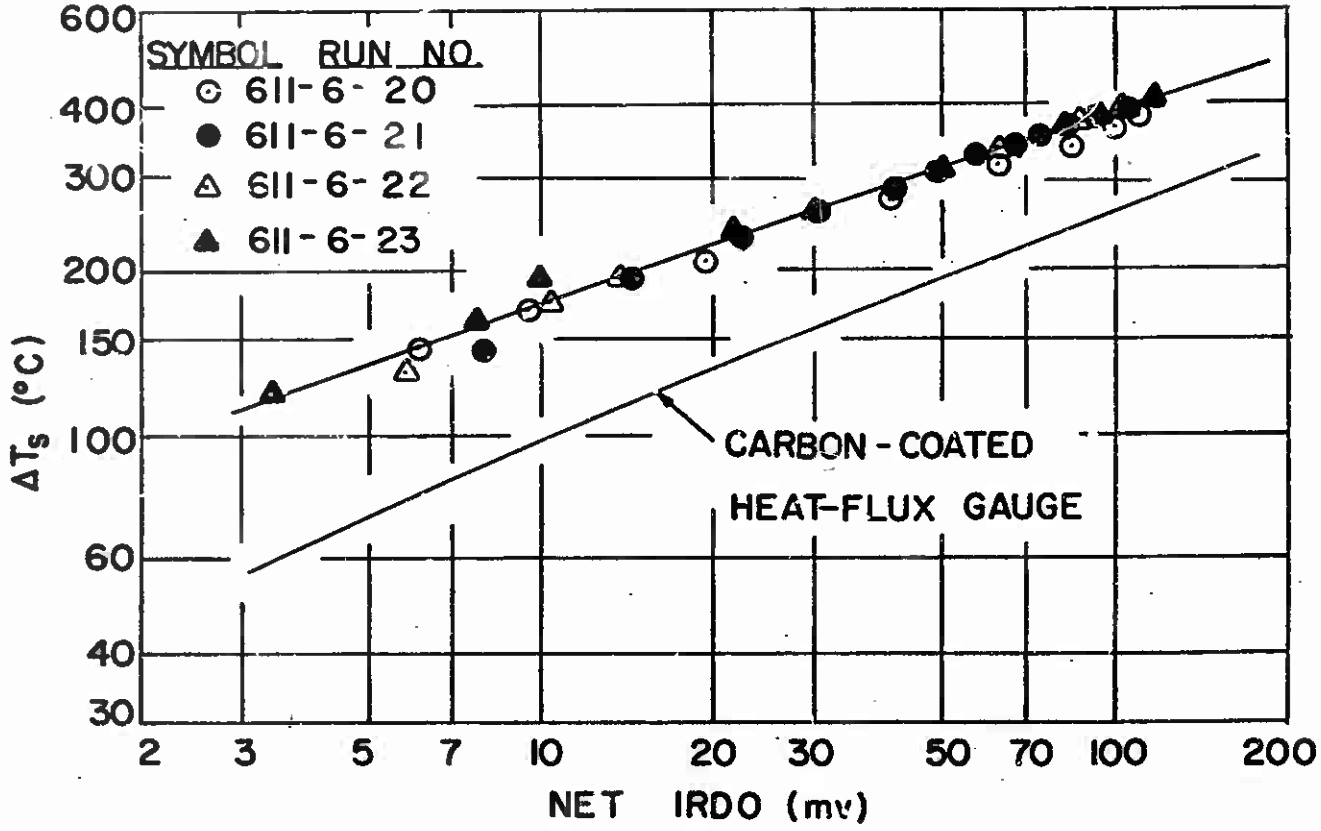

FIGURE 11. Infrared-detector Output Versus Calculated Surface Temperature for Linear Heating of Propellant UA. (Data for Samples with Smooth Surfacea.)

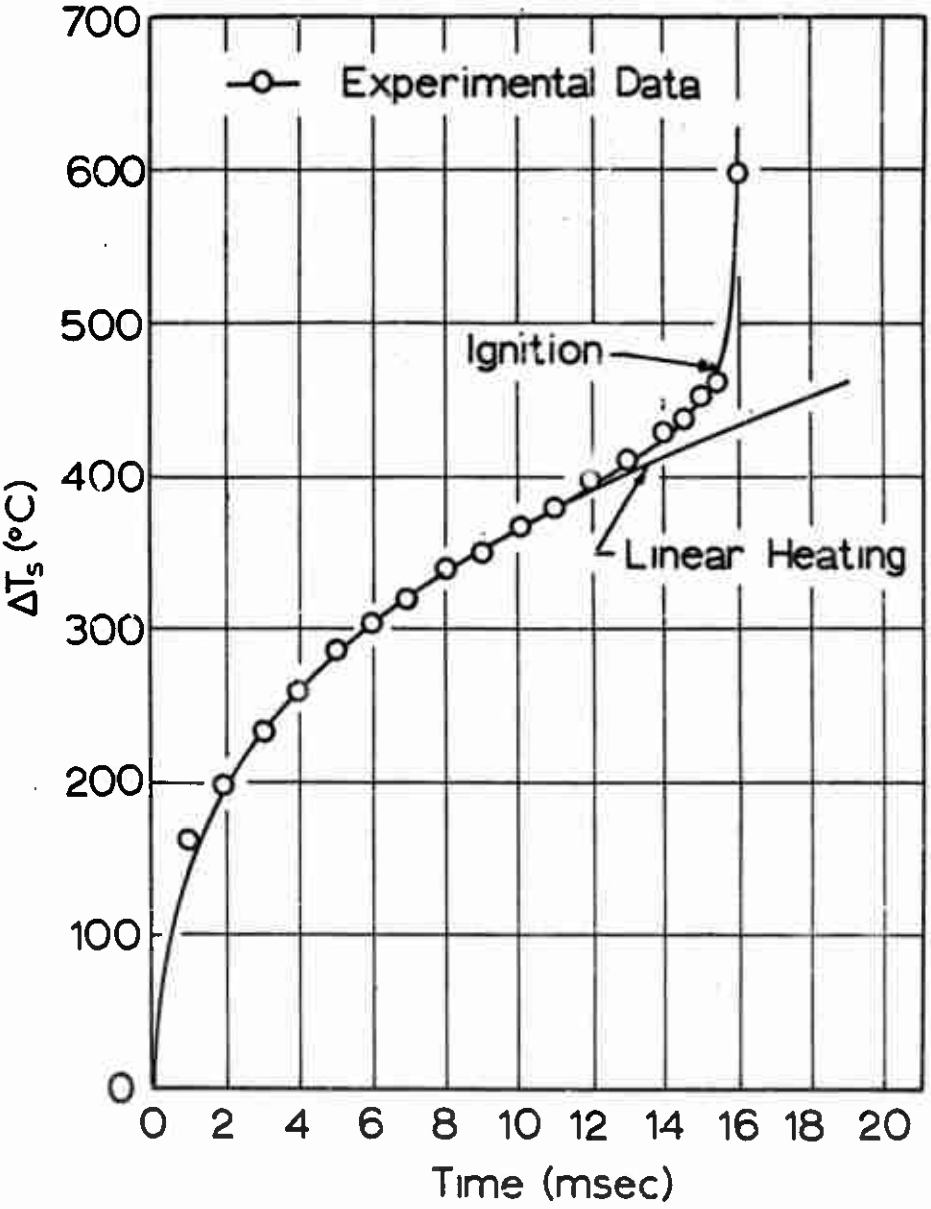

FIGURE 12 Temperature History for Smooth-surfaced Sample of Propellant UA (Run No. 611-6-21)

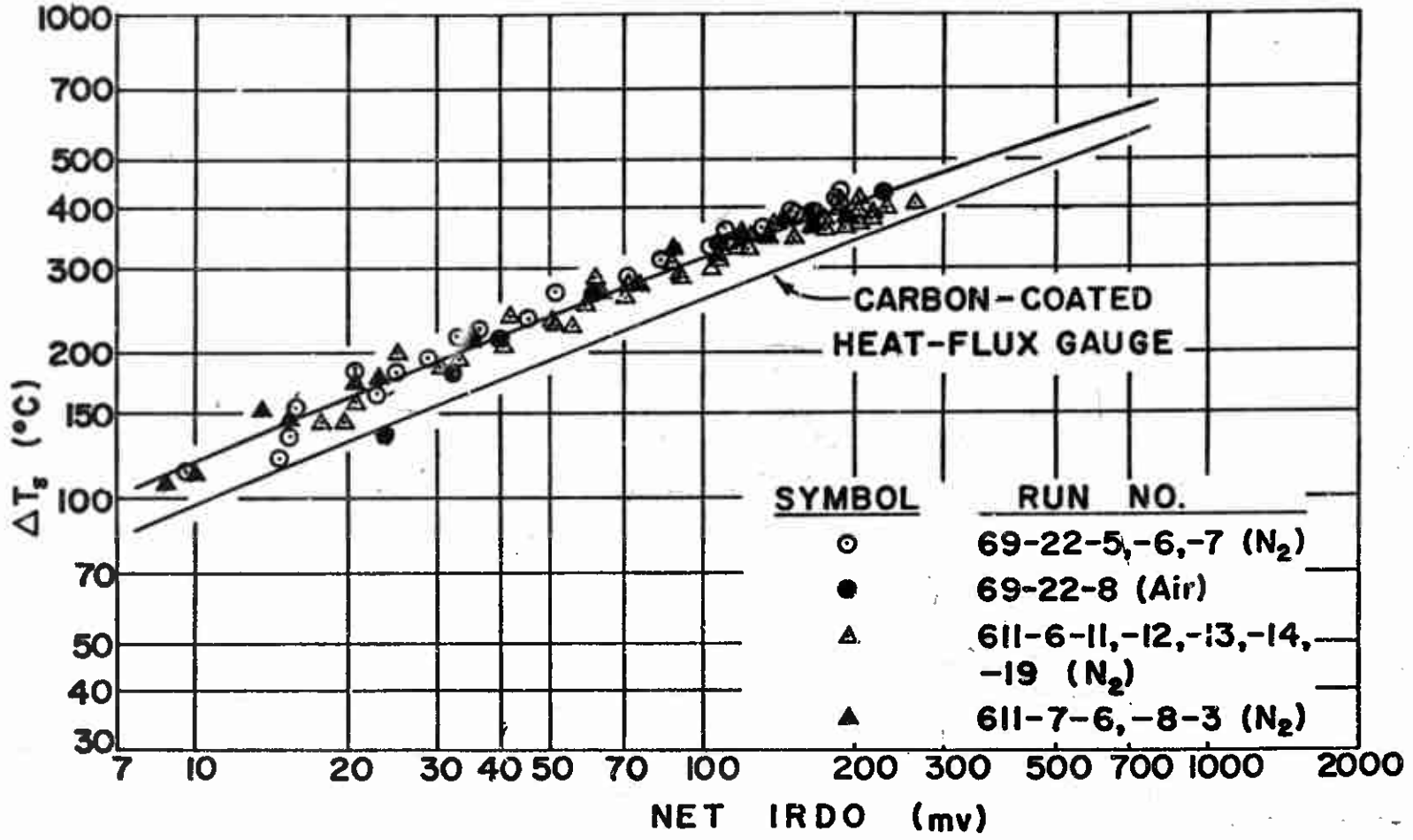

Figure 13. Infrared-detector Output Versus Calculated Surface Temperature for Linear Heating of Propellant AR (Samples with Smooth Surfaces).

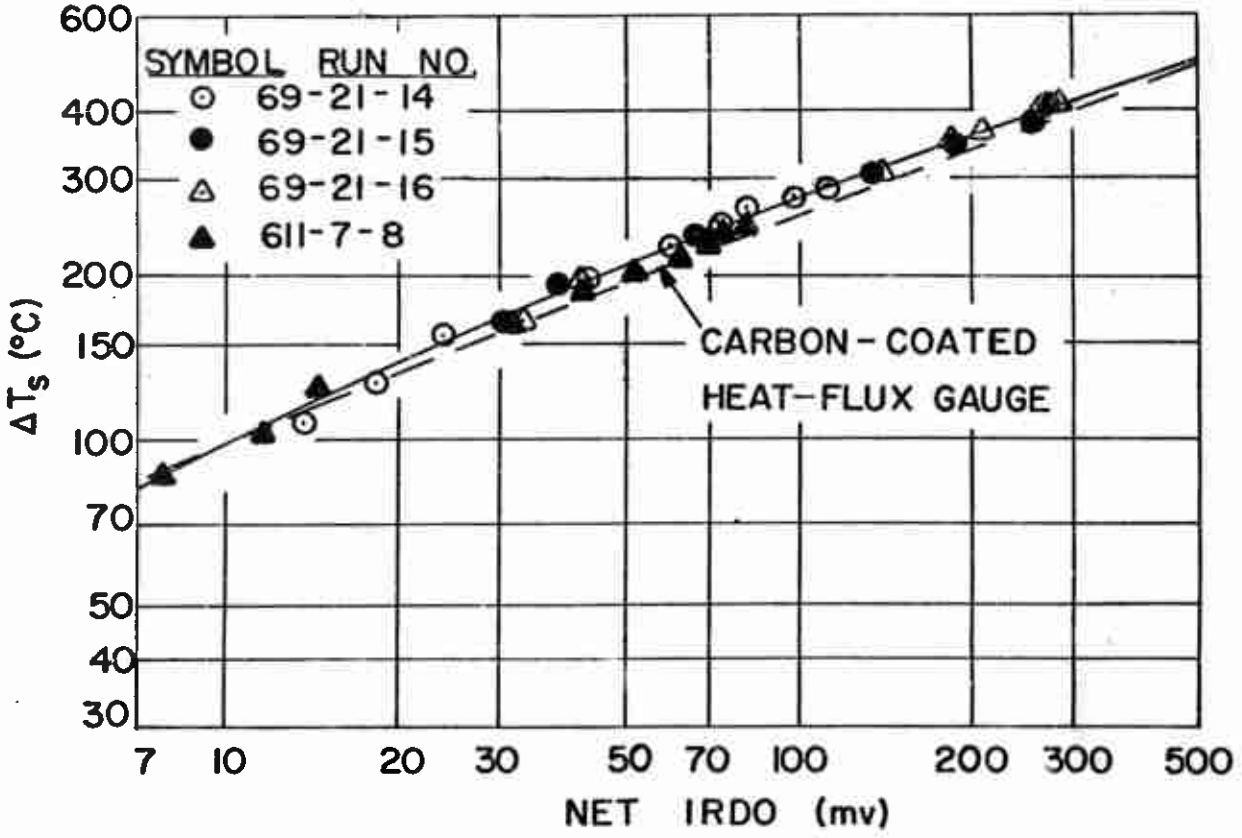

FIGURE 14. Infrared-detector Output Versus Calculated Surface Temperature for Linear Heating of Propellant AR. (Samples with Smooth Surfaces Coated with Thin

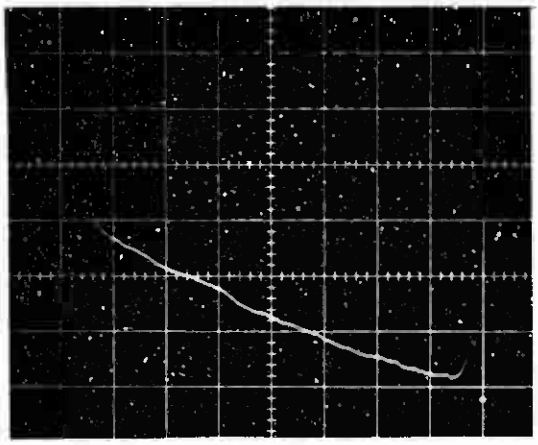

a. IR Detector Output, 100 mv/(div.) Sweep Rate: (Right to Left) 2 msec/(div.)

b. Inverted Trace: IR Detector Output, 200 mv/(div.). Normal Trace: Pressure in Shock Tube, 50 psig/(div.) Sweep Rate: (Right to Left), 5 msec/(div.)

FIGURE 15. Oscillograph of IR Detector Output for Surface Temperature Measurements on a Smooth-surfaced Sample of Propellant AR. Run No. 611-6-13. Shock Mach No.: 3.1. Convective Gas Temperature: 1490°K.

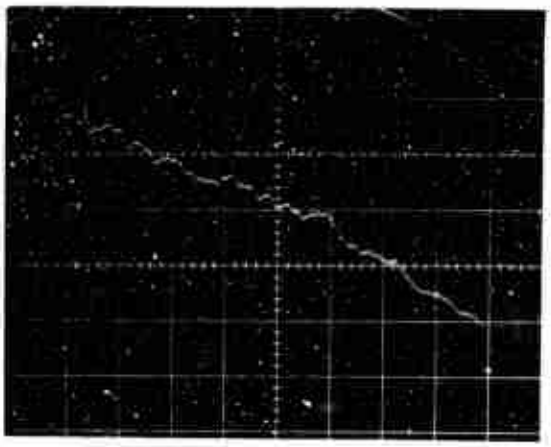

a. IR Detector Output: 50 mv/(div.), Sweep Rate: (Right to Left), 2 maec/(div.).

b. Inverted Trace: IR Detector Output, 200 mv/(div.), Normal Trace: Presaure in Shock Tube, 50 paig/(div.), Sweep Rate: (Right to Left), 5 maec/(div.).

FIGURE 16. Oscillographa of IR Detector Output for Surface Temperature Measurements on a Sample of Propellant AR with a Rough Surface. Run No. 611-6-25, Shock Mach Number: 2.7, Convective Gas Temperature: 1230°K.

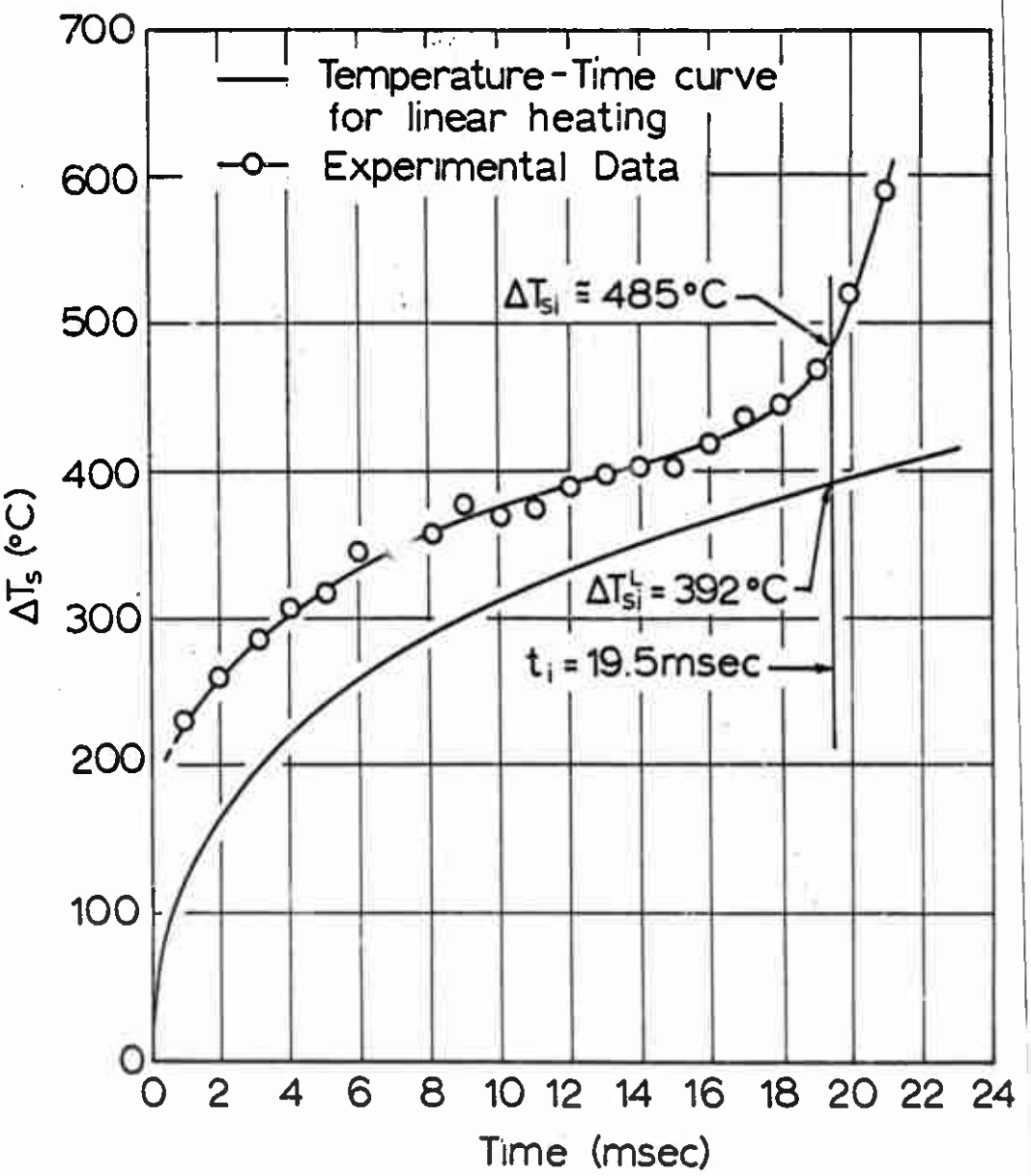

FIGURE 17. Temperature History for Ignition of a Sample of Propellant AR with a Rough Surface. Run No. 611-B-25.

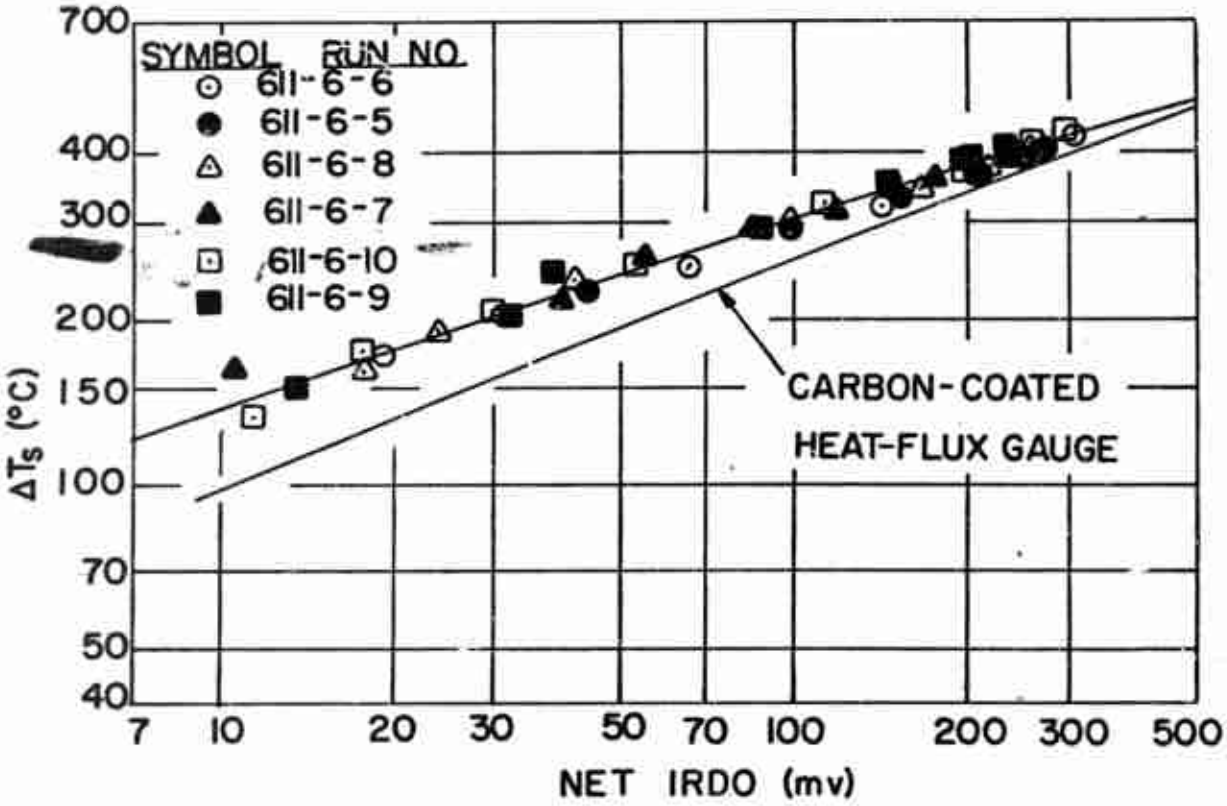

FIGURE 18. Infrared-detector Output Versus Calculated Surface Temperature for Linear Heating of Propellant AQ (Samples with Smooth Surfacea).

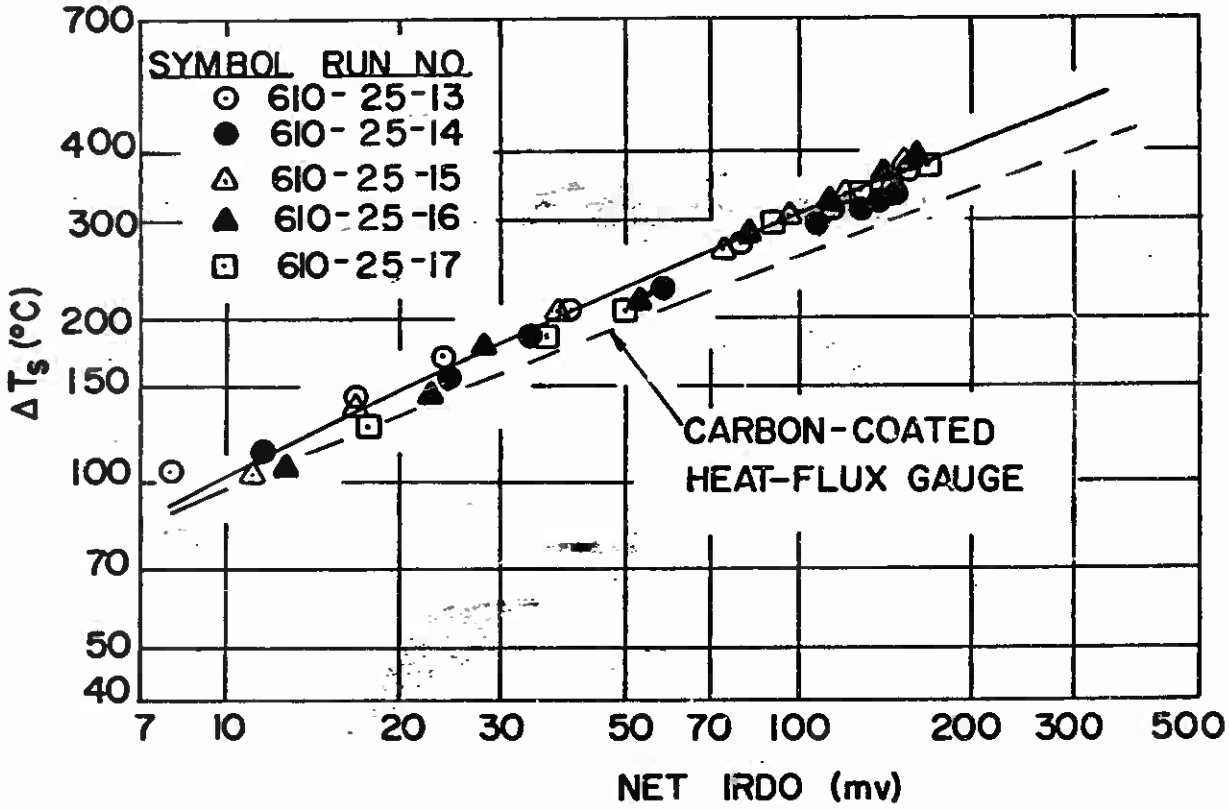

FIGURE 19. Infrared-detector Output Versus Calculated Surface Temperature for Linear Heating of Pressed Propellant PP-CBM (Samples with Smooth Surfaces).

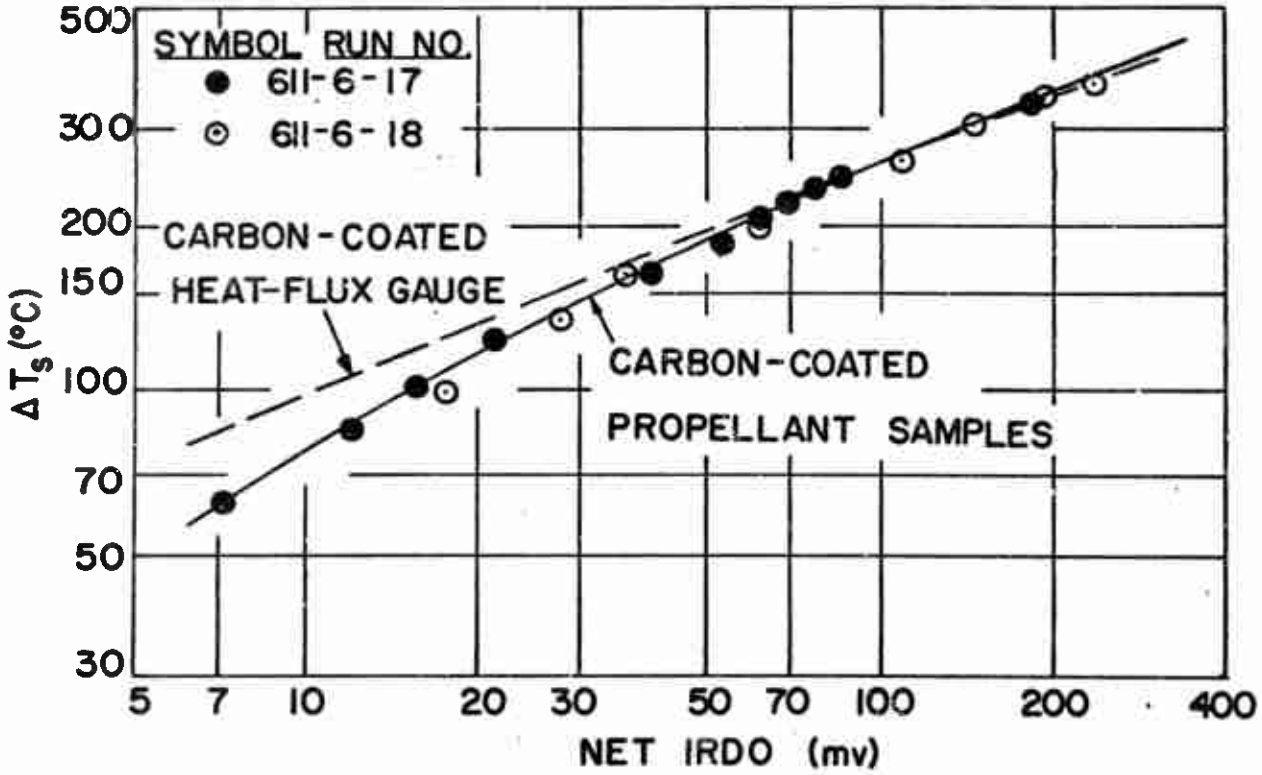

FIGURE 20. Infrared-detector Output Versus Calculated Surface Temperature for Linear Heating of Carbon-coated Samplea of Pressed Propellant PP-CBM.

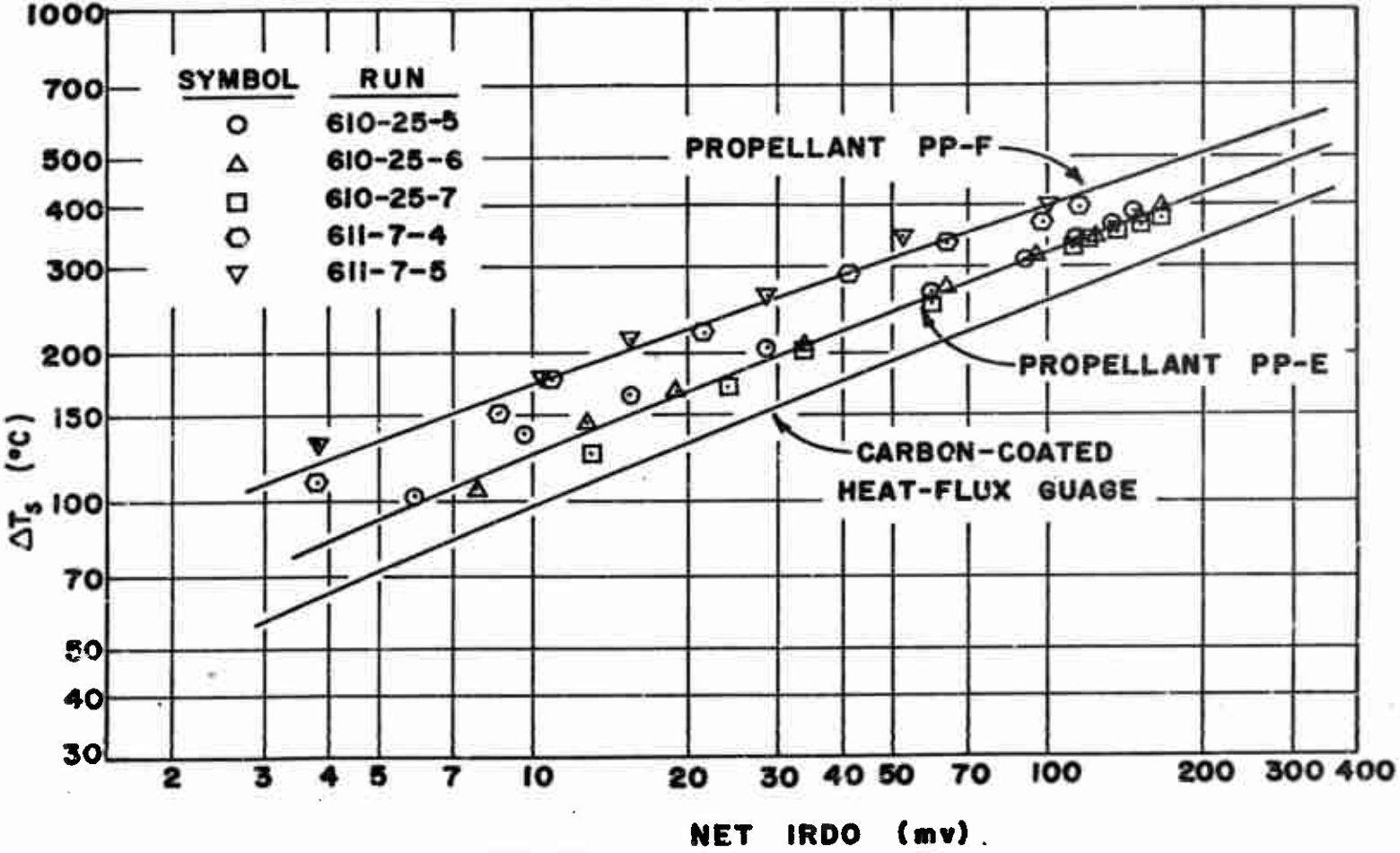

Figure 21. Infrared-detector Output Versus Calculated Surface Temperature for Linear Heating of Pressed Propellant PP-E and PP-F.

a. Run No. 610-25-7 on Pressed Propellant PP-E. Normal Trace: IR Detector Output, 50 mv/(div.), Sweep Rate: (Left to Right), 5 msec/(div.).

b. Run No. 611-7-5 on Pressed Propellant PP-F. Normal Trace: IR Detector Output, 50 mv/(div.), Sweep Rate: (Left to Right), 5 msec/(div.).

FIGURE 22. Oscillographs of Infrared-Detector Output for Preased Propellants PP-E and PP-F for Runs in Which Ignition of Samples Occurred.

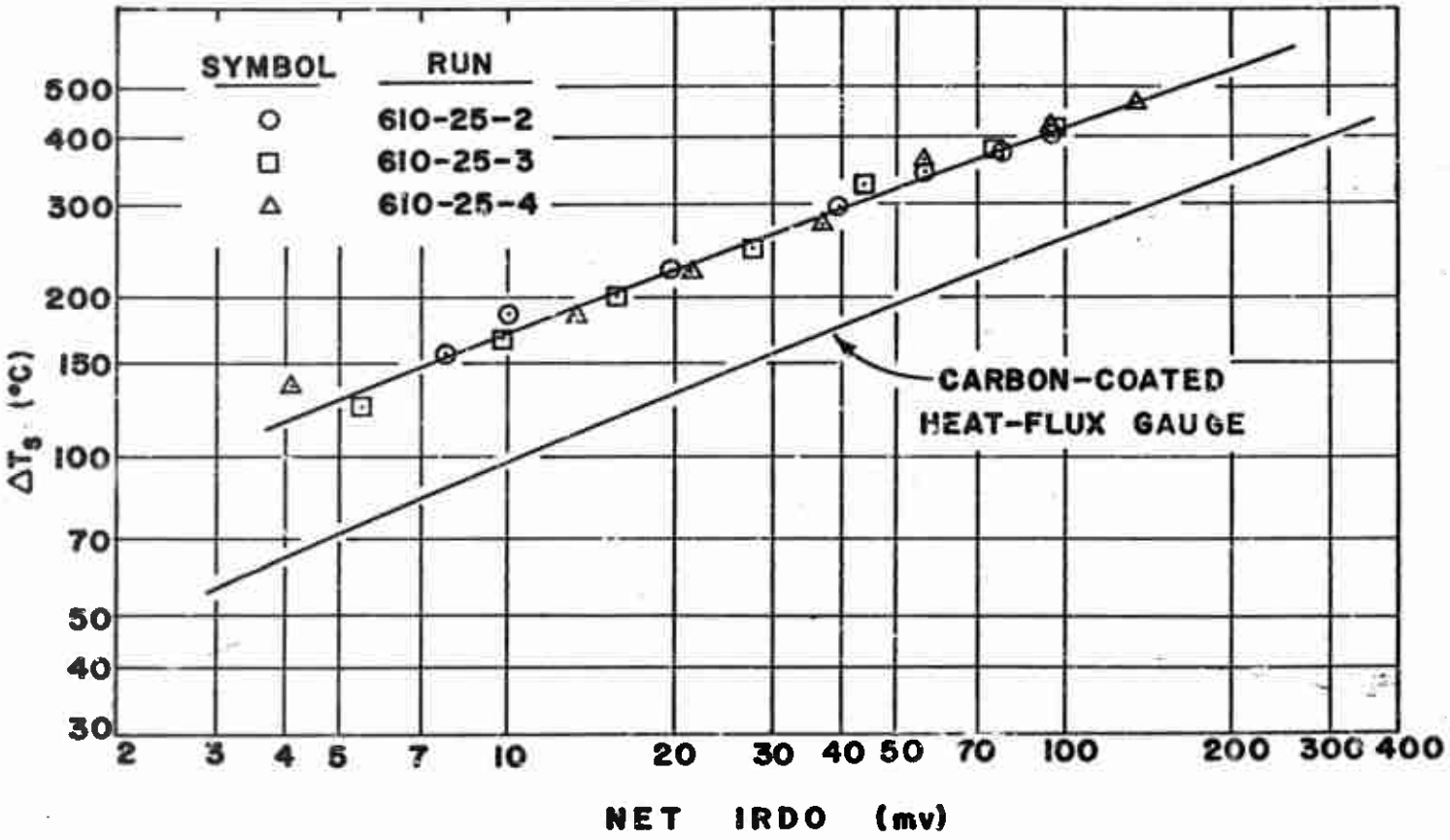

FIGURE 23. Infrared-detector Output Versus Calculated Surface Temperature for Linear Heating of Pressed

FIGURE 24. Oscillograph of Infrared-Detector Output for Run No. 69-21-12 on JPN Double-base Propellant. Normal Trsce: IR Detector Output, 50 mv/(div.), Sweep Rste: (Left to Right), 5 msec/(div.), Inverted Trace: Pressure in Shock-tube Driven Section, 50 psig/(div.), Test Gas: Nitrogen, Test-gas Temperature: 1265°K, Mesn Heat Flux: 50 csl/(cm^2)(sec).

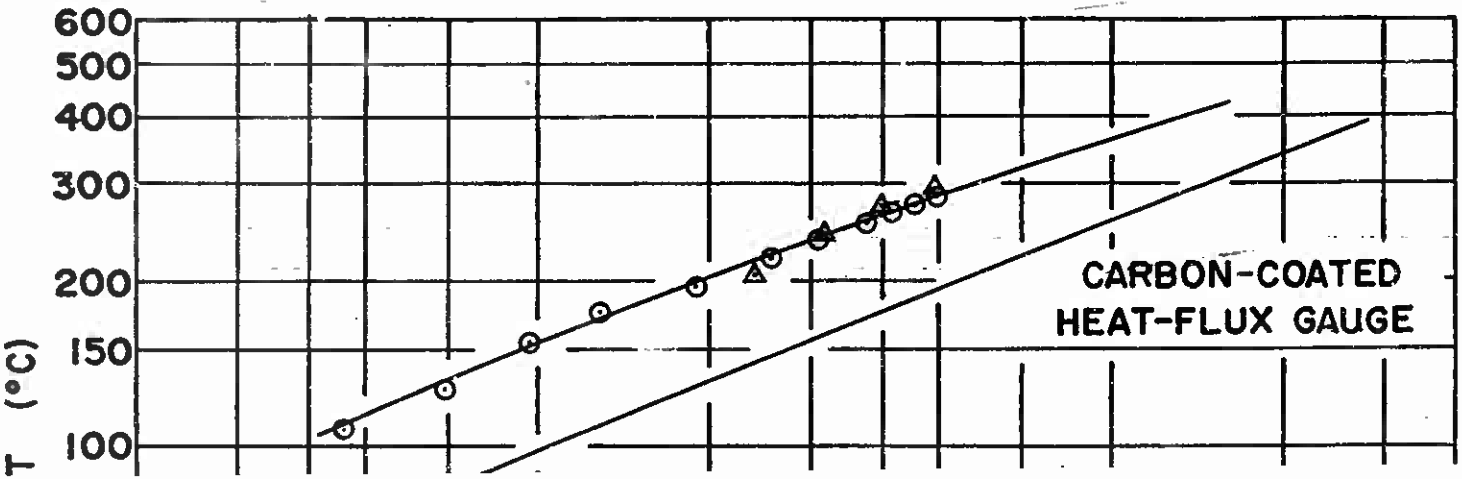
600
500
400
300
200
150
100
T (°C)
CARBON-COATED
HEAT-FLUX GAUGE

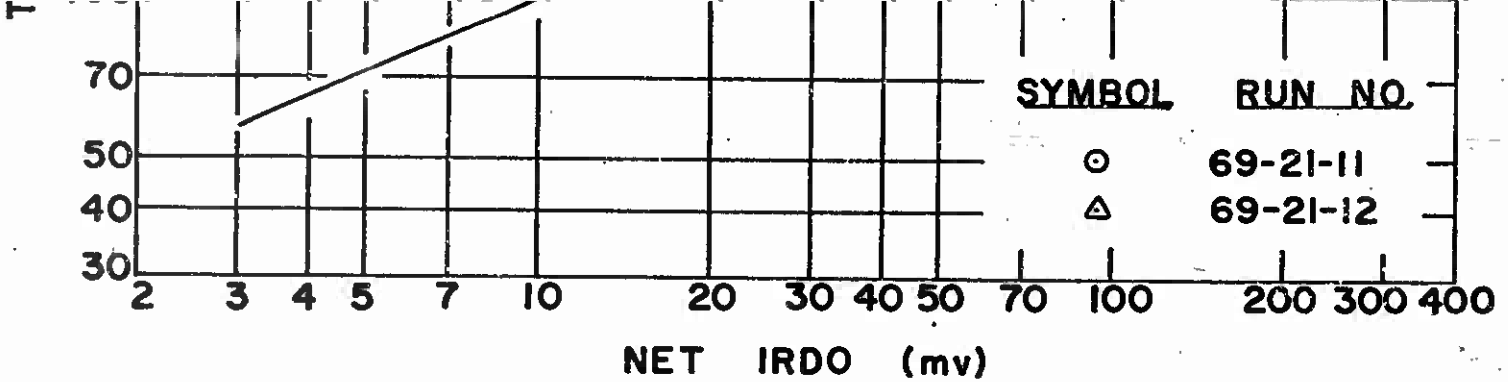

FIGURE 25. Infrared-detector Output Versus Calculated Surface Temperature for Linear Heating of Double-base Propellant JPN.

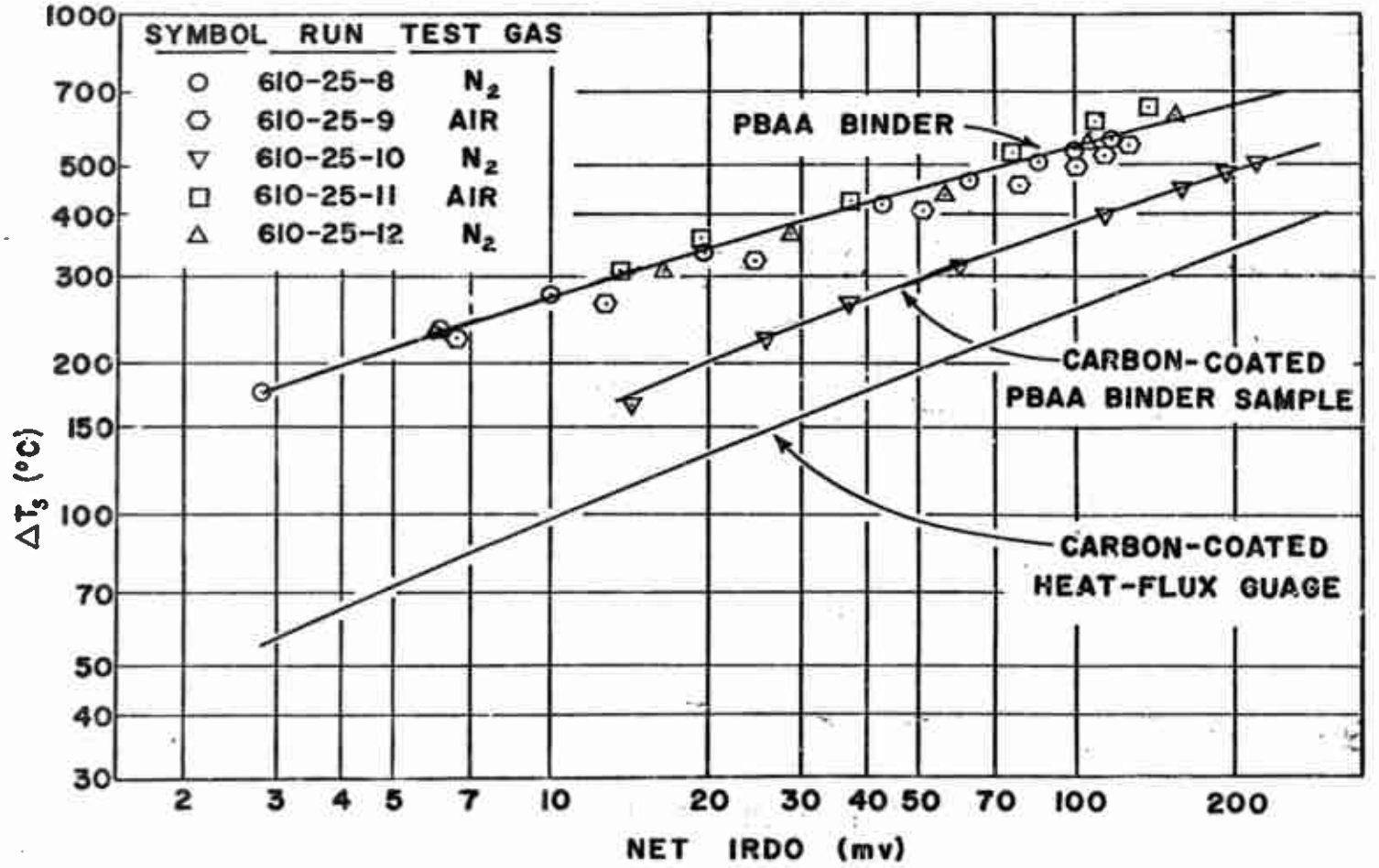

FIGURE 26. Infrared-detector Output Versus Calculated Surface Temperature

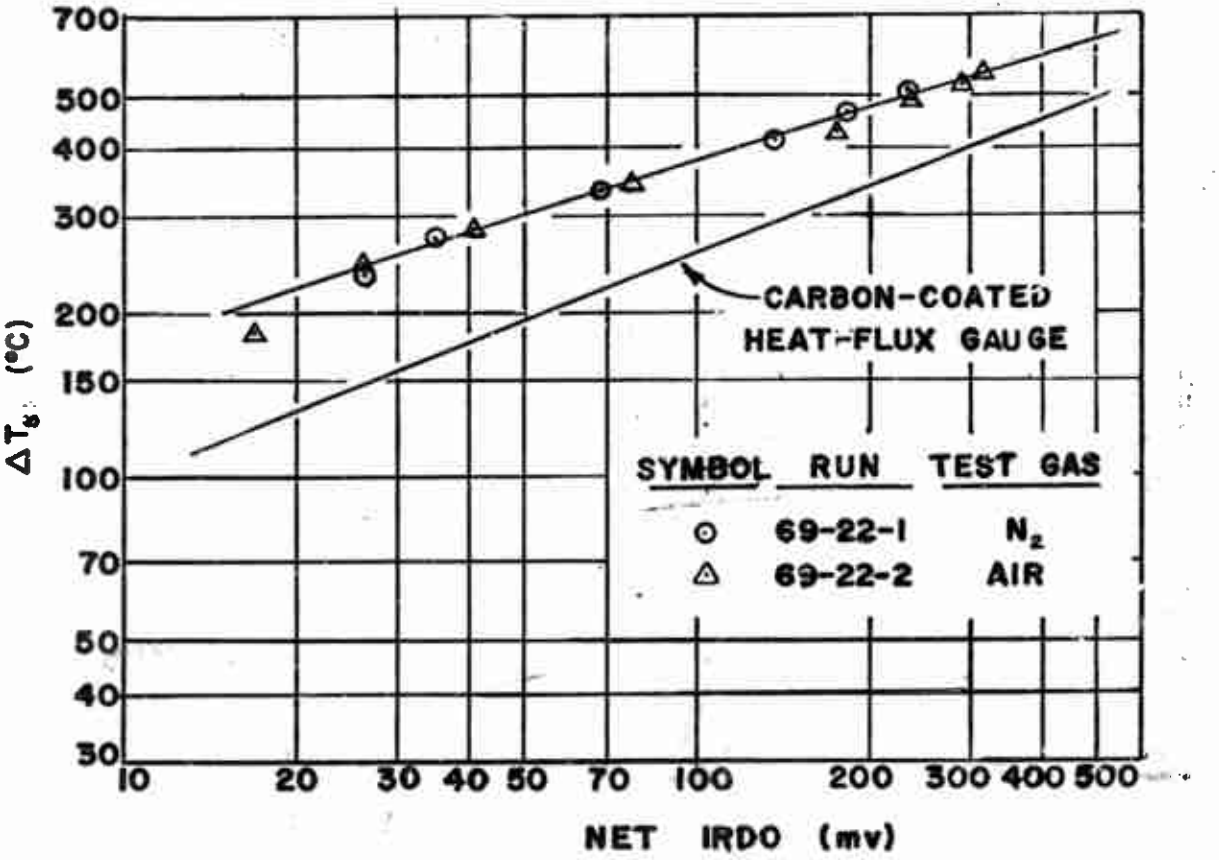

FIGURE 27. Infrared Detector Output Versus Calculated Surface Temperature for Linear Heating of Polyurethane Binder Samples.

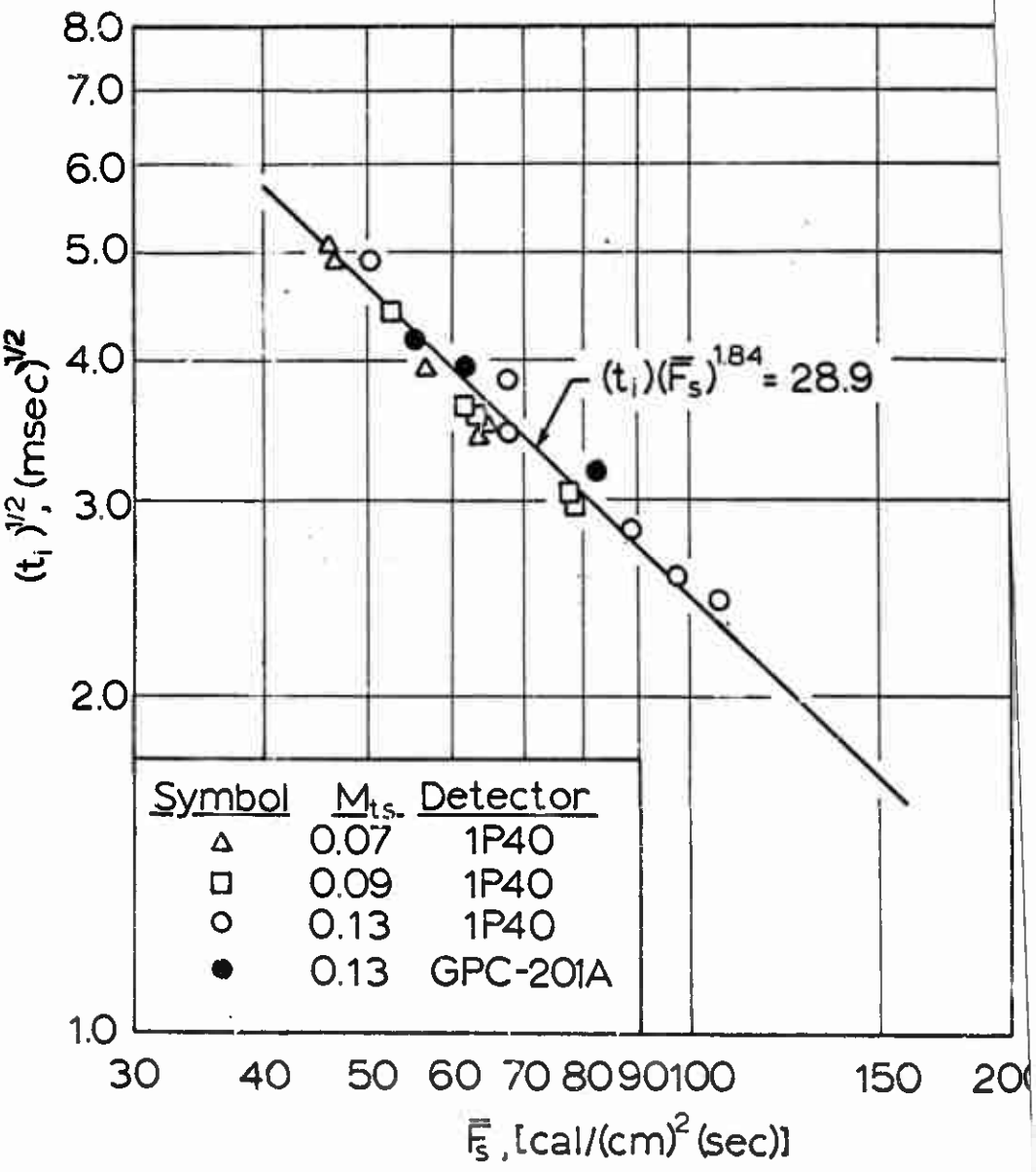

FIGURE 28. Ignition Data for Propellant UA.

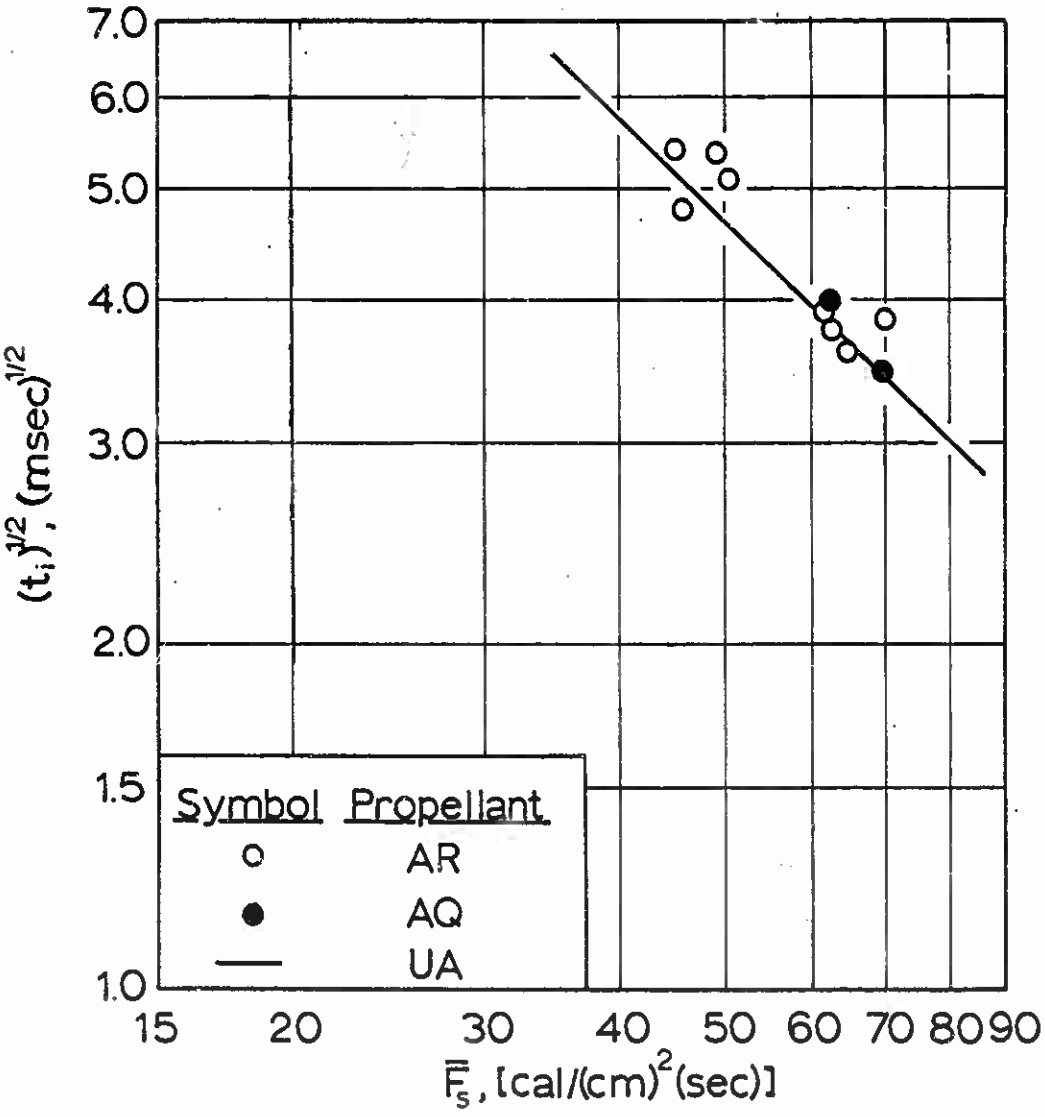

FIGURE 29. Ignition Data for Propellants AR and AQ as Measured with the GPC-201A IR Detector.

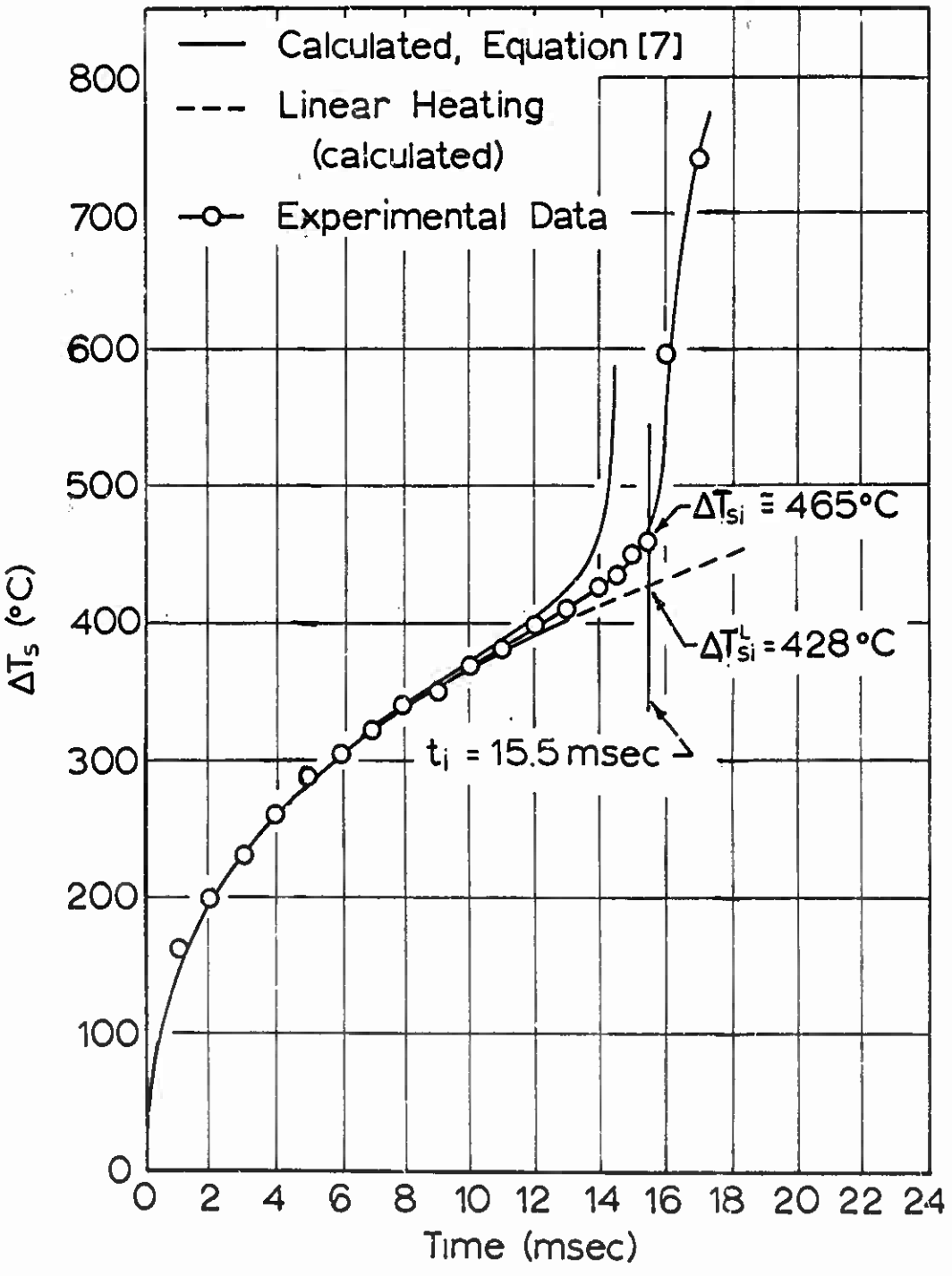

FIGURE 30. Calculated and Measured Surface-temperature Histories for Propella
UA. Run No. 611-6-21.

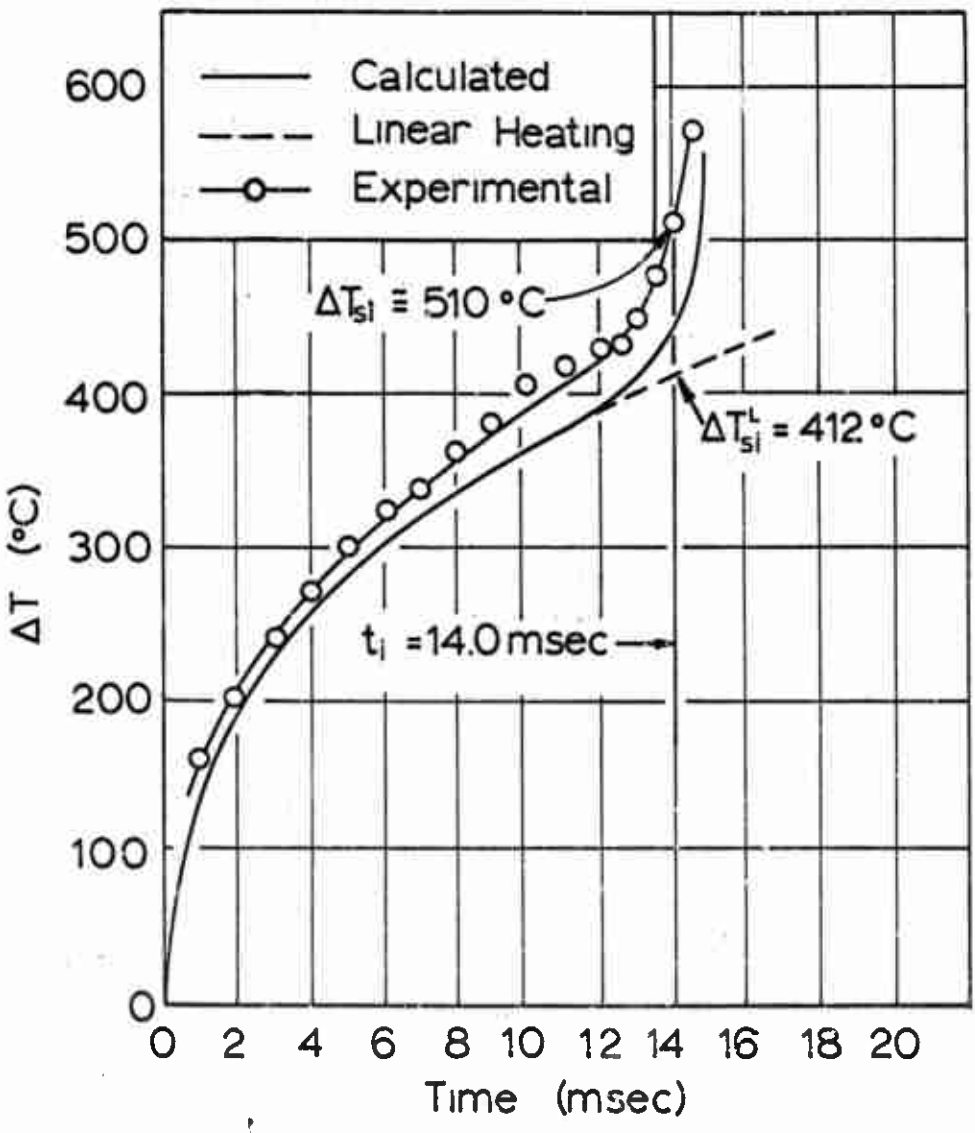

FIGURE 31. Calculated and Measured Surface-temperature Histories for Propellant AR. Run No. 611-6-11.

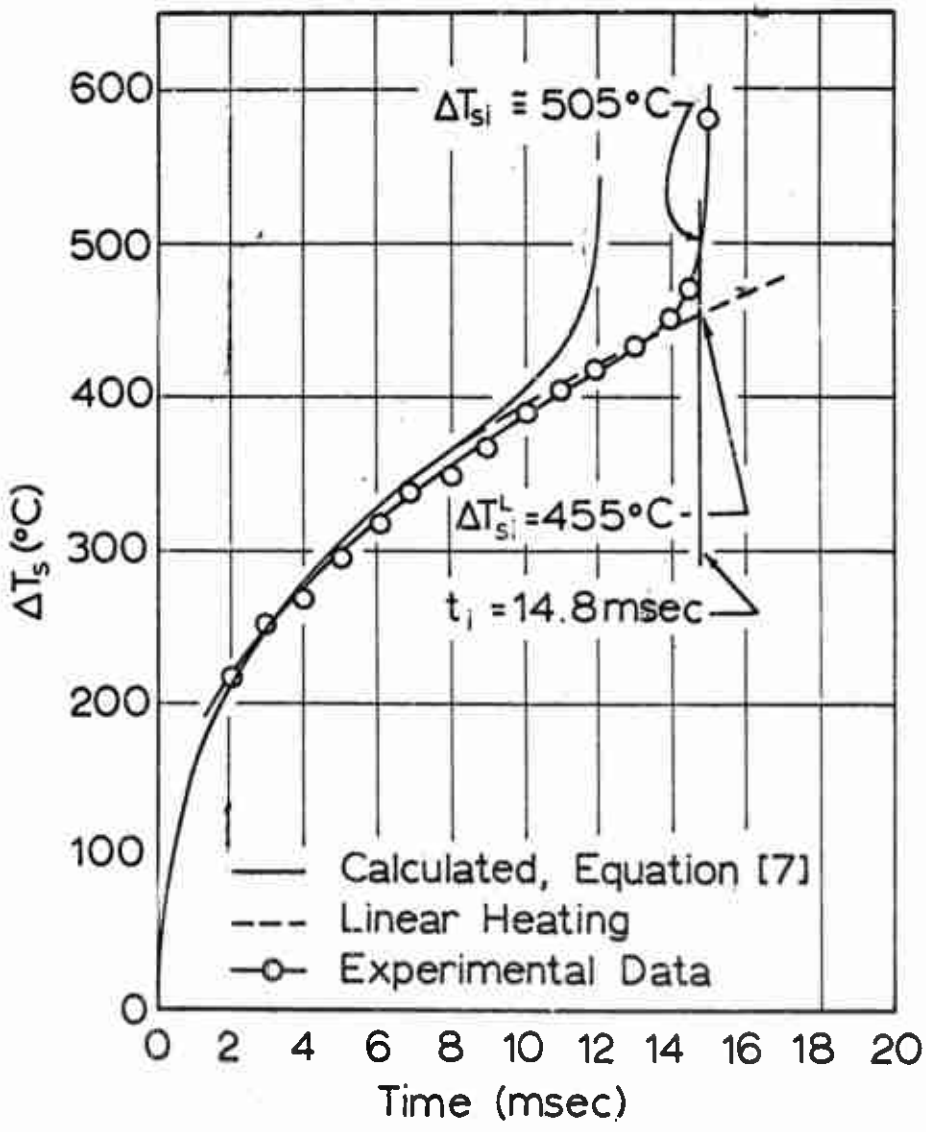

FIGURE 32. Calculated and Measured Surface-Temperature Histories for Propellant AR. Run No. 611-C-13.

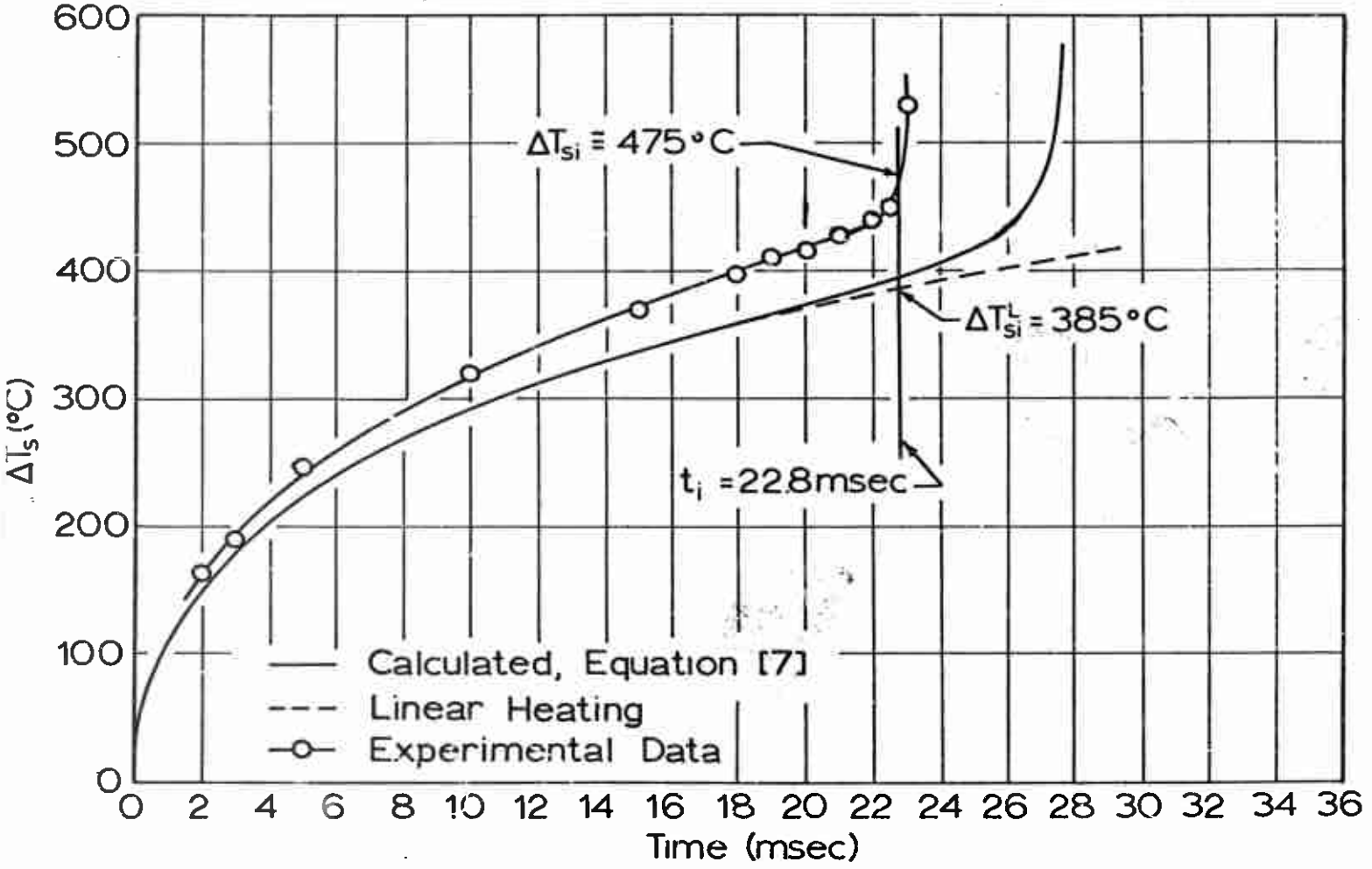
600
500
400
300
200
100
0
ΔT_s (°C)
$\Delta T_{si} \equiv 475°C$
$\Delta T_{si}^{L} = 385°C$
$t_i = 22.8$msec
Calculated, Equation [7]
Linear Heating
Experimental Data
0 2 4 6 8 10 12 14 16 18 20 22 24 26 28 30 32 34 36
Time (msec)

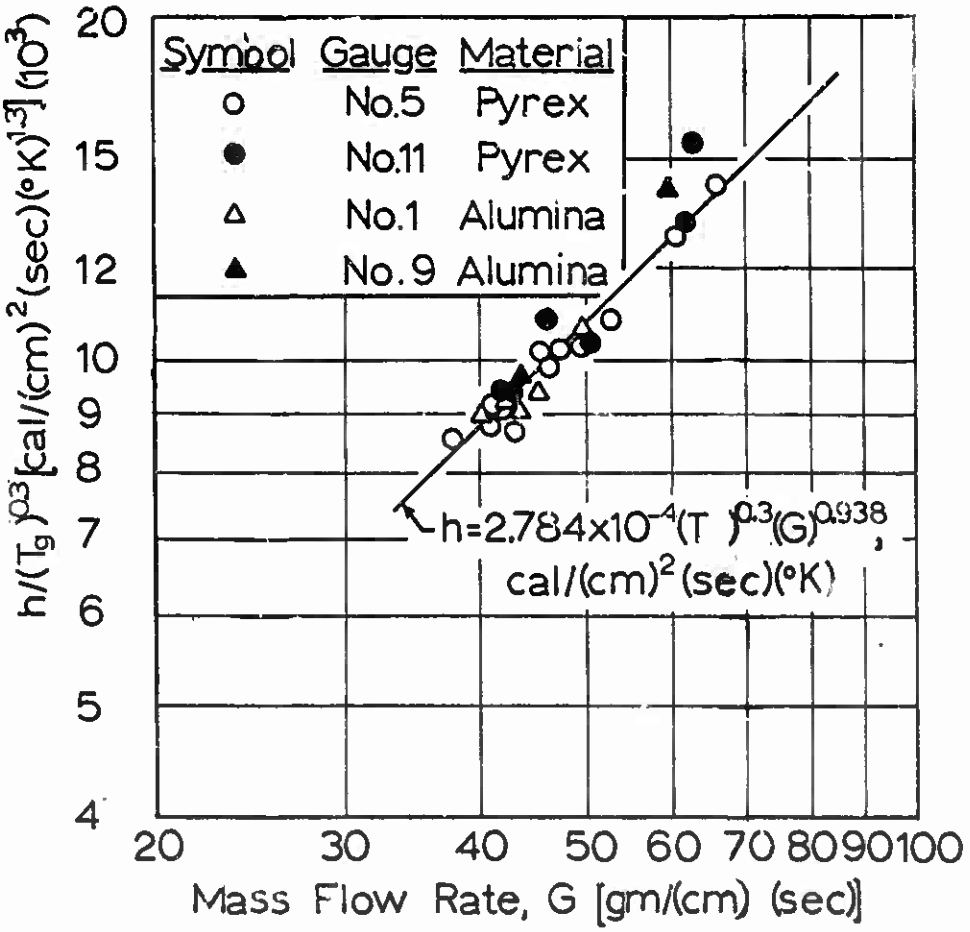

FIGURE 34. Wall Heat-transfer Coefficients for Flow-control Orifice No. 3A Correlated in Terms of Mass Flow Rate through the Flow Channel and Gas Temperature (Data are for Modified Test Section with Hot Nitrogen as the Test Gas.)

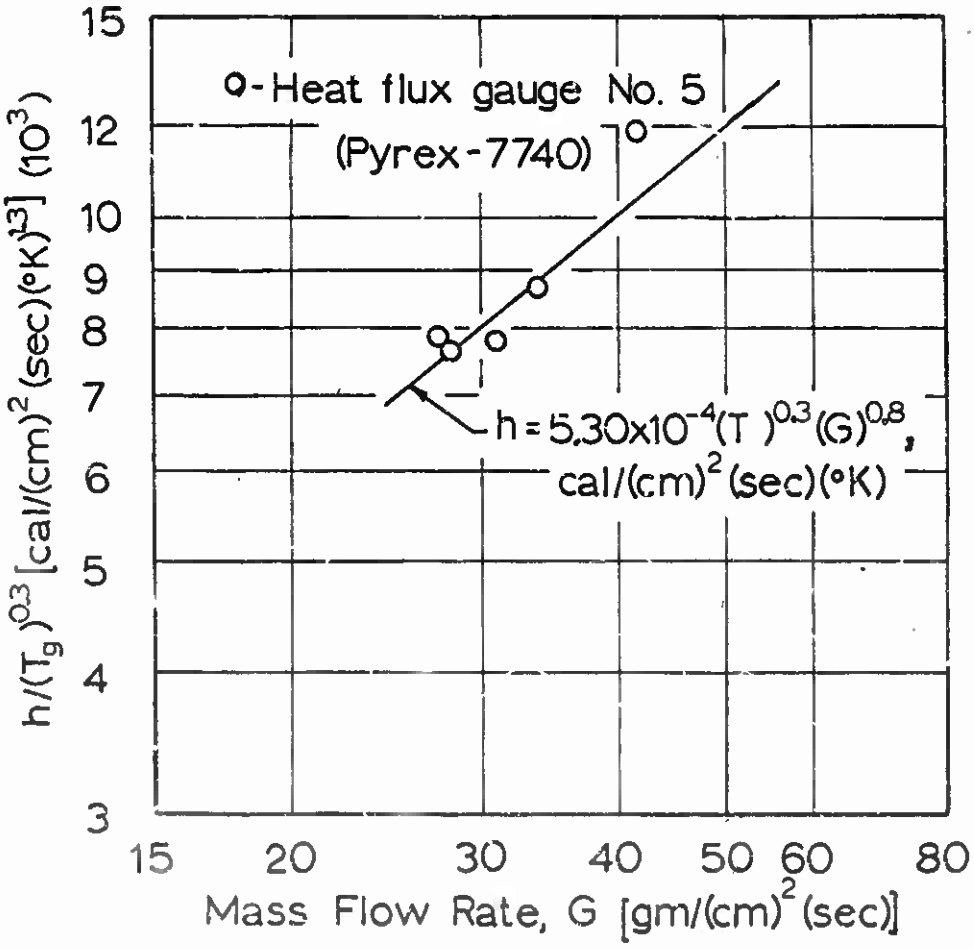

FIGURE 35. Wall Heat-transfer Coefficients for Flow-control Orifice No. 4A Correlated in Terms of Mass Flow Rate through the Flow Channel and Gas Temperature. (Data are for Modified Test Section with Hot Nitrogen as the Test Gas.)

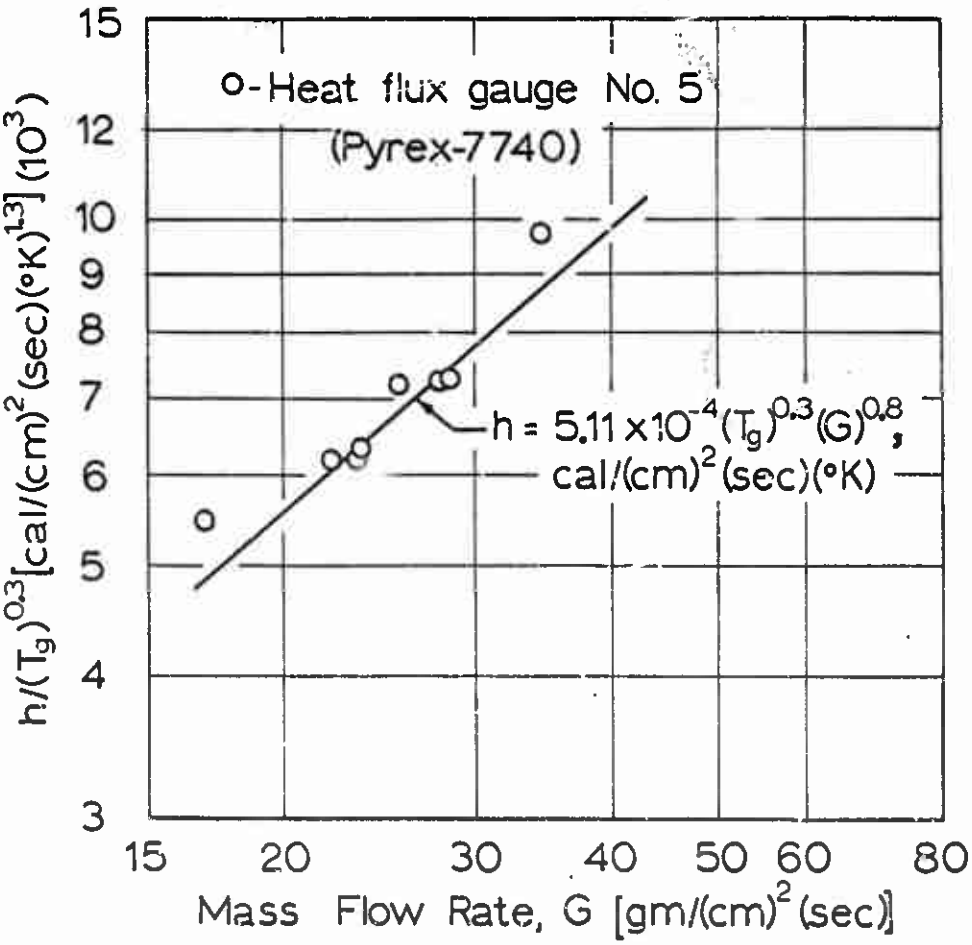

Figure 36. Wall Heat-transfer Coefficients for Flow-control Orifice No. 5A Correlated in Terms of Mass Flow Rate through the Flow Channel and Gas Temperature. (Data are for Modified Test Section with Hot Nitrogen as the Test Gas.)

a. Data for Uncoated Heat-flux Gage. Sweep Rate: (Left to Right), 50 msec/(div.). Temperature: 1.5°C/(div.).

b. Data for Carbon-coated Heat-flux Gage. Sweep Rate: (Left to Right), 50 msec/(div.), Temperature: 1.5°C/(div.).

FIGURE 37. Oscillographs of Temperature-time Data for Heat-flux Gages Initially at Room Temperature, Which Were Rapidly Immeraed in a Bath of Carbon Tetrachloride at 0°C.

APPENDIX F

NOMENCLATURE

Symbol	Definition	Typical Units
b	pre-exponential factor (see Equation 3) Product of the frequency factor, z, and energy supplied at the propellant surface per unit area, Q_s, by the key ignition reaction.	cal/(cm^2)(sec)
c	specific heat	cal/(g)(°K)
E_a	activation energy for key ignition reaction	cal/mole
F_s	externally applied heat flux to propellant surface	cal/(cm^2)(sec)
$\bar{F}_s$	mean externally applied heat flux to propellant surface	cal/(cm^2)(sec)
F_T	total heat flux to propellant surface	cal/(cm^2)(sec)
G	mass flow rate of test gas through flow channel of test section	g/(cm^2)(sec)
h	convective heat-transfer coefficient	cal/(cm^2)(sec)(°K)
IRDO	infrared-detector output	millivolta
k	thermal conductivity	cal/(cm)(aec)(°K)
M_E	Mach number of incident shock wave at entrance to test section	dimensionless
P_u	pressure immediately behind reflected shock wave	atm
P_u'	maximum pressure rise behind reflected shock wave	atm
R	gas constant :h value of 1.987	cal/(mole)(°K)
t	time	aec, msec
t_i	ignition time	sec, msec
T	temperature	°K
T_0	initial uniform temperature of solid	°K

APPENDIX F. NOMENCLATURE
(continued)

Symbol	Definition	Typical Units
T_4	gas temperature immediately behind reflected shock wave	°K
T_4'	maximum gas temperature behind reflected shock wave	°K
ΔT_{ps}	temperature rise at surface of Pyrex heat-flux gage during convective heating	°K
T_s	surface temperature	°K
ΔT_s	temperature rise at surface during transient convective heating	°K
T_{si}	temperature at propellant surface at ignition	°K
T_{si}^L	ignition temperature calculated assuming linear heating of surface	°K
ΔT_{si}^L	ignition temperature relative to T_o	°K
x	distance into the solid, measured from its surface	cm
α	thermal diffusivity	$(cm^2)/(sec)$
Γ	thermal responsivity (square root of the product of k, ρ, c)	$cal/(cm^2)(sec)^{1/2}(°K)$
Γ_p	thermal responsivity of the propellant	$cal/(cm^2)(sec)^{1/2}$ °C
π	numerical constant (3.14159. . .)	dimensionless
ρ	density	$g/(cm^3)$

APPENDIX G

REFERENCES

[1] Niesson, W. R., and Baatress, E. K. "Solid Propellant Ignition Studies," Arthur D. Little, Inc. Air Force Rocket Propulsion Laboratory, Edwards Air Force Base, California, Technical Report No. AFRPL-TR-66-32, Final Report (February, 1966).

[2] Powling, J., and Smith, W. A. W. "Measurement of the Burning Surface Temperature of Propellant Compositions by Infra-red Emission," *Combustion and Flame, 6,* 173-181 (1962).

[3] Powling, J., and Smith, W. A. W. "The Surface Temperature of Burning Ammonium Perchlorate," *Combustion and Flame, 7,* 269-275 (1963).

[4] Powling, J., and Smith, W. A. W. "The Surface Temperature of Ammonium Perchlorate Burning at Elevated Pressures," *Tenth Symposium (International) on Combustion* (The Combustion Institute, Pittsburgh, 1965), pp. 1373-1380.

[5] Cheng, J., Bouck, L. S., Keller, J. A., Baer, A. D., and Ryan, N. W. "Ignition and Combustion of Solid Propellants," Department of Chemical Engineering, University of Utah, Final Report on Air Force Grant AFOSR 40-65, AD-637-496 (1966).

[6] Keller, J. A. "Studies on the Ignition of Ammonium Perchlorate-based Propellants by Convective Heating," Ph.D. Thesis, University of Utah, Department of Chemical Engineering (Salt Lake City, Utah, August, 1965). (Also publiahed as Technical Report: Keller, J. A., Baer, A. D., and Ryan, N. W. "Studies on Ignition of Ammonium Perchlorate-based Propellants by Convective Heating," Department of Chemical Engineering, University of Utah, Technical Report under Air Force Grant AFOSR 40-63 and 64, AD 638647 (1966).

[7] Keller, J. A., Baer, A. D., and Ryan, N. W. "Ignition of Ammonium Perchlorate Propellants by Convective Heating," *AIAA Journal, 4,* 1358-1365 (1966).

[8] Camac, M. and Feinberg, R. M. "High Speed Infrared Balometer," *Review of Scientific Instruments,* 33, 964-962 (1962).

[9] Camac, M., and Feinberg, R. M. "High Speed Infrared Balometer." Avco-Everett Research Laboratory, Research Report 120 (AFCRL 942, AFOSR 1564) March, 1962.

[10] Baer, A. D., and Ryan, N. W. "Ignition of Composite Propellants by Low Radiant Fluxes," *AIAA Journal, 3,* 884-889 (1965).

[11] Bouck, L. S., "A Model of the Ignition of a Heterogeneous Solid Propellant," M.S. Thesis, University of Utah, Department of Chemical Engineering (Salt Lake City, Utah, August, 1966).

[12] Rosser, W. A., Jr., Inami, S. H., and Wise, H. "Thermal Diffusivity of Ammonium Perchlorate," *AIAA Journal, 4,* 663-666 (1966).

APPENDIX G. REFERENCES
(continued)

[13] Carslaw, H. S., and Jseger, J. C. *Conduction of Heat in Solids*, Second Edition (Oxford Univsrsity Press, London, 1959).

[14] Roth, J. F., and Wachtell, C. P. "Hest Transfer and Chemical Kinetics in the Ignition of Solid Propellants," *Ind. Eng. Chem., Fundamentals, 1*, 62-67 (1962).

UNCLASSIFIED

Security Classification

DOCUMENT CONTROL DATA - R&D

(Security classification of title, body of abstract and indexing annotation must be entered when the overall report is classified)

1. ORIGINATING ACTIVITY (Corporate author)

University of Utah
Chemical Engineering Department
Salt Lake City, Utah 84112

2a. REPORT SECURITY CLASSIFICATION

UNCLASSIFIED

2b GROUP

3. REPORT TITLE

SURFACE TEMPERATURE MEASUREMENTS ON SOLID PROPELLANTS DURING IGNITION

4. DESCRIPTIVE NOTES (Type of report and inclusive dates)

Scientific Interim

5. AUTHOR(S) (Last name, first name, initial)

John A. Keller
Alva D. Baer
Norman W. Ryan

6. REPORT DATE	7a. TOTAL NO. OF PAGES	7b. NO. OF REFS
1 August 1967	122	14

8a. CONTRACT OR GRANT NO.	9a. ORIGINATOR'S REPORT NUMBER(S)
AF-AFOSR-40-67	
b PROJECT NO. 9711-01	
c. 61445014	9b. OTHER REPORT NO(S) (Any other numbers that may be assigned this report)
d. 681308	AFOSR 68-0034

10. AVAILABILITY/LIMITATION NOTICES

2. This document is subject to special export controls and each transmittal to foreign governments or foreign nationals may be made only with prior approval of AFOSR (SRGO).

11. SUPPLEMENTARY NOTES	12. SPONSORING MILITARY ACTIVITY
TECH, OTHER	AF Office of Scientific Research (SREP) 1400 Wilson Boulevard Arlington, Virginia 22209

13. ABSTRACT

Surface temperatures were measured on ammonium perchlorate propellants during ignition by convective heating by use of an infrared radiation sensor. This study was conducted in a shocktube apparatus, and air or nitrogen was used for heating the propellant samples. Heat fluxes were in the range of 30 to 80 cal/(cm^2) (sec). Surface-temperature histories measured on propellant samples with smooth blackened surfaces are in good agreement with predictions of a thermal ignition model that considers the key ignition reaction to be localized at the propellant surface. Surface roughness effects and sample transparency to thermal radiation result in difficulties in relating the infrared detector output to surface temperature.

DD FORM 1 JAN 64 1473

UNCLASSIFIED

Security Classification

14. KEY WORDS	LINK A		LINK B		LINK C	
	ROLE	WT	ROLE	WT	ROLE	WT
Propellant Ignition						
Composite Propellants						
Ammonium Perchlorate						
Convective Heating						
Shock Tube						
Heat Transfer						
Surface Temperature Measurements						
Infrared Detectors						
Ignition Temperatures						

INSTRUCTIONS

1. ORIGINATING ACTIVITY: Enter the name and address of the contractor, subcontractor, grantee, Department of Defense activity or other organization *(corporate author)* issuing the report.

2a. REPORT SECURITY CLASSIFICATION: Enter the overall security classification of the report. Indicate whether "Restricted Data" is included. Marking is to be in accordance with appropriate security regulations.

2b. GROUP: Automatic downgrading is specified in DoD Directive 5200.10 and Armed Forces Industrial Manual. Enter the group number. Also, when applicable, show that optional markings have been used for Group 3 and Group 4 as authorized.

3. REPORT TITLE: Enter the complete report title in all capital letters. Titles in all cases should be unclassified. If a meaningful title cannot be selected without classification, show title classification in all capitals in parenthesis immediately following the title.

4. DESCRIPTIVE NOTES: If appropriate, enter the type of report, e.g., interim, progress, summary, annual, or final. Give the inclusive dates when a specific reporting period is covered.

5. AUTHOR(S): Enter the name(s) of author(s) as shown on or in the report. Enter last name, first name, middle initial. If military, show rank and branch of service. The name of the principal author is an absolute minimum requirement.

6. REPORT DATE: Enter the date of the report as day, month, year; or month, year. If more than one date appears on the report, use date of publication.

7a. TOTAL NUMBER OF PAGES: The total page count should follow normal pagination procedures, i.e., enter the number of pages containing information.

7b. NUMBER OF REFERENCES: Enter the total number of references cited in the report.

8a. CONTRACT OR GRANT NUMBER: If appropriate, enter the applicable number of the contract or grant under which the report was written.

8b, 8c, & 8d. PROJECT NUMBER: Enter the appropriate military department identification, such as project number, subproject number, system numbers, task number, etc.

9a. ORIGINATOR'S REPORT NUMBER(S): Enter the official report number by which the document will be identified and controlled by the originating activity. This number must be unique to this report.

9b. OTHER REPORT NUMBER(S): If the report has been assigned any other report numbers *(either by the originator or by the sponsor)*, also enter this number(s).

10. AVAILABILITY/LIMITATION NOTICES: Enter any limitations on further dissemination of the report, other than those imposed by security classification, using standard statements such as:

(1) "Qualified requesters may obtain copies of this report from DDC."

(2) "Foreign announcement and dissemination of this report by DDC is not authorized."

(3) "U. S. Government agencies may obtain copies of this report directly from DDC. Other qualified DDC users shall request through

_____."

(4) "U. S. military agencies may obtain copies of this report directly from DDC. Other qualified users shall request through

_____."

(5) "All distribution of this report is controlled. Qualified DDC users shall request through

_____."

If the report has been furnished to the Office of Technical Services, Department of Commerce, for sale to the public, indicate this fact and enter the price, if known.

11. SUPPLEMENTARY NOTES: Use for additional explanatory notes.

12. SPONSORING MILITARY ACTIVITY: Enter the name of the departmental project office or laboratory sponsoring *(paying for)* the research and development. Include address.

13. ABSTRACT: Enter an abstract giving a brief and factual summary of the document indicative of the report, even though it may also appear elsewhere in the body of the technical report. If additional space is required, a continuation sheet shall be attached.

It is highly desirable that the abstract of classified reports be unclassified. Each paragraph of the abstract shall end with an indication of the military security classification of the information in the paragraph, represented as *(TS), (S), (C), or (U)*.

There is no limitation on the length of the abstract. However, the suggested length is from 150 to 225 words.

14. KEY WORDS: Key words are technically meaningful terms or short phrases that characterize a report and may be used as index entries for cataloging the report. Key words must be selected so that no security classification is required. Identifiers, such as equipment model designation, trade name, military project code name, geographic location, may be used as key words but will be followed by an indication of technical context. The assignment of links, rules, and weights is optional.